

**Exploring the neural basis of touch  
through selective and stable genetic tagging  
in the chick somatosensory system**

**Dissertation**

for the award of the degree

*'Doctor rerum naturalium'*

Division of Mathematics and Natural Sciences  
of the Georg-August-University Göttingen

submitted by

**Lukas Cyganek**

from Neustadt

Göttingen 2012

### **Thesis committee members**

Dr. Till Marquardt (Supervisor, Reviewer)

Developmental Neurobiology  
European Neuroscience Institute, Göttingen

Prof. Dr. Gregor Eichele (Reviewer)

Genes and Behavior  
Max Planck Institute for Biophysical Chemistry, Göttingen

Prof. Klaus-Armin Nave, Ph.D.

Neurogenetics  
Max Planck Institute for Experimental Medicine, Göttingen

### **Extended committee members**

Prof. Dr. Ernst Wimmer

Developmental Biology  
Johann-Friedrich-Blumenbach-Institute for Zoology and Anthropology, Göttingen

Prof. Dr. André Fischer

German Center for Neurodegenerative Diseases  
European Neuroscience Institute, Göttingen

Camin Dean, Ph.D.

Trans-synaptic Signaling  
European Neuroscience Institute, Göttingen

Date of the oral examination: December 20<sup>th</sup>, 2012

## I. List of contents

I.	List of contents .....	3
II.	List of figures .....	6
III.	List of tables .....	9
IV.	List of abbreviations .....	10
<b>1.</b>	<b>Introduction.....</b>	<b>13</b>
1.1.	Somatosensation .....	13
1.2.	Somatosensory neurogenesis.....	15
1.3.	Somatosensory neuron specification and connectivity .....	19
1.3.1.	Nociceptive neurons.....	21
1.3.2.	Proprioceptive neurons .....	23
1.3.3.	Mechanoreceptive neurons.....	25
1.4.	Low-threshold mechanoreceptor characteristics .....	28
1.5.	NetrinG-NGL interactions in neuronal circuit formation .....	32
1.6.	Identification of cis-regulatory elements.....	35
1.7.	Aim of the study .....	38
<b>2.</b>	<b>Materials and methods .....</b>	<b>40</b>
2.1.	Laboratory consumables and plastic ware.....	40
2.1.1.	Antibodies.....	40
2.1.2.	Enzymes.....	41
2.1.3.	Kits.....	42
2.1.4.	Chemicals and reagents .....	42
2.1.5.	Solutions.....	44
2.1.6.	Vectors .....	45
2.1.7.	Software .....	46
2.2.	Molecular biology.....	46
2.2.1.	Polymerase chain reaction.....	46

2.2.2.	DNA restriction digest .....	46
2.2.3.	Alkaline phosphatase treatment.....	47
2.2.4.	Agarose gel electrophoresis .....	47
2.2.5.	DNA purification from agarose gels .....	47
2.2.6.	DNA ligation.....	47
2.2.7.	Plasmid preparation .....	48
2.2.8.	DNA concentration measurements .....	48
2.2.9.	Sequencing.....	48
2.2.10.	Preparation of chemically competent <i>E.coli</i> .....	48
2.2.11.	Transformation .....	48
2.2.12.	Preservation and recovery of <i>E.coli</i> .....	49
2.2.13.	DNA extraction .....	49
2.2.14.	RNA extraction .....	49
2.2.15.	cDNA synthesis .....	50
2.3.	Plasmid construction.....	50
2.4.	<i>In ovo</i> electroporation .....	52
2.5.	Immunohistochemistry.....	53
2.6.	<i>In situ</i> hybridization .....	54
2.7.	Cell culture .....	55
2.8.	Electrophysiology.....	56
2.9.	Imaging .....	57
2.10.	Quantifications and measurements.....	57
<b>3.</b>	<b>Results.....</b>	<b>59</b>
3.1.	Stable genetic tagging of somatosensory neurons in chick.....	59
3.2.	Analysis of the sensory neuron-specific enhancer <i>Isl1<sup>Crest3</sup></i> .....	65
3.3.	Analysis of the sensory neuron-specific enhancer <i>Avil<sup>Lucy1</sup></i> .....	72
3.4.	Analysis of ipsilaterally and contralaterally migrating neural crest cells .....	76
3.5.	Analysis of the mechanoreceptor-specific enhancer <i>Ntng1<sup>Mech1</sup></i> .....	88
3.6.	Overall organization of somatosensory central collaterals in chick .....	103
3.7.	Peripheral connectivity of <i>Ntng1<sup>Mech1+</sup></i> somatosensory neurons .....	109
3.8.	<i>Ntng1</i> - <i>NGL1</i> interactions in laminar targeting of sensory afferents.....	114



<b>4. Discussion</b> .....	<b>120</b>
4.1. <i>STEVE</i> -mediated stable genetic tagging of somatosensory neurons .....	120
4.2. Establishment of <i>Isl1<sup>Crest3</sup></i> and <i>Avil<sup>Lucy1</sup></i> as pan-sensory neuron markers ...	121
4.3. Neurogenic equivalence of ipsilaterally and contralaterally migrating neural crest cells.....	124
4.4. A novel subclass of touch receptor neurons defined by <i>Ntng1<sup>Mech1</sup></i> .....	126
4.5. NetrinG-NGL interactions in mechanoreceptive circuit formation .....	132
<b>5. Summary</b> .....	<b>135</b>
6. References .....	137
7. Acknowledgements .....	154
8. Curriculum Vitae .....	155
9. Declaration.....	156

## II. List of figures

Figure 1.1: Connectivity of somatosensory neurons .....	14
Figure 1.2: Vertebrate neurulation.....	16
Figure 1.3: Waves of sensory neurogenesis.....	18
Figure 1.4: Genetic cascades of somatosensory subtype specification.....	20
Figure 1.5: Connectivity of nociceptive neurons .....	21
Figure 1.6: Connectivity of proprioceptive neurons.....	24
Figure 1.7: Connectivity of mechanoreceptive neurons.....	25
Figure 1.8: Electrophysiology of somatosensory neuron subtypes .....	29
Figure 1.9: Subtypes of low-threshold mechanoreceptors in hairy skin .....	30
Figure 1.10: NetrinG-NGL interactions in lamina-specific connectivity .....	33
Figure 1.11: Expression analysis of <i>NetrinG1</i> and <i>NGL1</i> in vertebrates.....	34
Figure 1.12: Enhancer identification via genomic comparison .....	37
Figure 2.1: Plasmid construction for enhancer activity analysis .....	51
Figure 2.2: Plasmid construction for transgene expression analysis.....	52
Figure 3.1: Selective and stable genetic tagging of spinal and somatosensory neurons in chick .....	61
Figure 3.2: <i>In silico</i> ECR screen of the <i>Islet1</i> gene locus .....	66
Figure 3.3: Genetic tagging of somatosensory neurons by <i>Isl1<sup>Crest3</sup></i> in early stage chick embryos .....	67
Figure 3.4: Tagging of somatosensory neurons by <i>Isl1<sup>Crest3</sup></i> in late-gestation chick embryos .....	68
Figure 3.5: Analysis of <i>Isl1<sup>Crest3+</sup></i> peripheral collaterals in late-gestation chick embryos .....	69
Figure 3.6: Development of central afferent projections in chick I.....	70
Figure 3.7: Development of central afferent projections in chick II.....	71
Figure 3.8: <i>In silico</i> ECR screen of the <i>Advillin</i> gene locus .....	73

Figure 3.9: Tagging of somatosensory neurons by <i>Avil<sup>Lucy1</sup></i> in late-gestation chick embryos .....	74
Figure 3.10: Mapping of central afferent projections by <i>Avil<sup>Lucy1</sup></i> throughout gestation in chick .....	75
Figure 3.11: Scenarios of ipsilaterally and contralaterally migrating NCC progeny in chick .....	76
Figure 3.12: Direct fate-tracking of ipsilaterally and contralaterally migrating NCCs in chick.....	77
Figure 3.13: Genetic tagging of ipsilateral and contralateral somatosensory neurons in chick .....	78
Figure 3.14: DRG neuron type composition of ipsilateral and contralateral NCC progeny in chick .....	79
Figure 3.15: Central connectivity pattern of ipsilateral and contralateral NCC progeny in chick .....	81
Figure 3.16: Peripheral collaterals of ipsilateral and contralateral NCC progeny in chick .....	82
Figure 3.17: Ipsilateral and contralateral NCC derivatives in the periphery of chick embryos .....	83
Figure 3.18: Projection density map of ipsilaterally-derived <i>Isl1<sup>Crest3+</sup></i> central collaterals in chick.....	84
Figure 3.19: Projection density map of contralaterally-derived <i>Isl1<sup>Crest3+</sup></i> central collaterals in chick.....	85
Figure 3.20: Projection density map of <i>TrkA<sup>+</sup></i> central collaterals in chick.....	86
Figure 3.21: <i>In silico</i> ECR screen of the <i>NetrinG1</i> gene locus .....	88
Figure 3.22: Selective tagging of a somatosensory neuron subtype by <i>Ntng1<sup>Mech1</sup></i> in chick.....	90
Figure 3.23: Development of <i>Ntng1<sup>Mech1+</sup></i> central afferent projections in chick.....	91
Figure 3.24: Molecular analysis of <i>Ntng1<sup>Mech1+</sup></i> somatosensory neurons in chick .....	92
Figure 3.25: Morphological analysis of <i>Ntng1<sup>Mech1+</sup></i> somatosensory neurons in chick.....	94
Figure 3.26: Electrophysiological analysis of <i>Ntng1<sup>Mech1+</sup></i> somatosensory neurons in chick I .....	96
Figure 3.27: Electrophysiological analysis of <i>Ntng1<sup>Mech1+</sup></i> somatosensory neurons in chick II .....	97
Figure 3.28: Central connectivity pattern of <i>Ntng1<sup>Mech1+</sup></i> somatosensory neurons in chick .....	98

Figure 3.29: Projection density map of Ntng1 <sup>Mech1+</sup> central collaterals in chick.....	100
Figure 3.30: Trajectories of individual molecularly defined central collaterals in chick .....	104
Figure 3.31: Trajectory tracings of nociceptive central afferents in chick.....	105
Figure 3.32: Trajectory tracings of mechanoreceptive central afferents in chick ....	106
Figure 3.33: Trajectory tracings of proprioceptive central afferents in chick .....	107
Figure 3.34: Tagging of contralateral central collaterals throughout gestation in chick .....	108
Figure 3.35: Analysis of Ntng1 <sup>Mech1+</sup> peripheral collaterals in chick glabrous skin ..	110
Figure 3.36: Analysis of Ntng1 <sup>Mech1+</sup> peripheral collaterals in chick feathery skin ...	111
Figure 3.37: Analysis of Ntng1 <sup>Mech1+</sup> peripheral terminations in chick glabrous skin at E12 .....	112
Figure 3.38: Analysis of Ntng1 <sup>Mech1+</sup> peripheral terminations in chick glabrous skin at E19 .....	113
Figure 3.39: Selective and stable transgene overexpression in late-gestation chick embryos .....	115
Figure 3.40: Verification of transgene overexpression in early stage chick embryos .....	116
Figure 3.41: NGL1 overexpression analysis of chick somatosensory central connectivity .....	117
Figure 3.42: Ntng1 overexpression analysis of chick somatosensory central connectivity .....	118
Figure 4.1: Connectivity of Ntng1 <sup>Mech1+</sup> A $\beta$ -LTMR neurons in chick.....	128
Figure 4.2: DRG explant culture of Isl1 <sup>Crest3+</sup> somatosensory neurons in chick.....	130

### III. List of tables

Table 1.1: Correlation of mechanoreceptive subtypes with their innervated end organs .....	27
Table 2.1: Incubation timeline for chicken embryos .....	53
Table 3.1: <i>In silico-to-in vivo</i> ECR screen of sensory neuron-specific candidate genes.....	62
Table 3.2: Statistical analysis of ipsilateral and contralateral NCC progeny experiments.....	87
Table 3.3: Statistical analysis of <i>Ntng1<sup>Mech1</sup></i> colocalization and cell size experiments.....	101
Table 3.4: Statistical analysis of <i>Ntng1<sup>Mech1</sup></i> electrophysiology and projection density experiments .....	102

## IV. List of abbreviations

μ	Micro
%	Percent
°C	Degree Celsius
AHP	Afterhyperpolarization
Avil	Advillin
BDNF	Brain-derived neurotrophic factor
BMP	Bone morphogenetic protein
bp	Base pair
BSA	Bovine serum albumin fraction V
Btx	Bungarotoxin
CAG	CMV early enhancer / chicken β-actin
cDNA	Complementary DNA
chr	Chromosome
cKO	Conditional knockout
CNS	Central nervous system
DEPC	Diethylpyrocarbonate
DF	Dorsal funiculus
DIG	Digoxigenin
DMSO	Dimethyl sulfoxide
DNA	Deoxyribonucleic acid
DRG	Dorsal root ganglion
E	Embryonic day
ECR	Evolutionary conserved non-coding region
EDTA	Ethylenediaminetetraacetic acid
eGFP	Enhanced GFP
EGTA	Ethyleneglycoltetraacetic acid
etc	Et cetera
g	Gram

galGal	Gallus gallus
GDNF	Glia-derived neurotrophic factor
GFP	Green fluorescent protein
GPI	Glycosyl-phosphatidyl-inositol
GRE	Gene regulatory element
h	Hour
HPD	Half peak duration
HH	Hamburger-Hamilton
IA	Intermediately adapting
IB4	Isolectin B4
Isl1	Islet1
kb	Kilo base pair
KO	Knockout
l	Liter
LF	Lateral funiculus
LT	Lateral tract
LTMR	Low-threshold mechanoreceptor
m	Milli
mm	Mus musculus
M	Molar
mGFP	Myristoylated GFP
min	Minute
MN	Motor neuron
Mrgpr	Mas-related G protein-coupled receptor
mRNA	Messenger RNA
NCC	Neural crest cell
NeuN	Neuronal nuclei
NF	Neurofilament
NGF	Nerve growth factor
NGL	NetrinG ligand
Ngn	Neurogenin
NT-3	Neurotrophin 3
NtnG	NetrinG

P	Postnatal day
Phal	Phalloidin
PBS	Phosphate buffered saline
PCR	Polymerase chain reaction
PFA	Paraformaldehyde
PN	Peripheral nerve
RA	Rapidly adapting
RNA	Ribonucleic acid
SA	Slowly adapting
SCG	Sympathetic chain ganglion
SDS	Sodium dodecyl sulfate
SEM	Standard <i>error</i> of the mean
Sox10	SRY box 10
<i>STEVE</i>	Stable expression vector
TF	Transcription factor
TFBS	Transcription factor binding site
TH	Tyrosine hydroxylase
Trk	Tropomyosin receptor kinase
Trp	Transient receptor potential cation channel
w/v	Weight per volume



# 1. Introduction

## 1.1. Somatosensation

Being exposed to myriad forces and environmental signals, higher organisms adapted by acquiring mechanisms to detect external stimuli, to process the information and to react accordingly. Force sensing is essential for nearly all behaviors that range from avoiding bodily harm to social exchange and is therefore fundamental for development and survival (Lumpkin *et al.*, 2010). Many types of specialized receptors transduce light, heat, mechanical or chemical stimuli into a change in the cell's membrane potential, the common language of neurons (Squire *et al.*, 2008). Somatosensory neurons detect the information about noxious stimuli, touch, temperature and proprioception in skin, viscera and muscle and bridge the distance between peripheral transduction and central processing in the central nervous system (CNS) (Lewin and Moshourab, 2004; Bourane *et al.*, 2009; Lumpkin *et al.*, 2010). These pseudo-unipolar neurons cluster in the dorsal root ganglia (DRGs) and extend one axon collateral branch to the periphery, whereas the other collateral branch penetrates the spinal cord. The central axon collaterals form, depending on the type of stimulus they relay, synapses upon second order neurons in the dorsal horn, in the intermediate spinal cord or directly connect with motor neurons in the ventral horn (Figure 1.1) (Li *et al.*, 2011). The CNS then constructs a topographical representation of the body, compares the input with further sensory signals and past events and processes the information, enabling animals to adapt their behavior to the changing environment (Squire *et al.*, 2008).

All species rely on touch-dependent behaviors ranging from the simplest activities in daily life to extremely sophisticated tasks, like highly precise object manipulation or braille reading (Luo *et al.*, 2009; Lumpkin *et al.*, 2010). Different types of functionally specialized mechanoreceptors along with their corresponding receptor end organs in the skin encode the different qualities of touch and selectively respond to vibration, static indentation or stretch (Heidenreich *et al.*, 2011; Li *et al.*, 2011). The receptor density covering the body's surface is tightly correlated with the spatial acuity, ranging from higher frequency at the finger tips to lower frequency at the back (Squire *et al.*,

2008). The interplay of the distinct mechanoreceptive subtypes provides sensory richness to touch-related percepts and encodes complex textures with fine tactile acuity (Bourane *et al.*, 2009; Luo *et al.*, 2009). Additionally, nociceptors and proprioceptors provide an organism with knowledge of pain sensations for avoidance behaviors and give feedback to control and coordinate muscle action, respectively (Squire *et al.*, 2008; Arber, 2012).

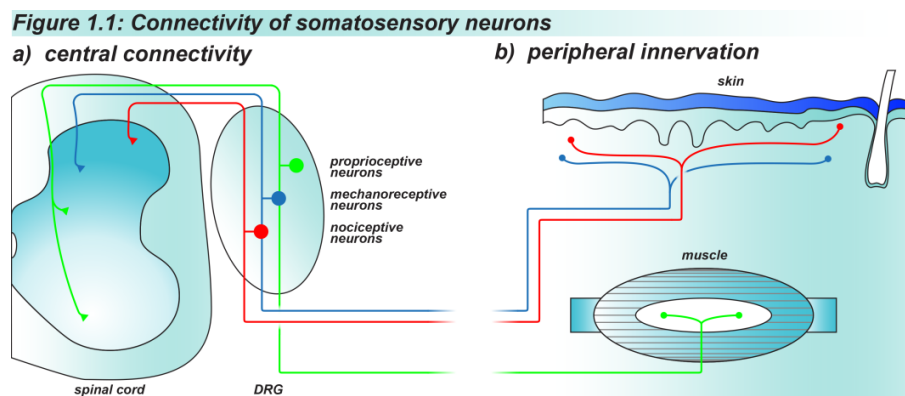


**Figure 1.1: Connectivity of somatosensory neurons**

**(a)** Somatosensory neurons accumulated in dorsal root ganglia (DRGs) penetrate the spinal cord and form synapses upon second order neurons in the dorsal horn and intermediate spinal cord or directly connect motor neurons, dependent on their distinct subtypes for signal transduction.

**(b)** Somatosensory afferents detect and transmit the sensory information about noxious stimuli, touch, temperature and proprioception from the skin and muscle to the central nervous system.

(Adapted from Lallemand and Ernfors, 2012)

Dysregulation of sensory signaling caused by disease or injury can lead to hypersensitivity and chronic pain (Lumpkin *et al.*, 2010). Recent studies reported of a congenital insensitivity to pain caused by gene mutations (Frenzel *et al.*, 2012). Further groups provided evidence that shared genetic factors influence different mechanosensitive systems, such as hearing and touch (Frenzel *et al.*, 2012). Despite more than 100 years of study and its overwhelming importance in daily life, surprisingly little is known about the cellular substrate of touch sensations, including the specification of the corresponding primary somatosensory neurons, their unique function and the logic of mechanoreceptive circuit organization (Marmigère and Ernfors, 2007; Lumpkin *et al.*, 2010; Nilius, 2010; Li *et al.*, 2011).

## 1.2. Somatosensory neurogenesis

The assembly of precise neuronal circuits is crucial for the function of the nervous system and depends on the specification of well-defined neuronal subpopulations that arise during embryogenesis (Kandel *et al.*, 2000). Neurulation is initiated by the induction of the neural plate from the dorsal ectoderm of the gastrula-stage embryo, whereby the most anterior region of the neural plate forms the forebrain, progressively more posterior regions give rise to midbrain, hindbrain and spinal cord structures (Figure 1.2 a) (Tanabe and Jessell, 1996). The neural plate is subsequently converted into a tube by the shaping and folding of the neuroepithelium, involving coordinated changes in cell shape, cell division, cell migration and cell-cell interaction (Figure 1.2 b) (Squire *et al.*, 2008; Greene and Copp, 2009). Finally, the inner neural tube and the outer surface ectoderm are created by adhesion, fusion and remodeling of the midline (Figure 1.2 c) (Copp *et al.*, 2003). The patterning of the neuraxis is mediated by factors released from the axial and paraxial mesoderm (Tanabe and Jessell, 1996; Lumsden and Krumlauf, 1996).

These secreted factors induce the localized expression of cell-intrinsically acting factors along the rostrocaudal and dorsoventral axis of the neural tube, which, in turn, are involved in the generation of a large diversity of neuronal cell types (Muhr *et al.*, 1999; Le Dréau and Martí, 2012). The dorsal cell fate determination depends on a cascade of secreted proteins, which are initiated by cells of the epidermal ectoderm and propagated by roof plate cells within the neural tube. The main instructive cues are members of the Transforming growth factor  $\beta$  / Activin / Bone morphogenetic protein (BMP) family, complemented by additional signals involving the Wnt and Fibroblast growth factor families, which also contribute to the dorsal neuronal identity (Liem *et al.*, 1997; Lee and Jessell, 1999; Helms and Johnson, 2003; Le Dréau and Martí, 2012). The ventral neuronal patterning of the CNS is induced by signaling of the notochord and later on by the floor plate through secretion of the glycoprotein Sonic hedgehog, which has been shown to direct different cell fates, such as motor neurons and ventral interneurons, at different concentration thresholds (Chiang *et al.*, 1996; Briscoe *et al.*, 2000). Selective cross-repressive interactions convert the dorsoventral

signaling activity into discrete progenitor domains (Sander *et al.*, 2000; Liem *et al.*, 2000; Jessell, 2000).

**Figure 1.2: Vertebrate neurulation**

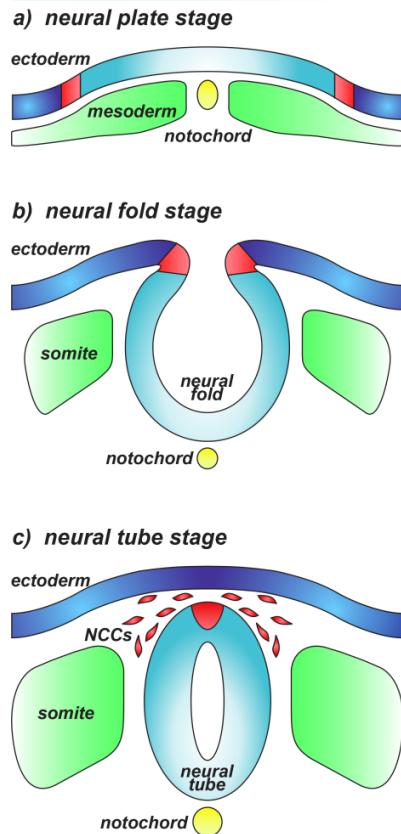


**Figure 1.2: Vertebrate neurulation**

**(a)** The induction of the neural plate is initiated from the dorsal ectoderm of the gastrula-stage embryo as a consequence of inducing factors released from the mesoderm and notochord.

**(b)** Shaping and folding of the neuroepithelium converts the tube in a neural fold. Somites originate from the paraxial mesoderm.

**(c)** Fusion and remodeling of the midline creates the neural tube and the outer ectoderm. Neural crest cells (NCCs) emerge from the dorsal part of the neural tube.

(Adapted from Jessell, 2000)

Concomitant with the fusion of the neural folds during neurulation, neural crest cells (NCCs) subsequently emerge from the most dorsal portion of the neural tube. These multipotent, SRY box 10 (Sox10)-positive progenitor cells give rise to a wide variety of cell types and form most of the peripheral nervous system, including dorsal root, sympathetic, parasympathetic and enteric ganglia. Furthermore, NCCs generate non-neuronal cells like glia, Schwann cells, adrenal cells and melanocytes (Bronner-Fraser and Fraser, 1988; Frank and Sanes, 1991; Gilbert, 2000; Kim *et al.*, 2003). NCC progenitor cell fate arises prior to neurulation within a band of cells at the border between the neural plate and the non-neuronal ectoderm (Le Douarin and Kalcheim, 1999; Squire *et al.*, 2008). Premigratory NCC development is induced by signaling factors, including BMP and WNT, whereas a variety of further factors can bias the cells toward certain lineages (Bronner-Fraser, 2004; Huang and Saint-Jeannet, 2004;

Marmigère and Ernfors, 2007). NCCs undergo a transition from epithelial to migratory mesenchymal cells with changes in their adhesive properties (Sauka-Spengler and Bronner-Fraser, 2008; Squire *et al.*, 2008). Downregulation of cell adhesion molecules like N-cadherin and cadherin 6 are thought to drive the transition from epithelial to motile mesenchymal characteristics (Nakagawa and Takeichi, 1998; Pla *et al.*, 2001). During this process, the basal lamina around the neural tube dissolves, NCCs delaminate and directionally emigrate, a process involving homotypic cell-cell interactions (Kandel, 2000; Carmona-Fontaine *et al.*, 2008). Many NCCs appear to be multipotent both before and after emigration, and their fate is to large degree determined in response to extracellular signals (Hari *et al.*, 2012). However, several lines of evidence suggest the existence of subpopulations of lineage-restricted premigratory NCCs (George *et al.*, 2007; Lefcort and George, 2007). NCCs migrate along defined pathways in chain-like structures towards their respective peripheral targets between embryonic day (E) 8 and E10 in the mouse and between Hamburger-Hamilton stage 11 and 21 in the chick (Hamburger and Hamilton, 1951; Serbedzija *et al.*, 1990; Frank and Sanes, 1991; Kasemeier-Kulesa *et al.*, 2005; Krispin *et al.*, 2010). Attractive and repulsive environmental adhesion molecules and secreted guidance cues influence NCC migration before they differentiate into their target-appropriate cell types (Ruhrberg and Schwarz, 2010; Theveneau and Mayor, 2012). Currently, little is known about how NCCs stop their migration after reaching their appropriate destination (Squire *et al.*, 2008; Theveneau and Mayor, 2012).

Neurogenesis occurs in three successive waves of NCC migration between E9.5 and E11 in the mouse, in which the Wnt/ $\beta$ -catenin pathway and the BMP signaling play an instructive role concerning the specification of the sensory lineage (Hari *et al.*, 2002; Lee HY *et al.*, 2004; Bronner-Fraser, 2004; Kléber *et al.*, 2005; Marmigère and Ernfors, 2007). After their delamination a subpopulation of NCCs migrates along a ventral pathway and coalesces into dorsal root ganglia (DRGs) adjacent to the neural tube at regular intervals (Lallemend and Ernfors, 2012). The first wave of neurogenesis is initiated during early NCC migration by the expression of the transcription factor (TF) Neurogenin 2 (Ngn2) that directs NCC differentiation mainly into mechanoreceptive and proprioceptive sensory neurons, which localize in the ventrolateral part of the DRG (Figure 1.3 a) (Ma *et al.*, 1999; Perez *et al.*, 1999). These

$\text{Ngn2}^+$  cells show limited cell division with three neurons per NCC and constitute around four percent of the adult DRG neurons (Frank and Sanes, 1991; Anderson, 2000).

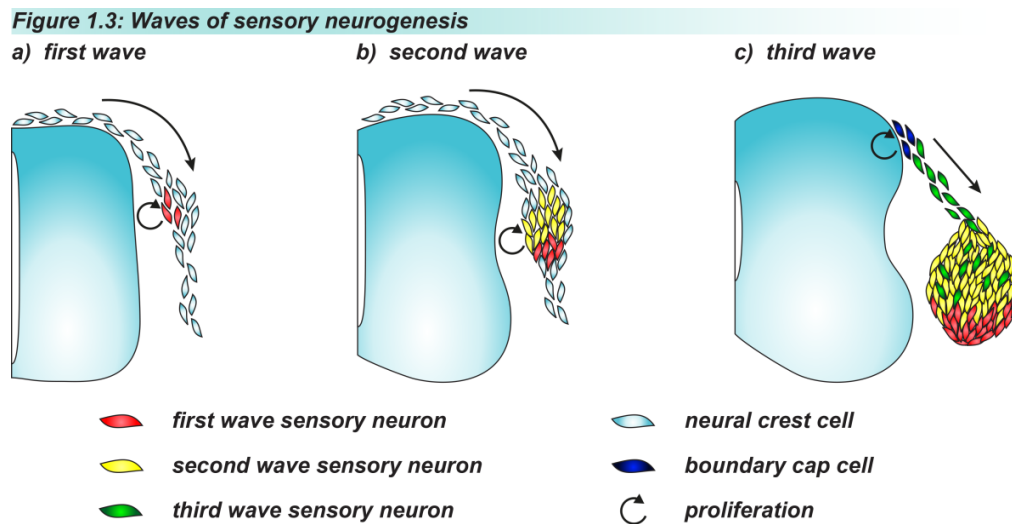


**Figure 1.3: Waves of sensory neurogenesis**

(a) Multipotent neural crest cells (NCCs) delaminate from the neural tube and migrate along ventral pathways to accumulate in dorsal root ganglia (DRGs). Neurogenin 2 initiates a first wave of neurogenesis producing mechanoreceptive and proprioceptive neurons (4% of total DRG neurons).

(b) Postmigratory differentiation of NCCs towards nociceptive, mechanoreceptive and proprioceptive neurons is mediated by Neurogenin 1 in a second wave of neurogenesis. High cell division rates lead to the emergence of around 91% of total DRG neurons.

(c) In a late neurogenic wave boundary cap cells generate a small amount of nociceptive neurons (5% of total DRG neurons).

(Adapted from Marmigère and Ernfors, 2007)

With around 91%, the major proportion of the DRG neurons is generated in the second wave of sensory neurogenesis due to a high cell division rate that produces an average of 36 neurons per NCC (Figure 1.3 b) (Frank and Sanes, 1991; Marmigère and Ernfors, 2007). High levels of the TF Neurogenin 1 ( $\text{Ngn1}$ ) drive the postmigratory differentiation of the multipotent  $\text{Sox10}^+$  NCCs towards small nociceptive neurons located in the dorsomedial region of the DRG, as well as towards large-size mechanoreceptive and proprioceptive neurons (Ma *et al.*, 1999; Kim *et al.*, 2003). Furthermore, in a third wave of neurogenesis, boundary cap cells, a specialized population of postmigratory NCCs contributing to up to five percent of total DRG neurons, are thought to produce DRG neurons of exclusively nociceptive type

(Figure 1.3 c) (Maro *et al.*, 2004; Lallemand and Ernfors, 2012). NCCs of the second and third waves also differentiate into peripheral glia in addition to neurons (Frank and Sanes, 1991; Maro *et al.*, 2004). The Neurogenin TFs initiate pan-neuronal programs leading to the establishment of neuronal fate accompanied by the expression of other key TFs like Brn3a, Islet1 or Foxs1 (McEvilly *et al.*, 1996; Perez *et al.*, 1999; Kim *et al.*, 2003; Montelius *et al.*, 2007). The initiated transcriptional programs cause downregulation of multipotency factors like Sox10 and suppression of dorsal spinal cord and other non-neuronal fates, while downstream signaling cascades promote neuronal differentiation and sensory neuron subtype specification (Marmigère and Ernfors, 2007; Sun *et al.*, 2008; Lanier *et al.*, 2009).

### **1.3. Somatosensory neuron specification and connectivity**

The determination of a neuronal cell fate is controlled by the interplay between environmental cues and cell-intrinsic information. Therefore, the birth of a neuron at a specific time and position determines its identity (Lallemand and Ernfors, 2012). Shortly after their accumulation in DRGs the immature NCC-derived neurons start to differentiate into various types of sensory neurons, including nociceptive and mechanosensitive neurons terminating in the skin, as well as proprioceptive neurons innervating deep structures, such as muscle spindles and golgi tendon organs (Lupkin *et al.*, 2010). Intrinsic and local environmental signals drive the segregation into unique subtypes by transcriptional activation and repression of specific genes, encoding key cell fate determinants. The earliest known markers for sensory subtypes are the growth factor receptors Tropomyosin receptor kinase A (TrkA), TrkB, TrkC, Met and Ret which serve as receptors for the Neurotrophins (Nerve growth factor, NGF; Brain-derived neurotrophic factor, BDNF; Neurotrophin 3, NT-3), Hepatocyte growth factors and Glia-derived neurotrophic factor (GDNF) ligands produced by cells from sensory target tissue (Snider and Wright, 1996; Huang and Reichardt, 2001).

Figure 1.4: Genetic cascades of somatosensory subtype specification

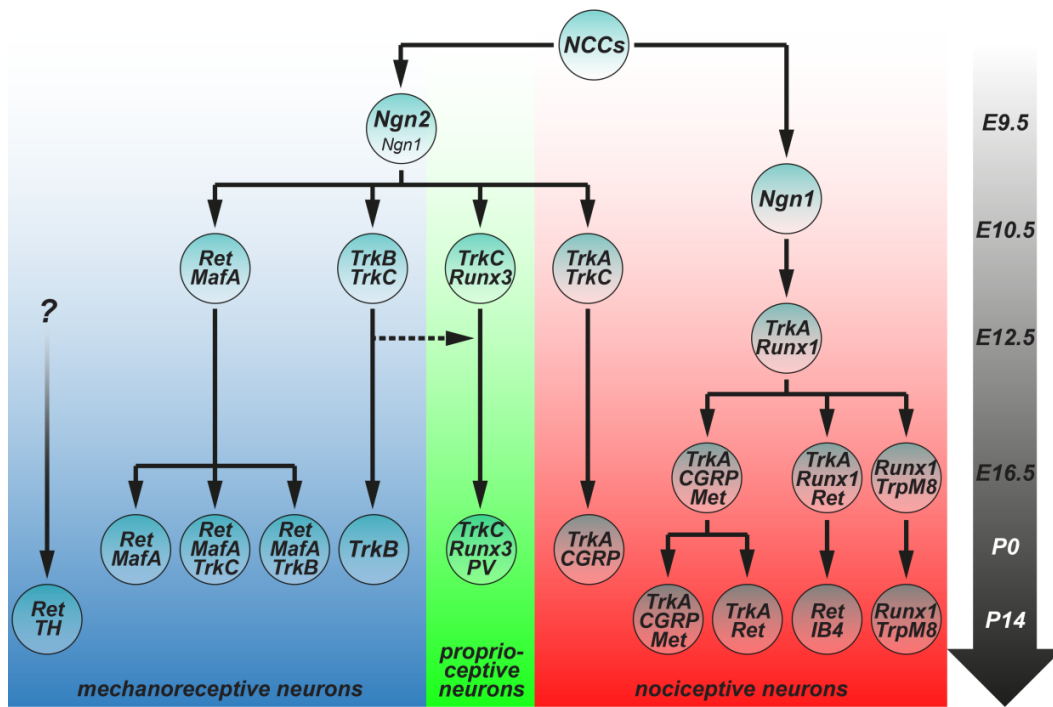


Figure 1.4: Genetic cascades of somatosensory subtype specification

All sensory neurons arise from neural crest cells (NCCs). Further in their development, they become specified according to the combinatorial expression of key regulators like the growth factor receptors TrkA, TrkB, TrkC, Ret and Met and the transcription factors Runx1, Runx3 and MafA. Sensory specification and maturation of mechanoreceptors, proprioceptors and nociceptors extends to postnatal stages in mice. E, embryonic day; P, postnatal day; interrogation mark, unknown origin.

(Adapted from Lallemand and Ernfors, 2012)

These factors and their receptors play important roles in shaping the functionality and specific connectivity of the primary somatosensory neurons by their involvement in neuron diversification, peripheral innervation, cell survival and central axon collateral targeting (Huang *et al.*, 1999; Fünfschilling *et al.*, 2004; Marmigère and Ernfors, 2007; Luo *et al.*, 2009; Gascon *et al.*, 2010). Furthermore, several differentially expressed TFs begin to be expressed in early neurogenesis, including MafA and c-Maf, as well as the Runx family members Runx1 and Runx3 (Kramer *et al.*, 2006; Bourane *et al.*, 2009; Wende *et al.*, 2012). It is generally thought that these factors participate via combinatorial expression profiles in the basic establishment of sensory neuron diversification and maturation, a process that extends well into postnatal stages in mammals (Figure 1.4). Genetic programs that direct neuronal subtype specification are likely to also control connectivity. However, the regulatory mechanisms driving



both sensory subtype specification and connectivity remain incomplete and additional participating factors need to be identified (Liu and Ma, 2011; Lallemand and Ernfors, 2012).

### 1.3.1. Nociceptive neurons

The major part of unmyelinated nociceptive neurons is generated from the Ngn1 dependent wave of neurogenesis, followed by the upregulation of high TrkA and Runx1 expression levels at E11.5 in mice (Ma *et al.*, 2003; Kramer *et al.*, 2006; Chen CL *et al.*, 2006). Runx1 is important for the emergence of Ngn1-dependent small-diameter neurons by activation of TrkA via direct promoter binding (Marmigère *et al.*, 2006). At later embryonic stages around E12.5 - E15.5 in mice, Runx1 expression becomes more subtype-restricted and the function switches from a general nociceptive transcriptional activator to a repressor (Chen CL *et al.*, 2006). Thus, Runx1 mediates the further diversification of immature TrkA<sup>+</sup> neurons. Maintained Runx1 expression drives a TrkA<sup>-</sup> non-peptidergic phenotype, whereas downregulation of Runx1 allows neurons to acquire a TrkA<sup>+</sup> peptidergic phenotype (Chen CL *et al.*, 2006; Marmigère and Ernfors, 2007).

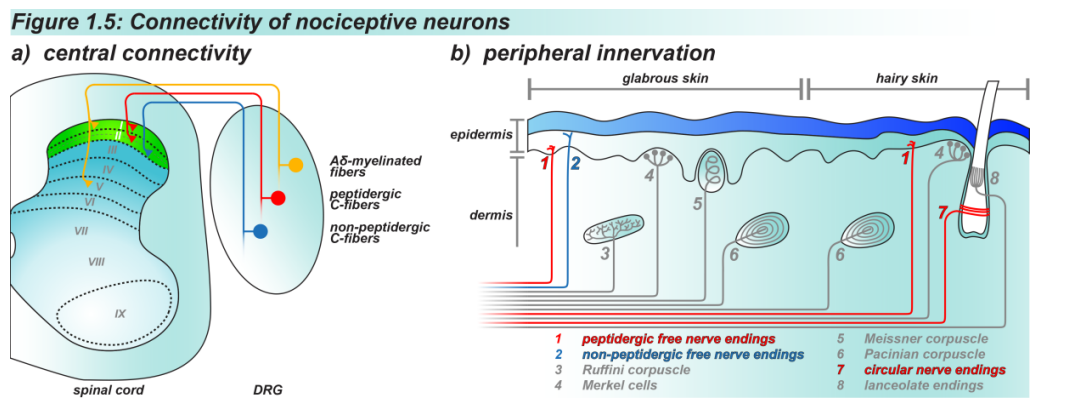


**Figure 1.5: Connectivity of nociceptive neurons**

**(a)** Nociceptive subtypes terminate in different laminae in the spinal cord. Peptidergic C-fibers innervate laminae I and II (outer), non-peptidergic neurons project mainly into lamina II (inner), whereas lightly myelinated A $\delta$ -nociceptors terminate in laminae I and V of the dorsal horn.

**(b)** In the periphery, peptidergic C-fibers terminate as free nerve endings in the epidermis close to the dermis border and as circular nerve endings at hair follicles. Non-peptidergic peripheral projections terminate superficially in the epidermis.

(Adapted from Lallemand and Ernfors, 2012)

Peptidergic nociceptors, which serve as polymodal pain-sensing neurons responding to noxious heat and mechanical stimuli, express high levels of TrkA, Met and the neuropeptides CGRP and Substance P (Lewin and Moshourab, 2004). Their slowly conducting C-fibers terminate close to the epidermis-dermis border as free nerve endings and as circular nerve endings at hair follicles (Figure 1.5). Their central afferents project into laminae I and II (outer) in the spinal cord for pain transmission (Fitzgerald, 2005; Zylka *et al.*, 2005; Squire *et al.*, 2008). Activation of TrkA has been shown to induce Met, which defines the peptidergic phenotype by extinguishing Runx1 expression via cross-repressive interactions between Met and Runx1 (Kramer *et al.*, 2006; Gascon *et al.*, 2010). Additionally, Met and TrkA activate peptidergic expression profiles (Lumpkin and Caterina, 2007; Lallemand and Ernfors, 2012).

Non-peptidergic nociceptors are responsible for the detection of thermal pain, inflammatory pain and are involved in neuropathic pain (Chen CL *et al.*, 2006). Their C-fiber terminals innervate the epidermis and their central projections terminate in lamina II (inner) in the spinal cord (Figure 1.5) (Fitzgerald, 2005; Zylka *et al.*, 2005; Squire *et al.*, 2008). Non-peptidergic neurons display a unique expression of Runx1 and Ret, which together induce the progressive extinction of TrkA around P14 in mice, while at the same time these neurons acquire isolectin B4 (IB4) binding (Molliver *et al.*, 1997; Abdel Samad *et al.*, 2010). During segregation of the peptidergic and non-peptidergic subtypes, Runx1 is important for inducing Ret expression and for repression of the peptidergic neuron markers CGRP and Met (Luo *et al.*, 2009; Gascon *et al.*, 2010). The upregulation of non-peptidergic-specific ion channels and transmembrane receptors shapes the receptive properties and the neuronal connectivity (Lumpkin and Caterina, 2007; Golden *et al.*, 2010). Additionally, Ret, whose expression is initiated by NGF and consolidated by Ret itself, accompanies the Runx1 function in repressing TrkA during the segregation of the lineages (Luo *et al.*, 2007). At approximately E16.5 in mice further nociceptive subtype specification occurs by the expression of different Mas-related G protein-coupled receptors (Mrgprs) whose functions are thought to underlie the acquisition of distinct pain sensitivities (Liu *et al.*, 2008; Lallemand and Ernfors, 2012).

It has been shown, that Runx1 is also necessary for the specification of DRG neurons expressing the Transient Receptor Potential channel family member TrpM8 (Chen CL *et al.*, 2006). These TrpM8<sup>+</sup>, but CGRP<sup>-</sup> and IB4<sup>-</sup> unmyelinated or lightly myelinated neurons probably arise from early TrkA<sup>+</sup>/Runx1<sup>+</sup> progenitors and mediate innocuous and painful sensations to cold and cooling compounds (Peier *et al.*, 2002; Takashima *et al.*, 2010). New data further revealed an early TrkA lineage of A $\delta$ -nociceptors, generated at E10.5 by a Ngn1-independent neurogenesis terminating in laminae I and V of the dorsal horn (Lallemend and Ernfors, 2012). This DRG neuron subtype expresses CGRP and the myelination marker Neurofilament 200 (NF200), whereas no expression of Runx1, Ret or Met could be detected (Gascon *et al.*, 2010; Bachy *et al.*, 2011). In summary, based on current literature, at least two bursts of birth of TrkA<sup>+</sup> neurons exist in sensory neurogenesis (Figure 1.4).

### 1.3.2. Proprioceptive neurons

Large-size proprioceptive neurons play a prominent role in coordinated muscle control by detecting changes in muscle length (Arber, 2012). Type Ia heavily myelinated A $\alpha$ -fibers innervate muscle spindles, whereas the central afferents project to the intermediate and ventral spinal cord where they directly synapse with  $\alpha$ -motor neurons to establish monosynaptic reflex circuits (Chen *et al.*, 2003). Group Ib A $\alpha$ -afferents which innervate golgi tendon organs project mainly to lamina VI in the intermediate spinal cord. Proprioceptive A $\beta$ -fibers of group II DRG neurons also terminate at muscle spindles and, like type Ia afferents, concentrate their central afferents in the intermediate and ventrolateral gray matter (Figure 1.6) (Scott, 1992; Riddell and Hadian, 2000).

The progenitors that give rise to proprioceptive neurons arise from the first and second waves of neurogenesis in the DRG (Ma *et al.*, 1999). Early in sensory DRG neuron diversification, two TrkC<sup>+</sup> populations can be observed until E12.5 in mice: one population expresses TrkC in combination with TrkB, whereas the other one expresses TrkC alone. At approximately E10.5, expression of Runx3 is initiated leading to the repression of TrkB and Shox2 (Kramer *et al.*, 2006; Abdo *et al.*, 2011; Scott *et al.*, 2011). This direct repression can be explained by the dependence of a

TrkB gene silencer on the Runx protein complex and on NT-3 signaling (Inoue *et al.*, 2007).

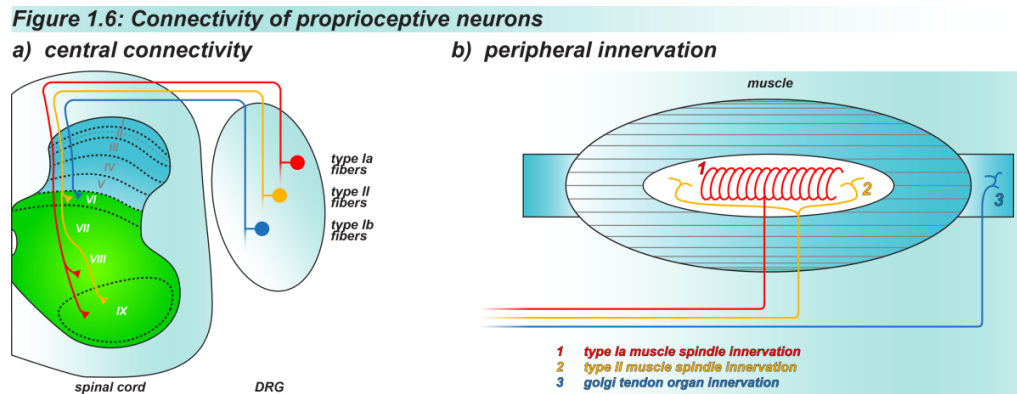


**Figure 1.6: Connectivity of proprioceptive neurons**

**(a)** Type Ia proprioceptive neurons terminate in the ventrolateral spinal cord and directly connect motor neurons (IX). Type Ib afferents project to the intermediate zone (mainly lamina VI), whereas type II neurons occupy both intermediate and ventral domains of the spinal cord.

**(b)** Type Ia A $\alpha$ -fibers and type II A $\beta$ -fibers innervate muscle spindles. Type Ib A $\alpha$ -afferents form endings at golgi tendon organs.

(Adapted from Lallemand and Ernfors, 2012)

The initiation of Runx3 expression in immature proprioceptive neurons occurs before peripheral target innervation and implies the regulation of determinants in the local DRG environment for proprioceptive cell fate (Lallemand and Ernfors, 2012). Additionally, Runx3 maintains TrkC expression via cross-activating loops between Runx3 and TrkC to consolidate a proprioceptive phenotype between E11 and E13.5 (Figure 1.4) (Kramer *et al.*, 2006; Nakamura *et al.*, 2008). The TrkC ligand NT-3, which is expressed in early muscle mass and later on in muscle spindles, has been shown to induce the ETS family TF ER81, an important regulator of central connectivity (Patel *et al.*, 2003). Together, Runx3 and TrkC are the key factors in molecular specification and functional circuit formation of proprioceptive neurons (Inoue *et al.*, 2002; Levanon *et al.*, 2002; Chen Al *et al.*, 2006). At later embryonic stages, additional general proprioceptive markers like Parvalbumin begin to be expressed, but no genes exclusively expressed by type Ia, Ib or II neurons have been identified so far (Chen *et al.*, 2003).

### 1.3.3. Mechanoreceptive neurons

Mechanoreceptive neurons comprise various myelinated and unmyelinated types, terminating throughout laminae II (inner) and V in the dorsal horn of the spinal cord and innervating their corresponding peripheral end organs in the hairy and glabrous skin (Figure 1.7) (Brown, 1982; Squire *et al.*, 2008).

**Figure 1.7: Connectivity of mechanoreceptive neurons**

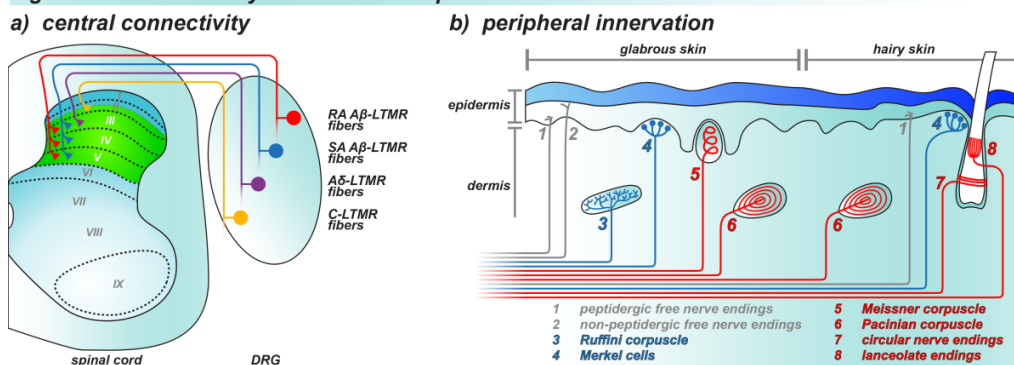


**Figure 1.7: Connectivity of mechanoreceptive neurons**

**(a)** Mechanoreceptive central afferents project into deeper laminae of the spinal cord. Rapidly adapting (RA) and slowly adapting (SA) low-threshold mechanoreceptors (LTMRs) terminate throughout laminae III-V, Aδ-LTMRs mainly connect with interneurons from lamina III and unmyelinated C-afferents project into lamina II (inner).

**(b)** Pacinian corpuscles and Merkel cells present in both, glabrous and hairy skin, are innervated by RA-afferents and SA-afferents, respectively. Meissner corpuscles exclusively found in glabrous skin and hair follicles are also innervated by RA Aβ-LTMRs, whereas SA-afferents additionally terminate at Ruffini corpuscles in glabrous skin. Aδ- and C-fibers were found to form lanceolate and circular nerve endings at hair follicles.

(Adapted from Lallemand and Ernfors, 2012)

In contrast to proprioceptors and nociceptors, little is known about the molecular mechanisms governing the early differentiation and later specification into mechanosensitive subtypes (Lecoin *et al.*, 2010). Mechanoreceptive neurons arise mainly from the Ngn2-dependent wave of neurogenesis (Ma *et al.*, 1999). Soon after DRG accumulation, mechanoreceptive progenitors segregate into Ret/Gfra2 expressing (earlyRet<sup>+</sup>) and TrkB<sup>+</sup>/TrkC<sup>+</sup> populations (Luo *et al.*, 2009; Honma *et al.*, 2010). This lineage diversifies further into Ret<sup>+</sup>/MafA<sup>+</sup>, Ret<sup>+</sup>/MafA<sup>+</sup>/TrkB<sup>+</sup> and Ret<sup>+</sup>/MafA<sup>+</sup>/TrkC<sup>+</sup> expressing neurons, for which Ret signaling appears to be crucial (Bourane *et al.*, 2009; Lecoin *et al.*, 2010). The more broadly expressed c-Maf controls MafA expression in these cells and further regulates the expression of ion channels

important for mechanoreceptor functions (Wende *et al.*, 2012). MafA, which is expressed in all of the three earlyRet<sup>+</sup> mechanoreceptive subtypes, shows the ability to repress TrkB (Ma, 2009). TrkB expression in one of the subtypes can only be maintained by additional expression of Shox2 (Abdo *et al.*, 2011). The regulatory mechanism of the differentiation into Ret<sup>+</sup>/MafA<sup>+</sup> or Ret<sup>+</sup>/MafA<sup>+</sup>/TrkC<sup>+</sup> mechanoreceptors still remains unknown (Lallemend and Ernfors, 2012). The earlyRet<sup>+</sup> neurons have been shown to predominantly label rapidly adapting low-threshold mechanoreceptors (LTMRs) innervating Meissner corpuscles, Pacinian corpuscles and hair follicles (Ma, 2009). Ret, MafA and c-Maf mutant mice all show dramatic defects in rapidly adapting mechanoreceptors function, as well as their central and peripheral connectivity (Table 1.1) (Bourane *et al.*, 2009; Luo *et al.*, 2009; Honma *et al.*, 2010; Wende *et al.*, 2012). Whether the different earlyRet<sup>+</sup> subtypes are restricted to different mechanoreceptive end organs demands further investigation. Therefore, additional participating factors, like ion channels responding to mechanical stimuli, still need to be identified (Ma, 2009). One putative candidate could be the potassium channel Kcnq4, which is expressed in earlyRet<sup>+</sup> neurons exclusively innervating Meissner corpuscles and hair follicles and plays an important role in controlled low-frequency vibration detection (Heidenreich *et al.*, 2011).

The TrkB<sup>+</sup> lineage of mechanoreceptive neurons arises from early TrkB<sup>+</sup>/TrkC<sup>+</sup> progenitors and might include slowly adapting LTMRs innervating Merkel and Ruffini end organs and lightly myelinated A $\delta$ -LTMRs (Abdo *et al.*, 2011; Li *et al.*, 2011). The co-expression of Shox2 in the progenitors promotes TrkB and represses TrkC expression and thereby directs the neurons to escape from a proprioceptive phenotype (Scott *et al.*, 2011). The cross-activation between Shox2 and TrkB and the cross-repression between Shox2 and TrkC are suggested to be the major determinants in TrkB<sup>+</sup> mechanoreceptive versus TrkC<sup>+</sup> proprioceptive cell fates (Lallemend and Ernfors, 2012).

Furthermore, Li and colleagues identified a DRG neuron population representing unmyelinated C-LTMRs, that is positive for Ret, tyrosine hydroxylase (TH) and vGlut3<sup>+</sup>, but negative for the common nociceptive markers TrkA, TrpV1, Mrgps and IB4 (Li *et al.*, 2011). These recent findings imply the existence of at least five molecularly

unique mechanoreceptive subtypes: Ret<sup>+</sup>/MafA<sup>+</sup>, Ret<sup>+</sup>/MafA<sup>+</sup>/TrkB<sup>+</sup>, Ret<sup>+</sup>/MafA<sup>+</sup>/TrkC<sup>+</sup>, TrkB<sup>+</sup> and Ret<sup>+</sup>/TH<sup>+</sup> (Figure 1.4). However, in most cases their correlation with distinct mechanoreceptive end organs needs to be examined in more detail (Table 1.1).

**Table 1.1: Correlation of mechanoreceptive subtypes with their innervated end organs**

lineage	method	innervated end organs				
		rapidly adapting			slowly adapting	
		hair follicles	Meissner corpuscles	Pacinian corpuscles	Merkel cells (hairy)	Merkel cells (glabrous)
earlyRet	earlyRet (genetically) Ret cKO (Luo et al., 2009)	yes affected	yes lost	yes lost	no ?	no ?
earlyRet	Ret (antibody) Ret cKO (Bourane et al., 2009)	yes affected	yes ?	? ?	yes affected	no ?
earlyRet	Ret (genetically) Ret KO (Honma et al., 2010)	yes	yes	yes	yes (not specified) generally impaired innervation	
earlyRet	cMaf cKO (Wende et al., 2012)	affected	affected	lost	unaffected	?
earlyRet subtype	Kcnq4 (antibody) (Heidenreich et al., 2011)	yes	yes	no	no	?
earlyRet subtype + TrkB	Shox2 cKO (Abdo et al., 2011)	affected	affected	unaffected	affected	affected

**Table 1.1: Correlation of mechanoreceptive subtypes with their innervated end organs**

The comparison of the results from different studies revealed consensuses and a few discrepancies in their observations of peripheral sensory end organ innervation. The labeling methods used for the sensory subtypes (genetically, antibody) and the mutant mice are stated. The innervation of Ruffini corpuscles was not analyzed by any of the groups. (c)KO, (conditional) knockout mouse; interrogation mark, not stated.

The current knowledge regarding the process of sensory neuron diversification is still rudimentary. The discovery of somatosensory subtype-specific direct cell lineage tracings, co-activators, co-repressors and further downstream substrates would help to understand the definite hierarchical organization, sensory cell fate determining mechanisms or the precise connectivity of somatosensory neuronal circuits (Marmigère and Ernfors, 2007; Lallemand and Ernfors, 2012).

#### 1.4. Low-threshold mechanoreceptor characteristics

Low-threshold mechanoreceptors (LTMRs) sense a range of innocuous mechanical stimuli and are subdivided according to their temporal response properties and their receptive field size. LTMRs differ in their conduction velocities which are affected by the nerve diameter, the myelination and the internal axon resistance. Accordingly, rapidly adapting (RA) and slowly adapting (SA) types can be distinguished (Lewin and Moshourab, 2004; Lumpkin and Caterina, 2007; Ma, 2009). LTMRs possessing a small receptive field size in the skin are referred to as type I, while LTMRs with a large receptive field are termed type II (Woolfe *et al.*, 2008). In mammals, RA type I and RA type II A $\beta$ -mechanoreceptors innervate Meissner corpuscles and Pacinian corpuscles, respectively, that dynamically respond to low and high-frequency vibration (Lewin and Moshourab, 2004; Heidenreich *et al.*, 2011). Hair follicles are innervated by heavily myelinated RA A $\beta$ -LTMRs, lightly myelinated A $\delta$ -LTMRs (D-hair receptors) and unmyelinated C-LTMRs, all of which are stimulated by hair deflection (Lewin and Moshourab, 2004; Lumpkin *et al.*, 2010). The peripheral collaterals of SA type I and SA type II A $\beta$ -mechanoreceptors terminate in Merkel discs and Ruffini corpuscles, respectively, that relay static responses to dermal stretch and indentation (Lewin and Moshourab, 2004; Lumpkin and Caterina, 2007; Lumpkin *et al.*, 2010). The different large-diameter A $\beta$ -LTMRs, as well as the medium-diameter A $\delta$ -neurons and small-diameter C-fibers can be differentiated electrophysiologically via *in vitro* skin nerve preparations, whereby response properties of single axon fibers are recorded after variable mechanical stimulation of the skin (Figure 1.8) (Lewin and Moshourab, 2004; Heidenreich *et al.*, 2011; Wende *et al.*, 2012).

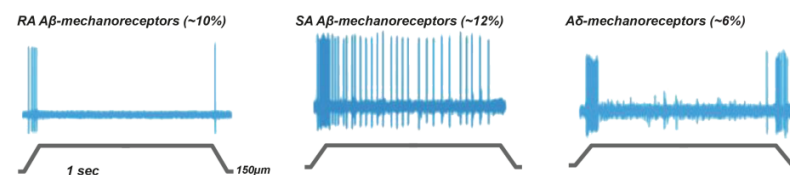
Through whole cell patch clamp recordings, it is further possible to discriminate isolated adult and embryonic nociceptive and mechanoreceptive sensory neurons by their characteristic action potential waveforms (Koerber *et al.*, 1988; Djouhri *et al.*, 1998; Fang *et al.*, 2005). The nociceptive action potentials show a 'hump' on the falling phase, long half peak durations and longer afterhyperpolarization durations. In contrast, mechanoreceptors fire narrow uninflected spikes with short half peak and afterhyperpolarization durations (Lechner *et al.*, 2009). Additionally, all sensory neurons acquire a mechanotransduction competence, the ability to transduce



mechanical stimuli into electrical signals (Lechner *et al.*, 2009). In mechanoreceptors and proprioceptors, this mechanically-activated rapid and highly sensitive mechanosensitive current activates and inactivates within a few milliseconds and appears as soon as the receptors innervate their peripheral targets (Lechner *et al.*, 2009). LTMRs thus possess a so-called RA-mechanosensitive current, while the majority of nociceptors exhibit intermediately adapting and SA inactivating currents (Drew *et al.*, 2002; Hu and Lewin, 2006; Lechner *et al.*, 2009).

**Figure 1.8: Electrophysiology of somatosensory neuron subtypes**

**a) mechanoreceptive neurons**



**b) nociceptive neurons**

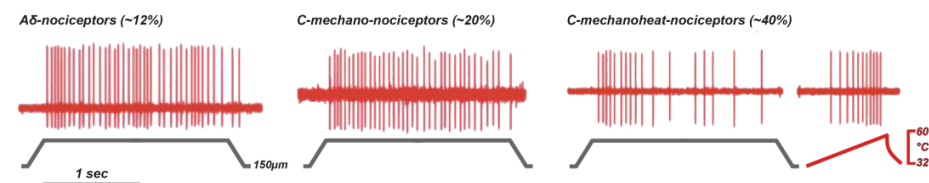


**Figure 1.8: Electrophysiology of somatosensory neuron subtypes**

*In vitro* mouse skin nerve preparations reveal typical electrophysiological differences between sensory neuron subtypes and their approximate incidence of total cutaneous sensory neurons.

**(a)** Low-threshold mechanoreceptors robustly respond to the ramp phase of the stimulated skin. RA, rapidly adapting; SA, slowly adapting.

**(b)** Nociceptors respond primarily to the static phase of the stimulus.

(Modified from Lewin and Moshourab, 2004)

It is therefore possible to classify LTMRs based on their peripheral innervation of distinct morphologically unique end organs, as well as on their characteristic physiological properties. The central afferents of LTMRs also differ from other sensory types in their termination zones in the spinal cord. RA and SA A $\beta$ -LTMRs terminate throughout laminae III to V, A $\delta$ -LTMRs mainly connect with interneurons from lamina III and unmyelinated C-afferents project into lamina II (inner) (Light and Perl, 1979; Li *et al.*, 2011). In contrast, the majority of nociceptive afferents project in the most superficial laminae I and II of the dorsal horn, while proprioceptive projections terminate in laminae VI and XI of the intermediate and ventrolateral gray matter

(Brown, 1982; Chen AI *et al.*, 2006). In analogy to the fine-grained laminar and sublamina segregation patterns of the molecularly defined nociceptor identities, the different subtypes of LTMRs could consequently also terminate in discrete laminar targets (Zylka *et al.*, 2005; Li *et al.*, 2011). Li and colleagues could recently show that the major hair follicle types (guard hair, zigzag hair and awl/auchene hair) are innervated by a unique and invariant combination of LTMRs (Figure 1.9). Strikingly, they could also show a topographical arrangement of the corresponding central afferents in columns, whereby the projections of the different LTMRs innervating the same or adjacent hair follicles terminate within narrow columns in the dorsal horn (Li *et al.*, 2011). The dorsal horn could therefore combine 2000-4000 columns of LTMR units in 3D space that reflect the respective peripheral receptive fields (Li *et al.*, 2011; Arber, 2012). A similar concept has been proposed for nociceptive withdrawal reflex modules (Ladle *et al.*, 2007; Arber, 2012).

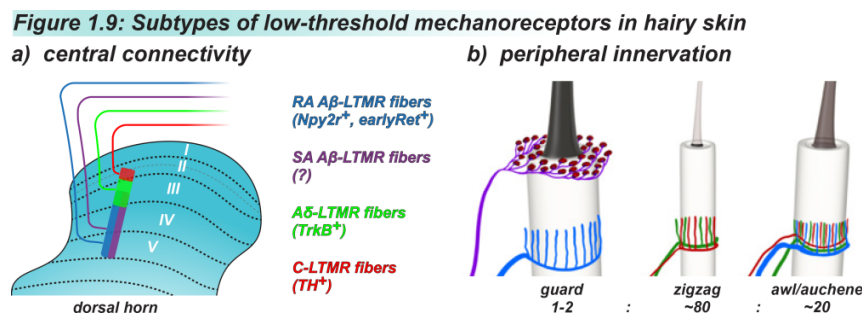


**Figure 1.9: Subtypes of low-threshold mechanoreceptors in hairy skin**

**(a)** Different types of low-threshold mechanoreceptors (LTMRs) innervating the same or adjacent hair follicles form narrow columns in the dorsal horn. The peripheral receptive fields are reflected by a central topographical arrangement in columns. RA, rapidly adapting; SA, slowly adapting; interrogation mark, no specific markers.

**(b)** The major hair follicle types, guard hair, zigzag hair and awl/auchene hair, are innervated by a unique and invariant combination of LTMRs. Merkel cells associated with guard hair are innervated by SA Aβ-LTMRs. The ratio indicates the composition of a peripheral LTMR unit.

(Modified from Li *et al.*, 2011)

Molecularly, at least five unique mechanoreceptive subtypes (Ret<sup>+</sup>/MafA<sup>+</sup>, Ret<sup>+</sup>/MafA<sup>+</sup>/TrkB<sup>+</sup>, Ret<sup>+</sup>/MafA<sup>+</sup>/TrkC<sup>+</sup>, TrkB<sup>+</sup>, Ret<sup>+</sup>/TH<sup>+</sup>) were identified, but their correlation with distinct mechanoreceptive end organs and their central terminations in the spinal cord need to be determined in more detail (Table 1.1) (Bourane *et al.*, 2009; Luo *et al.*, 2009; Honma *et al.*, 2010; Abdo *et al.*, 2011; Heidenreich *et al.*, 2011; Li

*et al.*, 2011; Wende *et al.*, 2012). Further analysis becomes difficult, however, due to the scarcity of available gene expression profiles or specific markers that would help to directly identify the mechanoreceptive subtypes (Ma, 2009; Lallemand and Ernfors, 2012).

Surprisingly, little is known about the establishment of well-defined sensory circuits. Gene programs that direct the sensory subtype specification are likely to control connectivity (Hippenmeyer *et al.*, 2004). It has been shown that key determinants for the establishment of sensory phenotypes like Runx1, Runx3 and Ret also have an impact on the neuron subtype-specific connectivity, presumably by influencing the expression of cell-surface receptors for axon guidance cues (Chen AI *et al.*, 2006; Chen CL *et al.*, 2006; Kramer *et al.*, 2006; Marmigère and Ernfors, 2007; Bourane *et al.*, 2009; Luo *et al.*, 2009). Recent evidence indicates that peripheral target-derived, yet-to-be-identified retrograde signals prompt sensory afferents to project to spatially stereotyped and conserved domains in the spinal cord and hindbrain (Sürmeli *et al.*, 2011). In these confined zones presynaptic sensory axons and postsynaptic interneuron/motor neuron dendrites overlap and form synaptic contacts presumably through the selective interaction of cell-surface signaling cues (Arber, 2012). Axon target finding results therefore from interplay between long-range signaling for modality-specific innervation and attractive and repulsive short-range forces for lamina-specific synaptic connectivity (Chen *et al.*, 2003; Marmigère and Ernfors, 2007). Target-derived neurotrophic factors like NT-3 in muscles and NGF signaling in the dermis are important participants in establishing somatosensory circuits (Patel *et al.*, 2000; Ernfors, 2001; Patel *et al.*, 2003). Another factor is the short-range diffusible chemorepellent Sema3a, which mediates a dorsal discrimination of nociceptive and mechanoreceptive afferents versus ventrally projecting proprioceptive afferents (Messersmith *et al.*, 1995; Pond *et al.*, 2002; Marmigère and Ernfors, 2007). However, the complex and unique wiring of sensory circuits is far from being understood (Arber, 2012). The identification of additional factors and downstream substrates that execute the effects of specification and connectivity would shine a light on the regulatory mechanisms of sensory neurons and bridge the gap between their molecular identity and their precise peripheral and central circuit formation (Liu and Ma, 2011; Lallemand and Ernfors, 2012).

### 1.5. NetrinG-NGL interactions in neuronal circuit formation

Cell adhesion molecules at neuronal synapses regulate diverse aspects of neuronal circuit formation, including axo-dendritic contact establishment, synapse formation and maturation (Woo *et al.*, 2009). The synaptic adhesion molecules NetrinG1 and NetrinG2 appear to be expressed by a subset of large-diameter sensory neurons in postnatal mouse DRGs and are therefore candidate factors in sensory circuit formation (Yin *et al.*, 2002; [www.brain-map.org](http://www.brain-map.org)). These receptors share a similar domain structure with the well-characterized secreted Netrin axon guidance molecule. In contrast to Netrins, NetrinGs are plasma membrane-linked via a Glycosyl-phosphatidyl-inositol (GPI) anchor and display isoform-specific interaction with the NetrinG ligands (NGL) 1 and NGL2, respectively, which are also known as LRRC4C and LRRC4 (Nakashiba *et al.*, 2002; Yin *et al.*, 2002; Niimi *et al.*, 2007; Nishimura-Akiyoshi *et al.*, 2007). NetrinG and NGL homologs are only found in vertebrates and are supposed to be involved in aspects of the nervous system of higher organisms with greater diversity of synapses (Woo *et al.*, 2009). Their multiple splice variants are differentially expressed in mainly non-overlapping neuronal populations in distinct regions of the brain during embryonic and postnatal developmental stages (Nakashiba *et al.*, 2002; Yin *et al.*, 2002; Meerabux *et al.*, 2005; Niimi *et al.*, 2007; Nishimura-Akiyoshi *et al.*, 2007).

NetrinG-NGL interactions have been implicated in the regulation of axonal outgrowth and synaptic differentiation (Nakashiba *et al.*, 2002, Lin *et al.*, 2003; Woo *et al.*, 2009). Transsynaptic NetrinG-NGL adhesion promotes the formation of excitatory, but not inhibitory synapses through recruitment of pre- and postsynaptic proteins like PSD95 and NMDA (Kim *et al.*, 2006; Biederer, 2006; Brose, 2009; Linhoff *et al.*, 2009). A study by Nishimura-Akiyoshi and colleagues associated NetrinG-NGL interactions with lamina-specific segmentation of dendrites (Nishimura-Akiyoshi *et al.*, 2007). Entorhinal cortex axon fibers selectively expressing NetrinG1 terminate on distal dendrites of CA1 pyramidal neurons of the hippocampus, whereas NetrinG2 expressing Schaffer collaterals from CA3 neurons mainly terminate on proximal regions of the CA1 dendrites. Accordingly, NGL1 and NGL2 localize in the distal and proximal dendritic

segments of CA1 pyramidal neurons, respectively (Figure 1.10) (Nishimura-Akiyoshi *et al.*, 2007).

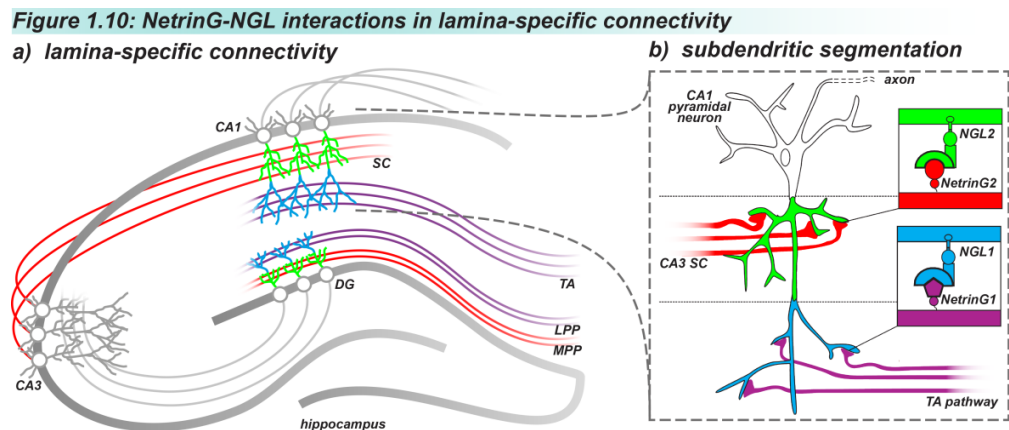


**Figure 1.10: NetrinG-NGL interactions in lamina-specific connectivity**

**(a)** NetrinG1 expressing axons arise from layer III of the entorhinal cortex, project along the temporoammonic (TA) pathway to terminate on distal dendrites of CA1 pyramidal neurons of the hippocampus. Schaffer collaterals (SC) from CA3 neurons express NetrinG2 and terminate on proximal regions of the CA1 dendrites. NetrinG interactions induce a subdendritic segmentation of their ligands NGL1 and NGL2. Dendritic NGL clustering in dentate gyrus (DG) neurons is induced by NetrinG1 and NetrinG2 expressing axons in the lateral and medial perforant paths (LPP and MPP) arising from entorhinal cortex layer II neurons.

**(b)** NetrinG-NGL binding selectivity drives subcellular NGL localization in hippocampal CA1 pyramidal cells.

(Modified from Woo *et al.*, 2009 and Seiradake *et al.*, 2011)

Knockout mice of NetrinG1 and NetrinG2 show a selective dispersal of their ligands. Therefore, it is believed that presynaptic NetrinGs localize and stabilize postsynaptic NGLs in specific segments of contacting dendrites through isoform-specific transneuronal adhesion for further synaptic protein recruitment and input-specific synapse formation (Nishimura-Akiyoshi *et al.*, 2007; Woo *et al.*, 2009; Seiradake *et al.*, 2011). Furthermore, knockout mice revealed the importance of NetrinG-NGL interactions for auditory synaptic responses (Zhang *et al.*, 2008). Whirlin, a direct interaction partner of NGL1, has been detected in stereocilia on the outer surface of hair cells in the cochlear system and has been linked to congenital hearing impairment (Mburu *et al.*, 2003; Delprat *et al.*, 2005). In humans, single nucleotide polymorphism studies associated NetrinGs with schizophrenia, bipolar disorder and a rare cause of

atypical Rett syndrome (Aoki-Suzuki *et al.*, 2005; Borg *et al.*, 2005; Archer *et al.*, 2006; Nectoux *et al.*, 2007; Eastwood and Harrison, 2008; Ohtsuki *et al.*, 2008).

**Figure 1.11: Expression analysis of *NetrinG1* and *NGL1* in vertebrates**

a) mouse P4 *in situ* hybridization

b) hypothesis of dorsal horn innervation

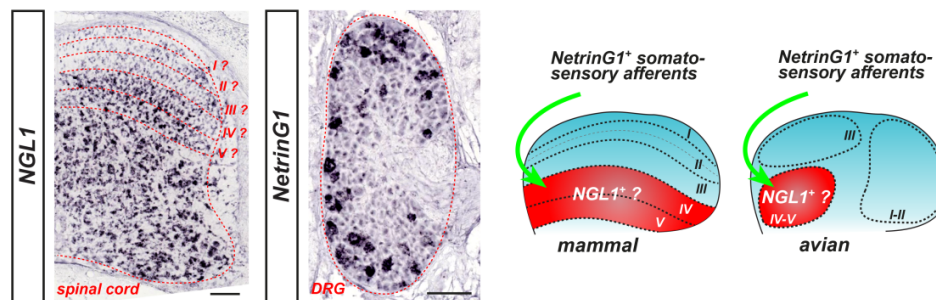


**Figure 1.11: Expression analysis of *NetrinG1* and *NGL1* in vertebrates**

(a) Mouse P4 *in situ* hybridization images from Allen Brain Atlas. *NGL1* mRNA expression in transverse spinal cord sections appears restricted to deeper laminae of the dorsal horn and intermediate and ventral spinal cord, while being excluded from superficial laminae. *NetrinG1* mRNA expression is detected in a scattered subset of large soma size sensory neurons in mouse P4 transverse DRG sections. Numbers indicate presumptive laminae. Scale bar: 100  $\mu$ m.

(b) Hypothesis of selective laminar targeting of *NetrinG1*<sup>+</sup> mechanoreceptive central afferent projections in laminae IV-V presumably expressing *NGL1* in mammals and avians.

(Modified from [www.brain-map.org](http://www.brain-map.org))

In summary, *NetrinG*-*NGL* interactions are short-range cues for axonal and dendritic behavior through bidirectional signaling and have a high impact on axonal outgrowth, lamina-specific dendritic segmentation and synapse formation, whereas deregulation of *NetrinGs*/*NGLs* has been implicated in diverse brain dysfunctions (Nakashiba *et al.*, 2002; Woo *et al.*, 2009). Based on literature and gene expression data bases, *Ntng1* mRNA expression is detected in a scattered subset of large soma size sensory neurons in mouse P4 and P20 DRGs (Yin *et al.*, 2002; [www.brain-map.org](http://www.brain-map.org)). Interestingly, the *Ntng1* ligand *NGL1* is highly expressed in the mouse P4 spinal cord and appears restricted to deeper laminae of the dorsal horn, which could correspond to laminae IV-V, while being excluded from superficial laminae. Consequently, *Ntng1*-*NGL1* interactions might be involved in the establishment of the specific and well-defined sensory connectivity during development (Figure 1.11).

## 1.6. Identification of cis-regulatory elements

Precise control of embryonic development and maintenance of the organism is mediated by a complex interaction network between a limited amount of around 20,000 genes and their products (Alberts *et al.*, 2008; Uchikawa, 2008). The identification of gene regulatory elements (GREs) is thus a first step to decipher the gene control machinery (Maher, 2012). Additionally, lineage-specific GREs can be used as genetic tools for tagging and manipulation of discrete cell types, like sensory neuron subtypes, to study their development and function (Echelard *et al.*, 1994; Marquardt *et al.*, 2001; Lee SK *et al.*, 2004).

In vertebrates, GREs comprise densely clustered TF binding sites which collectively form genomic instructions for the modulation of gene expression and act as switches to turn gene expression on or off (Woolfe *et al.*, 2005; Doh *et al.*, 2007). TFs accumulate to these GREs that can act as enhancers and silencers via specific binding motifs to attract and position the RNA polymerase and additional general TFs to the promoter region for gene activation. This process includes the recruitment of transcriptional co-regulators, mediator complexes, DNA looping and chromatin remodeling for greater DNA access (Blackwood and Kadonaga, 1998; Alberts *et al.*, 2008; Visel *et al.*, 2009). The majority of genes is regulated by complex arrays of enhancers for temporal and spatial expression, so that only when all required TFs are present in a tissue the enhancer becomes active (Alberts *et al.*, 2008; Visel *et al.*, 2009). Furthermore, insulator elements restrict enhancer-promoter interactions to defined chromatin domains (Alberts *et al.*, 2008; Visel *et al.*, 2009). GREs with varying lengths of 50 up to 1500 nucleotides can be located internal to the target gene, as well as up to 1 million base pairs upstream or downstream to the transcription start site, while being able to modulate gene expression independently of their orientation (Khoury and Gruss, 1983; Blackwood and Kadonaga, 1998; Pennacchio *et al.*, 2006; Doh *et al.*, 2007).

Gene coding regions make up a little more than 1% of the human genome, but recent studies revealed that at least 80% of non-coding regions, which were for a long time believed to be evolutionary accumulated 'junk DNA', constitute functional sequences

(Maher, 2012; Pennisi, 2012). However, in the 1970's, it has already been predicted that evolutionary changes in anatomy and way of life are more often based on changes in the mechanisms controlling the expression of genes than on changes in protein-coding sequences (King and Wilson, 1975). Biological trait-differences between humans and chimpanzees, for instance, appear to be primarily due to mutations in GREs (Wray and Babbitt, 2008). This hypothesis has been further corroborated, for instance, by the identification of evolutionary rapid changes of only 13 nucleotide substitutions in a limb-specific enhancer that are thought to have been driven by positive selection and that led to drastic gene expression changes with likely consequences for limb evolution (Prabhakar *et al.*, 2008; Wray and Babbitt, 2008). Additionally, changes in GREs are frequently involved in many disease-relevant processes (Visel *et al.*, 2009; Pennisi, 2012). The identification of enhancers is therefore crucial for the understanding of the immense complexity of organisms, yet the responsible information lays somewhere in the 'infinite deserts' between the genes proper, which complicates their localization (Nobrega *et al.*, 2003; Maher, 2012).

The ENCODE project, including 30 institutes, 440 scientists and the substantial investment of 185 million USD, aims to catalogue functional DNA sequences and their regulation and function in different cell types for a complex understanding of gene control. After almost 10 years of research with state-of-the-art techniques the participating groups uncovered 70,000 promoter and 400,000 distant enhancer regions (Maher, 2012; Pennisi, 2012). In contrast, hypothesis-driven traditional approaches analyze genomic fragments flanking a gene locus of interest for enhancer activity and narrow down the sequence to the functional enhancer (Uchikawa *et al.*, 2003; Lee SK *et al.*, 2004). In this way, Uchikawa and colleagues identified various specific enhancers driving Sox2 expression in different cell types at different developmental stages, respectively (Uchikawa *et al.*, 2003). Interestingly, the enhancers correspond to conserved non-coding regions between different species (Figure 1.12).

GREs important for accurate expression of vital genes experience selective pressure against change and therefore tend to have a high level of sequence conservation across a wide range of different species (Doh *et al.*, 2007). Accordingly, similarities in sequence between highly divergent organisms imply functional constraint (Woolfe



*et al.*, 2005). Comparison of genomic non-coding sequences reveals a full battery of potential regulatory elements and is a powerful filter to prioritize the search for functional activity sequences in vertebrates (Boffelli *et al.*, 2004; Uchikawa *et al.*, 2004; Uchikawa, 2008; Visel *et al.*, 2008). The server-based genomic alignment tool 'ECR Browser' permits fast and automated genome comparison between multiple species which allows pinpointing defined conserved regions as potential GREs within a given genomic locus of interest (Ovcharenko *et al.*, 2004; [ecrbrowser.dcode.org](http://ecrbrowser.dcode.org)).

**Figure 1.12: Enhancer identification via genomic comparison**

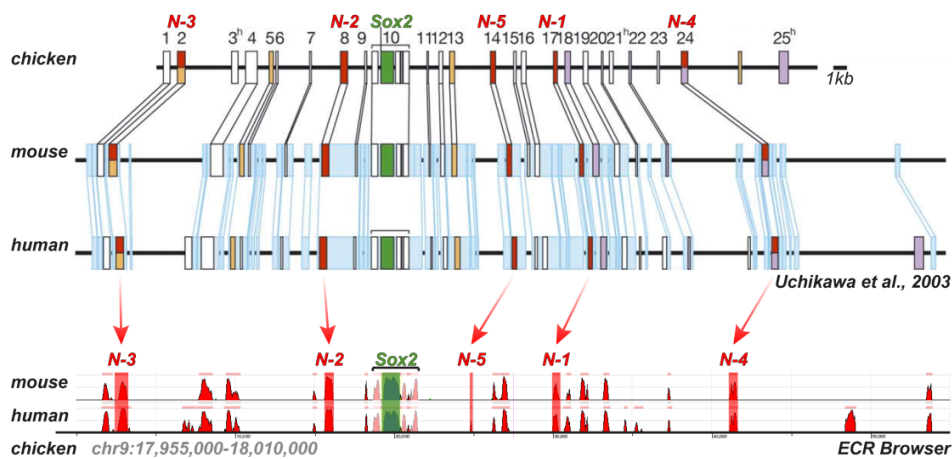


**Figure 1.12: Enhancer identification via genomic comparison**

Genomic comparison between chicken, mouse and human reveals a full battery of evolutionary conserved non-coding regions (1 to 25) in the gene locus of *Sox2*. The enhancers *N-1* to *N-5* driving gene expression in different cell types at different developmental stages correspond to conserved regions. In consequence, these regions can be identified by the genomic alignment tool 'ECR Browser'.

(Modified from Uchikawa *et al.*, 2003 and [ecrbrowser.dcode.org](http://ecrbrowser.dcode.org))

The identification of enhancers that are capable of driving transcription in specific cells or tissues by combining bioinformatics and experimental tests provides extremely powerful tools for a variety of studies (Timmer *et al.*, 2001; Wray and Babbitt, 2008). Sensory neuron subtype-specific enhancers would facilitate the analysis of the development, function and connectivity of distinct sensory lineages for a better understanding of how the complex somatosensory circuitries develop and function, and how they detect and transduce sensory information (Lallemend and Ernfors, 2012).

### 1.7. Aim of the study

Despite its decisive importance in somatosensory perception, the relationship between sensory modality, neuronal identity and the stereotypic connectivity of primary sensory neurons remains unclear (Arber, 2012). The available information regarding the mechanisms of molecular specification, precise connectivity and transduction of the many physiologically and morphologically defined sensory neuron subclasses that collectively relay mechanosensory input, is limited due to the lack of available molecular markers (Lumpkin and Caterina, 2007; Marmigère and Ernfors, 2007; Bourane *et al.*, 2009; Luo *et al.*, 2009; Ma, 2009; Lallemand and Ernfors, 2012).

The development of genetic tools for tagging and manipulation of discrete neuronal populations initiated a methodological revolution in virtually all areas of neurobiology (Zhang *et al.*, 2007; Lichtman and Sanes, 2008; Goulding, 2009; O'Conner *et al.*, 2009). In mouse, for instance, gene targeting and bacterial artificial chromosome transgenesis have led to the molecular identification of discrete sensory neuron subtypes and circuitries by mapping of their developmental lineage (Mombaerts, 1996; Zylka *et al.*, 2005; Kim *et al.*, 2008; Bourane *et al.*, 2009; Luo *et al.*, 2009; Chandrashekar *et al.*, 2010). An alternative approach is the selective screen of candidate gene activities putatively linked to given neuronal identities based on data mapped by individual researchers or public gene expression catalogues (Yin *et al.*, 2002; Alvarez-Bolado and Eichele, 2006; Jones *et al.*, 2009). This information can be used to isolate individual gene regulatory elements (GREs) of the candidate genes, to generate transgenic animals in which, hopefully, the desired neuronal population is labeled (Uchikawa *et al.*, 2003; Boffelli *et al.*, 2004; Ovcharenko *et al.*, 2004; Visel *et al.*, 2008). Therefore, the combination of gene expression database screening with GRE identification via genomic comparison between multiple species can potentially reveal sensory subtype-specific enhancers that, in turn, facilitate the analysis of the development, function and connectivity of distinct sensory lineages.

Rodent transgenic studies, however, implicate high costs, resource-intensiveness and time-consuming generations that can be prohibitive to individual researchers for performing neuron subtype-specific GRE screens on a larger basis (Timmer *et al.*,

2001). As a complementary model system, the straightforward and rapid *in vivo* transfection procedures developed in the chick (*Gallus gallus domesticus*) permit accelerated development of neuron subtype-specific genetic tools and have been proven extremely powerful for uncovering regulatory principles involved in early neural development of both avians and mammals (Novitsch *et al.*, 2001; Thaler *et al.*, 2002; Dasen *et al.*, 2005). The chicken is expected to share many features of developmental regulation and shows extensive homology in nervous system organization with mammals, indicating universal conserved gene regulatory mechanisms among vertebrates (Muramatsu *et al.*, 1997; Lee SK *et al.*, 2004; Uchikawa, 2008). Especially circuits involved in somatosensory perception, including morphologically and physiologically identified sensory neurons and their connectivity patterns, are highly conserved between birds and mammals (Necker, 1985; Necker, 1990; Woodbury and Scott, 1991; Duc *et al.*, 1993; Eide and Glover, 1997; Koltzenburg and Lewin, 1997; Guo *et al.*, 2011). Therefore, the *in ovo* electroporation approach greatly facilitates the study of sensory neuron specification and connectivity in vertebrates.

The initial aim of this work was the identification of genetic markers for distinct sensory subtypes by candidate gene screening and GRE identification via genomic comparison, combined with the establishment of an enhancer activity analysis assay in late-gestation chick embryos. Ultimately, the aim of this work was to evaluate and characterize the potential role of candidate genes in the function and circuit formation of distinct sensory lineages in the chick. The discovery of more restricted genetic markers provides more profound knowledge regarding the sensory system organization and function by linking molecularly identified neuronal subtypes with their preferred sensory modality and their peripheral and central connectivity, which together will allow uncovering of the neural substrates of somatosensation, including touch perception.

## 2. Materials and methods

### 2.1. Laboratory consumables and plastic ware

Consumables and plastic ware were purchased from Eppendorf AG, Starlab GmbH and Sarstedt AG. Dissection instruments were obtained from Fine Science Tools GmbH.

#### 2.1.1. Antibodies

##### Primary antibodies

Antigen	Host	Dilution	Code	Supplier
TrkA	Rabbit	1:2000		Gift from F. Lefcort
TrkB	Rabbit	1:2000		Gift from F. Lefcort
TrkC	Rabbit	1:2000		Gift from F. Lefcort
Sox10	Guinea Pig	1:1000		Gift from M. Wegner
NGL1	Mouse	1:50	Q9HCJ2	UC Davis/NIH NeuroMab Facility
Ntng1	Rabbit	1:200	H-55	Santa Cruz Biotechnology GmbH
Ret	Goat	1:200	C-19	Santa Cruz Biotechnology GmbH
NeuN	Mouse	1:1000	MAB377	Merck Millipore GmbH
TH	Rabbit	1:1000	657012	Merck Millipore GmbH
Tuj1 / βIII-tubulin	Mouse	1:2000	MMS- 435P	Covance GmbH
NF200	Mouse	1:2000	N0142	Sigma-Aldrich Chemie GmbH
NF (160 kDa)	Mouse	1:200	4H6	Developmental Studies Hybridoma Bank
Isl1/2	Mouse	1:200	39.4D5	Developmental Studies Hybridoma Bank
Lmx1b	Mouse	1:50	50.5A5	Developmental Studies Hybridoma Bank
MF20	Mouse	1:200	MF 20	Developmental Studies Hybridoma Bank
FLAG epitope	Mouse	1:1000	F3165	Sigma-Aldrich Chemie GmbH

GFP	Rabbit	1:2000	A-11122	Life Technologies GmbH
GFP	Sheep	1:2000	4745-1051	AbD Serotec MorphoSys AbD GmbH
$\alpha$ -Bungarotoxin	<i>Bungarus</i>	1:5000	B-35450	Life Technologies GmbH
Alexa Fluor 647 conjugate	<i>multicinctus</i> toxin			
Alexa Fluor 555	<i>Amanita</i>	1:100	A34055	Life Technologies GmbH
Phalloidin	<i>phalloides</i> toxin			

### Secondary antibodies

Target	Conjugate	Host	Dilution	Supplier
Mouse	Alexa fluorescent dye	Donkey	1:2000	Life Technologies GmbH
Rabbit	Alexa fluorescent dye	Donkey	1:2000	Life Technologies GmbH
Goat	Alexa fluorescent dye	Donkey	1:2000	Life Technologies GmbH
Sheep	Alexa fluorescent dye	Donkey	1:2000	Life Technologies GmbH
Guinea Pig	Alexa fluorescent dye	Donkey	1:500	Jackson ImmunoResearch Laboratories

### 2.1.2. Enzymes

Enzyme	Supplier
DNA Ligation Kit	Takara Bio Inc
Dream Taq DNA Polymerase	Thermo Fisher Scientific GmbH
Phusion High Fidelity DNA Polymerase	New England Biolabs GmbH
Platinum Taq DNA Polymerase High Fidelity	Life Technologies GmbH
Restriction enzymes	Thermo Fisher Scientific GmbH
Shrimp Alkaline Phosphatase	Thermo Fisher Scientific GmbH
SP6 RNA Polymerase	Roche Diagnostics GmbH
T4 DNA Ligase	Thermo Fisher Scientific GmbH
T4 Polynucleotide Kinase	Thermo Fisher Scientific GmbH
T7 RNA Polymerase	Roche Diagnostics GmbH

**2.1.3. Kits**

Kit	Supplier
iScript cDNA synthesis Kit	Bio-Rad Laboratories GmbH
PrimeScript First Strand cDNA Synthesis Kit	Takara Bio Inc
QIAGEN Plasmid Maxi Kit	Qiagen GmbH
QIAprep Spin Miniprep Kit	Qiagen GmbH
QIAquick Gel Extraction Kit	Qiagen GmbH
TOPO TA Cloning Kit	Life Technologies GmbH

**2.1.4. Chemicals and reagents**

Chemical	Supplier
Agar-Agar	Carl Roth GmbH
Agarose NEE0	Carl Roth GmbH
Ampicillin	Carl Roth GmbH
B-27 supplement	Life Technologies GmbH
BDNF	R&D Systems Inc
Benzyl alcohol	Carl Roth GmbH
Benzyl benzoate	Sigma-Aldrich Chemie GmbH
Blocking reagent	Roche Diagnostics GmbH
Bovine serum albumin fraction V (BSA)	Carl Roth GmbH
Calcium chloride	Carl Roth GmbH
D-PBS pH 7.2	Life Technologies GmbH
Diethylpyrocarbonate (DEPC)	Carl Roth GmbH
DIG RNA labeling mix	Roche Diagnostics GmbH
Dimethyl sulfoxide (DMSO)	Sigma-Aldrich Chemie GmbH
DMEM-F12	Life Technologies GmbH
DNA Ladder GeneRuler 1kb	Thermo Fisher Scientific GmbH
DNA loading dye 6x	Thermo Fisher Scientific GmbH
dNTP Mix	Thermo Fisher Scientific GmbH
Ethanol 99.9%	Carl Roth GmbH

Ethidium bromide solution 1%	Carl Roth GmbH
Ethylenediaminetetraacetic acid (EDTA)	Carl Roth GmbH
Ethyleneglycoltetraacetic acid (EGTA)	Carl Roth GmbH
Formamide	AppliChem GmbH
GDNF	R&D Systems Inc
Glucose	Sigma-Aldrich Chemie GmbH
Glycerol	Carl Roth GmbH
HEPES	Carl Roth GmbH
Isopropanol	Carl Roth GmbH
Horse serum	Life Technologies GmbH
Hydrochloric acid	Carl Roth GmbH
Hydrogen peroxide	AppliChem GmbH
L-15 medium Leibowitz	Sigma-Aldrich Chemie GmbH
L-Glutamic acid	Sigma-Aldrich Chemie GmbH
L-Glutamine	Life Technologies GmbH
Laminin	Life Technologies GmbH
Magnesium chloride	Carl Roth GmbH
Maleic acid	Carl Roth GmbH
Methanol	Carl Roth GmbH
NBT/BCIP tablets	Roche Diagnostics GmbH
Neurobasal medium	Life Technologies GmbH
NGF	R&D Systems Inc
NT-3	R&D Systems Inc
OCT embedding medium	Sakura Finetek GmbH
Paraformaldehyde (PFA)	Carl Roth GmbH
PBS pH 7.2	Life Technologies GmbH
Penicillin-Streptomycin	Life Technologies GmbH
Poly-D-Lysine	Merck Millipore GmbH
Poly-L-Lysine	Sigma-Aldrich Chemie GmbH
Polyacrylamide	Carl Roth GmbH
Potassium chloride	Carl Roth GmbH
Potassium hydroxide	Carl Roth GmbH

Proteinase K	AppliChem GmbH
Salmon sperm DNA	AppliChem GmbH
Sodium chloride	Carl Roth GmbH
Sodium citrate	Carl Roth GmbH
Sodium dodecyl sulfate (SDS)	Carl Roth GmbH
Sodium hydroxide	Carl Roth GmbH
Sucrose	Carl Roth GmbH
Tris	Carl Roth GmbH
Triton X-100	Carl Roth GmbH
TRIzol reagent	Life Technologies GmbH
Trypsin	Life Technologies GmbH
Tryptone	Carl Roth GmbH
Tween-20	Carl Roth GmbH
Yeast extract	AppliChem GmbH

### 2.1.5. Solutions

Solution	Contents
Antibody staining solution	PBS pH 7.2; 1% BSA; 1% Triton X-100
BABB clearing solution	66% Benzyl benzoate; 34% Benzyl alcohol
Culture medium	Neurobasal medium; 1x B-27, 0.5 mM L-Glutamic acid; 25 mM L-Glutamine; 1x Penicillin-Streptomycin
Dent's solution	80% Methanol; 20% DMSO
Growth factor solution	PBS pH 7.2; 100 µg/ml growth factor
Growth medium	DMEM-F12; 2 µM L-Glutamine; 8 mg/ml Glucose, 2x Penicillin-Streptomycin; 5% horse serum
<i>In situ</i> blocking buffer	MBST pH 7.5; 2% [w/v] Blocking reagent
<i>In situ</i> hybridization buffer	50% Formamide; SSC 5x pH 4.5; 1% SDS; 10 mg/ml Heparin; 10 mg/ml salmon sperm DNA
<i>In situ</i> wash buffer I	50% Formamide; SSC 5x pH 4.5
<i>In situ</i> wash buffer II	50% Formamide; SSC 2x pH 4.5
<i>In situ</i> wash buffer III	50% Formamide; SSC 1x pH 4.5



Laminin solution	D-PBS pH7.2; 1 mg/ml Laminin
LB agar	LB medium; 1% [w/v] Agar-Agar
LB medium	5 g/l Sodium chloride; 5 g/l Yeast extract; 10 g/l Tryptone
Lysis buffer	0.1 M Tris pH 8; 30 nM Sodium chloride; 0.2 mM EDTA; 0.05% SDS; 0.5 mg/ml Proteinase K
MBST	0.1 M Maleic acid; 0.15 M Sodium chloride; pH 7.5
Mounting solution	PBS pH 7.2; 50% Glycerol
NTMT	100 mM Sodium chloride; 10 mM Tris-Hydrochloric acid; 50 mM Magnesium chloride; pH 9.5
PBST	PBS pH 7.2; 0.1% Tween-20
PFA solution	PBS pH 7.2; 4% [w/v] Paraformaldehyde
PFA culture solution	PBS pH 7.2; 2% [w/v] Paraformaldehyde; 15% [w/v] Sucrose
SSC 20x solution	3 M Sodium chloride; 300 mM Sodium citrate; pH 4.5
Sucrose solution	PBS pH 7.2; 30% [w/v] Sucrose
TAE buffer	40 mM Tris; 1 mM EDTA adjust pH 7.5 with glacial acetic acid

### 2.1.6. Vectors

Plasmid	Supplier
<i>pCAG-loxP-ssFlag-IRES-mGFP-Tol2</i>	Workgroup Marquardt
<i>pCAG-loxP-ssFlag-IRES-tdTomato-Tol2</i>	Workgroup Marquardt
<i>pCAG-mGFP</i>	Addgene Inc
<i>pCAGGS-T2TP</i>	Gift from K. Kawakami (Sato <i>et al.</i> , 2007)
<i>pCRII-TOPO</i>	Life Technologies GmbH
<i>pGATA2V2X2</i>	Gift from S. K. Lee (Zhou <i>et al.</i> , 2000)
<i>pPGK-Cre-bpA</i>	Addgene Inc
<i>pT2KXIGΔin</i>	Gift from K. Kawakami (Sato <i>et al.</i> , 2007)
<i>pUC18</i>	Thermo Fisher Scientific GmbH

**2.1.7. Software**

Software	Supplier
Adobe Creative Suite CS5	Adobe Systems Inc
Chromas	Technelysium Pty Ltd
ECR Browser	<a href="http://ecrbrowser.dcode.org/">ecrbrowser.dcode.org/</a>
ImageJ	<a href="http://rsbweb.nih.gov/ij/">rsbweb.nih.gov/ij/</a>
Microsoft Office 2010	Microsoft Corp
pDraw	Acaclone Inc

**2.2. Molecular biology**

The methods described were performed according to 'Molecular cloning: a laboratory manual' (Sambrook and Russell, 2001) unless otherwise stated.

**2.2.1. Polymerase chain reaction**

The amplification of DNA fragments was performed with the Platinum Taq DNA Polymerase High Fidelity, the Phusion High Fidelity DNA Polymerase or the Dream Taq DNA Polymerase using the Mastercycler epGradient S (Eppendorf AG). The reaction mixture and the PCR program were used according to the manufacturer's protocols. Amplified DNA fragments were analyzed via agarose gel electrophoresis.

**2.2.2. DNA restriction digest**

The digestion of DNA was performed by the use of appropriate restriction enzymes (Thermo Fisher Scientific GmbH). The DNA was incubated with the enzymes and the reaction buffers at optimal reaction temperatures recommended by the manufacturer's reference for at least 3 h. Double digestions were carried out with reaction buffers enabling maximal enzyme activity for both endonucleases. Alternatively the digested DNA was purified with the QIAquick Gel Extraction Kit (Qiagen GmbH) before the second restriction digest.

### **2.2.3. Alkaline phosphatase treatment**

In order to prevent religation, the vector DNA was dephosphorylated by adding Shrimp Alkaline Phosphatase (Thermo Fisher Scientific GmbH) to the completed restriction digest of the vector DNA and incubation for 30 min at 37°C.

### **2.2.4. Agarose gel electrophoresis**

The separation of DNA fragments was performed by agarose gel electrophoresis. Therefore 1% [w/v] agarose was dissolved in TAE buffer by heating, followed by adding 0.05 µl/ml of ethidium bromide solution and transferring in a gel tray. After solidification, the gel was inserted into a gel chamber covered with TAE buffer, the DNA samples were mixed with DNA loading dye and loaded into the gel pockets. The electrical current was applied until a conclusive segregation of the DNA fragments was achieved.

### **2.2.5. DNA purification from agarose gels**

After the agarose gel electrophoresis, DNA bands were visualized under UV light illumination and the appropriate DNA fragments were extracted from the agarose gel. They were purified by using the QIAquick Gel Extraction Kit (Qiagen GmbH) according to the manufacturer's instructions.

### **2.2.6. DNA ligation**

The ligation mixture of digested vector and insert DNA fragments was prepared with a molar concentration ratio of 1:4. Therefore, the DNA concentrations were determined and incubated with T4 DNA Ligase and the appropriate buffer (Thermo Fisher Scientific GmbH) at 22°C for at least 6 h or with the DNA Ligation Kit (Takara Bio Inc) at 16°C for at least 4 h. For PCR products with low concentrations, the TOPO TA Cloning Kit (Life Technologies GmbH) was used according to the manufacturer's instructions.

### 2.2.7. Plasmid preparation

Single bacteria colonies were picked from agar plates and incubated in 5 ml LB medium containing ampicillin overnight at 37°C. A plasmid miniprep was performed using the QIAprep Spin Miniprep Kit (Qiagen GmbH) due to the manufacturer's instructions. Positive clones were verified via restriction digest and sequencing. For a plasmid maxiprep, the *E.coli* culture was grown from 100 µl of a glycerol stock in 200 ml LB medium with ampicillin overnight at 37°C and the plasmid DNA was extracted with the QIAGEN Plasmid Maxi Kit according to the manufacturer's manual.

### 2.2.8. DNA concentration measurements

The DNA and RNA concentration was determined using the Nanodrop 1000 UV-Vis Spectrophotometer (Thermo Fisher Scientific GmbH) based on UV light absorption of the nucleic acids at definitive wave lengths.

### 2.2.9. Sequencing

DNA sequencing was carried out by the Qiagen genomic services (Qiagen GmbH). DNA samples were submitted in a concentration of 500 ng per reaction. Only plasmids with strictly accurate sequences were used for further experiments.

### 2.2.10. Preparation of chemically competent *E.coli*

Chemically competent *E.coli* cells of the One Shot TOP10 strain (Life Technologies GmbH) were used for all molecular cloning experiments. The preparation was performed according to Inoue *et al.* (Inoue *et al.*, 1990) and stored at -80°C until use.

### 2.2.11. Transformation

Chemically competent *E.coli* were transformed by adding of 100 µl of the soluble cell suspension to the ligation mixture. After 30 min of incubation on ice, the cells were heat shocked at 42°C for 1 min and chilled on ice afterwards. *E.coli* were grown in 1 ml

of antibiotic-free LB medium at 37°C for one hour on a shaker and plated on an agar plate containing ampicillin. The plates were incubated overnight at 37°C.

#### **2.2.12. Preservation and recovery of *E.coli***

The preservation of the *E.coli* clones was performed by mixing 500 µl of soluble *E.coli* culture with 500 µl glycerol in a reaction tube and storing of the mixture at -80°C. For regrowing, 100 µl of the frozen *E.coli* stocks were incubated in 5 ml LB medium with ampicillin for a plasmid minipreparation or in 150 ml LB medium with ampicillin for a plasmid maxipreparation overnight at 37°C.

#### **2.2.13. DNA extraction**

Genomic DNA of mouse and chicken for enhancer amplification was extracted from mouse tail tip biopsies and whole chicken embryo of embryonic day 4 (E4) by incubation in lysis buffer overnight at 56°C. The lysate was cleared by centrifugation and the supernatant was mixed with 500 µl isopropanol. After centrifugation, the DNA pellet was washed with 500 µl 70% ethanol, air dried and eluted in water.

#### **2.2.14. RNA extraction**

Total RNA from mouse spinal cords and dorsal root ganglia (DRGs) from embryonic day 18.5 (E18.5) and chicken DRGs from embryonic day 12 (E12) was obtained via TRIzol isolation. The tissue was homogenized in 1 ml TRIzol reagent per 100 mg of tissue and incubated for 5 min. The samples were incubated with 0.2 ml chloroform per 1 ml TRIzol for 3 min and centrifuged for 15 min at 4°C. The aqueous phase containing the RNA was removed, transferred into a new reaction tube and incubated with 0.5 ml isopropanol per 1 ml of TRIzol and 3 µl of polyacrylamide for 10 min. After centrifugation for 15 min at 4°C, the supernatant was removed and the RNA pellet was washed with 1 ml 75% DEPC-ethanol. The samples were centrifuged, air dried and eluted in DEPC-H<sub>2</sub>O.

### 2.2.15. cDNA synthesis

The cDNA for the gene amplification and the *in situ* probe generation was synthesized using the iScript cDNA synthesis Kit (Bio-Rad Laboratories GmbH) or the PrimeScript First Strand cDNA Synthesis Kit (Takara Bio Inc) according to the manufacturer's instructions.

### 2.3. Plasmid construction

The plasmid *pSTEVE* was designed for reporter gene-based screening of cis-regulatory activities, combined with *Tol2* transposon-based transgenesis facilitating genomic integration upon *in ovo* electroporation (Kawakami and Shima, 1999; Sato *et al.*, 2007; Takahashi *et al.*, 2008). The plasmid *pSTEVE-eGFP* was constructed by insertion of the *Tol2* sites from *pT2KXIGΔin* vector in the *pUC18* vector, followed by insertion of a minimal *TATA box* promoter and *eGFP* from *pGATA2V2X2* between the *Tol2* sites. The *eGFP* reporter gene was replaced by the *mGFP* gene from *pCAG-mGFP* to generate *pSTEVE-mGFP*. The putative enhancers were subcloned upstream of the minimal promoter which do not drive a reporter gene expression without an additional enhancer. *Isl1<sup>Crest3</sup>* was amplified from mouse genomic DNA with following primers: 5'-TAAAAGAGCAAACACTACAGC-3' and 5'-AATAGTGTCTTGGCATC-3'. *Avil<sup>Lucy1</sup>* was amplified from mouse genomic DNA with following primers: 5'-GGGAATTGGAGGCTCCTG-3' and 5'-ACCCTCTGTCCTCCGAAGT-3'. *Ntn1<sup>Mech1</sup>* was amplified from chick genomic DNA with following primers: 5'-GATCCTTAATGTGCTTTGGT-3' and 5'-AGTCATAATGATGGTCGT-3'. *TrkA<sup>ECR1</sup>* was amplified from mouse genomic DNA with following primers: 5'-GCTCGCCTTCCTAATGTC-3' and 5'-CTCAGGATGCTTAGTGGGT-3'. *Runx3<sup>ECR1</sup>* was amplified from mouse genomic DNA with following primers: 5'-TAATAAATGGCCCGAGAA-3' and 5'-CACTCCCTCATTGACAGC-3'. *Runx3<sup>ECR2</sup>* was amplified from mouse genomic DNA with following primers: 5'-TTGTGTACCAGACAGGAGCA-3' and 5'-CCACTCTCTGCTGCCTCTAA-3'. *Runx3<sup>ECR3</sup>* was amplified from mouse genomic DNA with following primers: 5'-CAGTCGGCTGGACCTGAA-3' and

5'-TTGCTGCCCTTGACCTTT-3'. The *CMV early enhancer / chicken  $\beta$ -actin (CAG) promoter* was cut out from *pCAG-mGFP* via the *XbaI* and *SpeI* restriction sites. The created plasmids were verified via sequencing. *pSTEVE-eGFP* was used to visualize the cell somata of electroporated (dorsal root ganglion) DRG neurons, and *pSTEVE-mGFP* to trace sensory axons. The transposase in the *pCAGGS-T2TP* was co-electroporated for a stable genetic integration in the transfected cells (Figure 2.1).

**Figure 2.1: Plasmid construction for enhancer activity analysis**

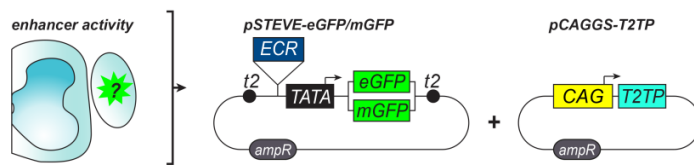


**Figure 2.1: Plasmid construction for enhancer activity analysis**

For the enhancer activity analysis, the ECRs were subcloned upstream of the minimal promoter driving the reporter gene *eGFP* or *mGFP*. Co-electroporation with the transposase (*pCAGGS-T2TP* vector) enables stable integration of the fragment between the *Tol2* sites (*t2*) into the genome of transfected cells.

For overexpression of *Ntng1* selectively in sensory neurons and the ligand *NGL1* in the entire spinal cord, the *Cre/loxP* system was used to combine a high expression level of the gene with maintaining the specificity in sensory neurons or the spinal cord (Livet *et al.*, 2007). Therefore the *pCAG-loxP-ssFlag-IRES-mGFP/tdTomato-Tol2* vector was designed consisting of six essential parts: the strong ubiquitous *CAG* promoter (1), the *loxP-STOP-loxP* cassette (2) for *Cre* recombination, followed by a signal sequence (3), which is necessary for the secretion pathway and a cellular membrane insertion, an *Flag* epitope tag (4) upstream of the gene insertion sites for protein detection and reporter genes *IRES-mGFP* or *IRES-tdTomato* (5). The expression cassette was flanked by *Tol2* sites (6) for transposase-mediated stable genomic integration.

The *Ntng1* coding sequence without its signal sequence was amplified from cDNA of mouse embryonic day 18.5 (E18.5) DRGs and inserted downstream of the *Flag* tag peptide sequence into the *pCAG-loxP-ssFlag-IRES-mGFP-Tol2* construct. The following primers were used: 5'-GTGATGCAGCCCTACCTTTTCG-3' and 5'-CTAGAACACCAGGGGACCGGCA-3'. The *NGL1* coding sequence without its signal sequence was amplified from cDNA of mouse embryonic day 18.5 (E18.5)

spinal cord and inserted downstream of the Flag tag peptide sequence into the *pCAG-loxP-ssFlag-IRES-tdTomato-Tol2* construct. The following primers were used: 5'-CAAACCTGCCCTTCAGTGTGCT-3' and 5'-TTATATCTGAGTCTCTTGTACA-3'. The sensory-specific *pIsl1<sup>Crest3</sup>-Cre* driver plasmid was created by insertion of a minimal *TATA box* promoter and *eGFP* from *pGATA2V2X2* in the *pUC18* vector, following the replacement of the *eGFP* gene by the *Cre* gene from the *pPGK-Cre-bpA* vector and insertion of the *Isl1<sup>Crest3</sup>* enhancer upstream of the minimal promoter. For the expression of NGL1 in the spinal cord, the constitutive *pPGK-Cre-bpA* vector was used. The final plasmids were verified via sequencing. The transposase in the *pCAGGS-T2TP* was co-electroporated for a stable genetic integration in the transfected cells (Figure 2.2).

**Figure 2.2: Plasmid construction for transgene expression analysis**

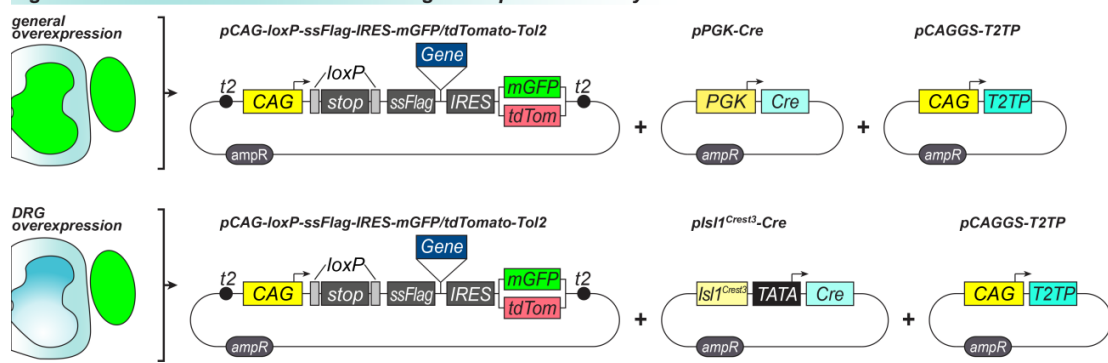


**Figure 2.2: Plasmid construction for transgene expression analysis**

For overexpression of NGL1 in the spinal cord, the gene was cloned into the expression vector and co-electroporated with the general *Cre* driver (*pPGK-Cre*) and the transposase for stable genomic integration. Overexpression of Ntng1 was achieved by subcloning of the gene coding sequence into the expression vector and co-electroporation with the sensory-specific *pIsl1<sup>Crest3</sup>-Cre* driver and the transposase for stable genomic integration.

#### 2.4. *In ovo* electroporation

Fertilized chick eggs (Horstmann Geflügelzucht GmbH) were incubated at 38°C and 80% humidity. The *in ovo* electroporation of DNA constructs was performed between Hamburger-Hamilton (HH) stages 11 and 13 (embryonic day 2 - 2.2) using the ECM 830 electroporation system (BTX Instrument Division, Harvard Apparatus Inc) with



following settings: 5 pulses of 25 mV for 50 ms in the LV 99 ms/500 V modus. All plasmids were injected into the central canal of the neural tube at final concentrations of 1.5 µg/µl in TE in a 4:1 mixture with the *pCAGGS-T2TP* plasmid. For overexpression the molar ratio for expression vector, Cre driver vector and transposase vector was 2:1:1. in the chick (embryonic day 2 - 2.2). Electroporated embryos were incubated until appropriate embryonic stages. All animal work has been conducted according to national and international guidelines.

## 2.5. Immunohistochemistry

Chicken spinal cords with attached dorsal root ganglia (DRGs), as well as hindlimbs and digits were dissected at appropriate developmental stages, fixed at 4°C in PFA solution, washed in PBS, immersed in sucrose solution and embedded into OCT embedding medium according to the incubation timeline (Table 2.1). 60 µm transversal cryosections were cut in a CM1900 cryostat (Leica Microsystems GmbH) at -20°C, placed on a super frost glass slide and stored at -20°C. For primary antibody detection the slides were washed three times for 30 min with PBS and incubated overnight at 4°C in staining solution. Slides were washed three times for 30 min with PBS and stained with secondary antibody solution for 1 h at room temperature. The slides were washed with PBS, mounted with mounting solution and cover slipped.

**Table 2.1: Incubation timeline for chicken embryos**

	<i>E4</i>	<i>E5</i>	<i>E6</i>	<i>E7</i>	<i>E9</i>	<i>E12</i>	<i>E15</i>	<i>E19</i>
<i>PFA</i>	1 h	1.5 h	2 h	3 h	4 h	6 h	10 h	15 h
<i>PBS</i>	5 h	6 h	7 h	8 h	10 h	12 h	15 h	20 h
<i>Sucrose</i>	3 h	4 h	5 h	6 h	7 h	8 h	10 h	15 h

**Table 2.1: Incubation timeline for chicken embryos**

For immunohistochemistry, chicken embryos at different developmental stages were successively treated with PFA, PBS and Sucrose according to the incubation timeline.

Whole mounts of embryonic day 5 (E5), whole hindlimbs of embryonic day 9 (E9) and whole digits of embryonic day 15 (E15) were fixed in PFA solution for 5 h, washed in PBS overnight, bleached with Dent's solution for 5 h, rehydrated in PBST overnight

and incubated in primary antibody solution for 4 days. The limbs were washed in PBST overnight, incubated in secondary antibody solution for 4 days, washed in PBST overnight, immersed in a graded series of methanol solution up to 100% and cleared with BABB solution. All steps were carried out at 4°C.

## 2.6. *In situ* hybridization

The *in situ* hybridization probe for the chicken Ntng1 coding sequence was generated by PCR amplification of a 654 bp fragment from cDNA of chicken embryonic day 9 (E9) dorsal root ganglia (DRGs) by the use of following primers: 5'-ATGATGTATTTGTCGAGATTTCT-3' and 5'-ACTGTTTGTTCATATATCCAG-3'. The probe was T/A subcloned into the *pCRII-TOPO* vector and verified via sequencing. The antisense RNA probe was synthesized by the T7 or Sp6 RNA polymerase using the DIG RNA labeling Kit according to the manufacturer's specifications. The quality and quantity was verified.

Chicken spinal cords with attached DRGs at different developmental stages were dissected, collected in D-PBS, fixed in PFA solution for 48 h, washed in D-PBS for 24 h and dehydrated in 30% sucrose solution. All steps were carried out at 4°C. The samples were embedded into OCT embedding medium, cryosectioned at 12 µm in a CM1900 cryostat (Leica Microsystems GmbH) at -20°C and placed on a super frost glass slide.

For the *in situ* hybridization, the slides were washed with D-PBS for 3 min, dehydrated in a graded series of methanol in D-PBS and stored in 100% methanol at -20°C overnight. The samples were rehydrated through methanol in D-PBS series for 5 min, bleached in 6% hydrogen peroxide in D-PBS and washed three times in D-PBS for 5 min. The sections were treated with 10 µg/ml Proteinase K in D-PBS for 10 min, washed with D-PBS and postfixed with PFA solution for 5 min. They were washed with D-PBS for 5 min and 0.85% NaCl in D-PBS, followed by dehydration through graded series of ethanol solutions for 10 min and air drying. The samples were transferred in a

humidified chamber containing *in situ* wash buffer I and prehybridized with *in situ* hybridization buffer for one hour at 68°C. The slides were treated with *in situ* hybridization buffer containing 500 ng/ml of the DIG-labeled antisense RNA probe, covered with parafilm and incubated overnight at 68°C. After hybridization, the parafilm was removed and the samples were immersed in *in situ* wash buffer I-III at 65°C for 30 min. The slides were washed two times with MBST at 70°C for 30 min and three times with MBST at room temperature for 5 min, before they were treated with *in situ* blocking buffer at room temperature for one hour. The samples were transferred in a humidified chamber containing water and incubated with 1:2500 diluted anti-digoxigenin alkaline phosphatase conjugated antibody in *in situ* blocking buffer overnight at 4°C. The slides were washed three times with MBST for 5 min and treated with NTMT for 10 min. The *in situ* signal was developed by incubation in NBT/BCIP dissolved in water at room temperature, followed by washing with D-PBS and mounting with mounting solution.

## 2.7. Cell culture

For the DRG explant culture assay, transfected embryonic day 6 (E6) chicken dorsal root ganglia (DRGs) from lumbar spinal segments were dissected, collected in culture medium on ice and transferred in a four-well plate on a glass coverslip precoated with 1 mg/ml Poly-D-Lysine and 100 µg/ml Laminin (Wang and Marquardt, 2012). BDNF, GDNF, NGF or NT-3 growth factor medium was added to the culture medium and the plate was transferred into the incubator overnight.

For immunohistochemistry, the explant samples were fixed by adding the equal amount of PFA culture solution to the culture medium for 30 min. After removing the top phase of the solution, another volume of the fixative was added for 1 h. The samples were washed three times for 10 min with PBST and incubated in primary antibody staining solution overnight at room temperature. After three washing steps with PBST, the secondary antibody solution was applied for 1 h at room temperature.

The samples were washed with PBST and mounted by inverting the coverslip with the explants on the mounting solution coated microscope slide.

For electrophysiological measurements, transfected embryonic day 9 (E9) chicken DRGs from all spinal segments were dissected, collected in  $\text{Ca}^{2+}$  and  $\text{Mg}^{2+}$ -free PBS and treated with 0.05% trypsin for 12 min at 37°C. Digested DRGs were washed twice with growth medium, triturated and plated in a droplet of growth medium on a glass coverslip precoated with 20  $\mu\text{g}/\text{cm}^2$  Poly-L-Lysine and 4  $\mu\text{g}/\text{cm}^2$  Laminin. Neurons were allowed to adhere to the coverslips for 3-4 hours at 37°C in a humidified 5% incubator before being used for patch-clamp experiments.

The DRG culture for electrophysiological measurements was performed in collaboration with Stefan G. Lechner and Gary R. Lewin at the 'Max-Delbrück-Center for Molecular Medicine' in Berlin.

## **2.8. Electrophysiology**

Whole cell patch clamp recordings were made at room temperature from cultures prepared as described above. Patch pipettes were pulled from borosilicate glass capillaries, filled with a solution consisting of 110 mM KCl, 10 mM NaCl, 1 mM MgCl, 1 mM EGTA and 10 mM HEPES, adjusted to pH 7.3 with KOH and had tip resistances of 2-4 M $\Omega$ . The bathing solution contained 140 mM NaCl, 4 mM KCl, 2 mM  $\text{CaCl}_2$ , 1 mM  $\text{MgCl}_2$ , 4 mM Glucose, 10 mM HEPES, adjusted to pH 7.4 with NaOH. All recordings were made using an EPC 10 amplifier (HEKA Elektronik Dr. Schulze GmbH) in combination with the Patchmaster and Fitmaster software (HEKA Elektronik Dr. Schulze GmbH). Pipette and membrane capacitance were compensated using the auto function of Patchmaster and series resistance was compensated by 70% to minimize voltage errors.

Action potentials were evoked by repetitive 80 ms current injections increasing from 40 pA to 800 pA in increments of 40 pA. The first action potential evoked with this

pulse protocol was used for analysis. Mechanically activated currents were recorded as previously described (Hu and Lewin, 2006; Lechner *et al.*, 2009). Briefly, neurons were clamped to -60 mV, stimulated mechanically with a fire-polished glass pipette (tip diameter 2-3  $\mu\text{m}$ ) that was driven by a piezo based micromanipulator called nanomotor (Kleindiek Nanotechnik GmbH) and the evoked whole cell currents were recorded with a sampling frequency of 200 kHz. The stimulation probe was positioned at an angle of 45° to the surface of the dish and moved with a velocity of 3.5  $\mu\text{m}/\text{ms}$ . Currents were fitted with single exponential functions and classified as RA-, IA- and SA-type currents according to their inactivation time constant (Hu and Lewin, 2006). All electrophysiological experiments were carried out on acutely dissociated dorsal root ganglion (DRG) neurons between 3 and 8 hours after plating.

The electrophysiological measurements were performed in collaboration with Stefan G. Lechner and Gary R. Lewin at the 'Max-Delbrück-Center for Molecular Medicine' in Berlin.

## 2.9. Imaging

All images, including those of transverse sections and whole mounts, were collected using a Leica TCS/MP confocal/two-photon microscope (Leica Microsystems GmbH) with 488 nm, 543 nm and 633 nm laser lines, *in situ* hybridization images were taken in the bright field. All images of a stack of  $\geq 18$  z-sections subsequently collapsed to a 2D rendering. The pictures were processed using Adobe Photoshop CS5.

## 2.10. Quantifications and measurements

For the quantification of ipsilaterally and contralaterally migrating  $\text{Isl1}^{\text{Crest3+}}$ ,  $\text{Avil}^{\text{Lucy1+}}$  and  $\text{CAG}^+$  sensory neurons, transverse sections of lumbar dorsal root ganglia (DRGs) of at least 8 embryos were selected.  $\text{GFP}^+$  /  $\text{Isl1}^+$  DRG neurons were counted on two

or more non-adjacent sections per embryo and presented as the mean  $\pm$  standard *error* of the mean (SEM). Statistical comparisons of cell counts were established using a two-tailed Student's *t* test with two samples and unequal variance.

For the comparison of Ntng1<sup>Mech1+</sup> and Isl1<sup>Crest3+</sup> DRG neurons, GFP<sup>+</sup> cells on transverse lumbar sections of at least 8 embryos were scored for colocalization with TrkA, TrkB, TrkC, Ret or NF200 and analyzed as the mean  $\pm$  standard *error* of the mean (SEM). Statistical comparisons of colocalization counts were established using a two-tailed Student's *t* test with two samples and unequal variance. Additionally the cell size area was measured of GFP<sup>+</sup>, TrkA<sup>+</sup>, TrkB<sup>+</sup> or TrkC<sup>+</sup> neurons by cell border determination of neurons with clear morphology and visible nucleus.

Projection density maps were generated from 18 sections from the lumbar dorsal horn segments out of  $\geq$  8 embryos. A stack with average intensity was performed that was rendered as a numerical grid based on pixel intensity values and converted into a normalized heat map. The statistical analysis of the laminae I-II versus laminae III-V axon density was performed by signal intensity comparison of the laminae based on mean pixel intensity values from 18 sections according to the projection density screen and presented as the mean  $\pm$  SEM by using a two-tailed Student's *t* test with two samples and unequal variance.

### 3. Results

#### 3.1. Stable genetic tagging of somatosensory neurons in chick

The assembly of circuitries for somatosensory perception relies on a complex interplay of neuronal diversification, specification, phenotypic modulation and precise connectivity. However, little is known about the molecular mechanisms controlling the establishment of well-defined somatosensory circuitries, which is to a large part due to the limitation of sensory neuron subtype-specific molecular markers (Arber, 2012; Lallemand and Ernfors, 2012). In order to identify novel markers for distinct sensory subtypes, published literature and public gene expression catalogues were selectively screened for candidate genes expressed by subsets of dorsal root ganglion (DRG) neurons. Through this information, potential gene regulatory elements of the corresponding candidate genes, capable of driving transcription in specific cell types, were defined by an *in silico* screen for evolutionary conserved non-coding regions (ECRs) via browser-based genome alignment between multiple species (Ovcharenko *et al.*, 2004; *ecrbrowser.dcode.org*). The chicken model system shares developmental and structural similarities with mammals, including highly conserved somatosensory system organization and overall connectivity, and allows a more rapid genetic manipulation and analysis than rodent transgenic studies (Necker, 1990; Eide and Glover, 1997; Koltzenburg and Lewin, 1997; Timmer *et al.*, 2001; Guo *et al.*, 2011). The *in ovo* electroporation technique has been widely used for enhancer activity analysis *in vivo* and has proven to be a powerful tool for uncovering regulatory principles involved in early neural development of both avians and mammals (Novitch *et al.*, 2001; Thaler *et al.*, 2002; Dasen *et al.*, 2005; Uchikawa, 2008). Therefore, a straightforward strategy was explored allowing effective, selective and stable genetic tagging of somatosensory neurons and their connectivity patterns in chick embryos (Figure 3.1 a).

For a precise analysis of enhancer activity, especially in late-gestation mature or nearly mature sensory neurons, a stable somatic transfection vector, termed *STEVE* (*STEVE*: stable expression vector), was designed. *STEVE* consists of three essential parts: a basal promoter, a reporter gene and flanking transposable elements. The

identified ECRs corresponding to putative enhancers were amplified from genomic DNA and subcloned upstream of the minimal promoter. The minimal promoter itself should not drive significant own activity in detectable expression levels, but was expected to faithfully reflect the activity of the enhancers contained within inserted ECRs. In addition, the sensitivity of the reporter gene should allow readily accessible detection of low-level expression driven by putative enhancers. By testing different basal promoters and reporter genes for their suitability for *in ovo* enhancer studies, a minimal *TATA box* basal promoter cassette, coupled to reporter genes encoding green fluorescent protein (GFP), proved to be the most appropriate choice to perform a systematic *in ovo* screen for enhancer activities. For different experimental purposes, either cytoplasm-localized *enhanced GFP* (eGFP) or membrane-tethered and axon-localized *myristoylated GFP* (mGFP) were inserted as reporter genes. The technique of *in ovo* transfection of the neural tube, including neural crest cells (NCCs), which give rise to DRG neurons, provides an accessible route for introducing transgenes into the sensory neuron lineage (Muramatsu *et al.*, 1997; Krispin *et al.*, 2010). However, the transient nature of these ‘pseudogenetic’ manipulations so far precluded their application to more mature aspects of sensory nervous system connectivity and function. Since the expression cassettes are not integrated into the host’s genome, their copies become diluted and ultimately disappear as NCCs undergo massive proliferation (Yokota *et al.*, 2011). To overcome these limitations, an effective, stable genetic tagging of transfected cells was achieved by transposon-based transgenesis based on the medaka fish hAT family *ToI2* transposon (Kawakami and Shima, 1999; Sato *et al.*, 2007; Takahashi *et al.*, 2008). The *ToI2* transposase (*T2TP*) recognizes a pair of core transposon sites (*t2*) flanking the ‘enhancer-promoter-reporter gene’ expression cassette, resulting in the recombination of the transgene sequence from the vector and its subsequent random integration in the genome. To achieve this, the transposase driven by the strong and ubiquitously active *CMV early enhancer / chicken  $\beta$ -actin (CAG) promoter (pCAGGS-T2TP)* was therefore co-electroporated with *STEVE*.

The efficiency of the designed strategy and the optimal electroporation conditions were first determined by examining the expression of a reporter gene driven by the *CAG* promoter (*pCAG-STEVE-eGFP*). The vast majority of cells on the transfected



(ipsilateral) side of the spinal cord expressed high levels of eGFP at E12 (Figure 3.1 b-c), while no activity was detected in embryos transfected with enhancer-less constructs (Figure 3.1 d-e). The electroporation showed no influence on embryonic development based on overall morphology, as well as neural marker gene expression, including *Isl1* protein expression, between the ipsilateral and contralateral side. The *in ovo* electroporation was performed between Hamburger-Hamilton (HH) stages 11 and 13 in the chick (embryonic day 2 - 2.2) before NCC emigration for a high transfection efficiency of somatosensory neuron progenitors (Hamburger and Hamilton, 1951; Krispin *et al.*, 2010).

**Figure 3.1: Selective and stable genetic tagging of spinal and somatosensory neurons in chick**

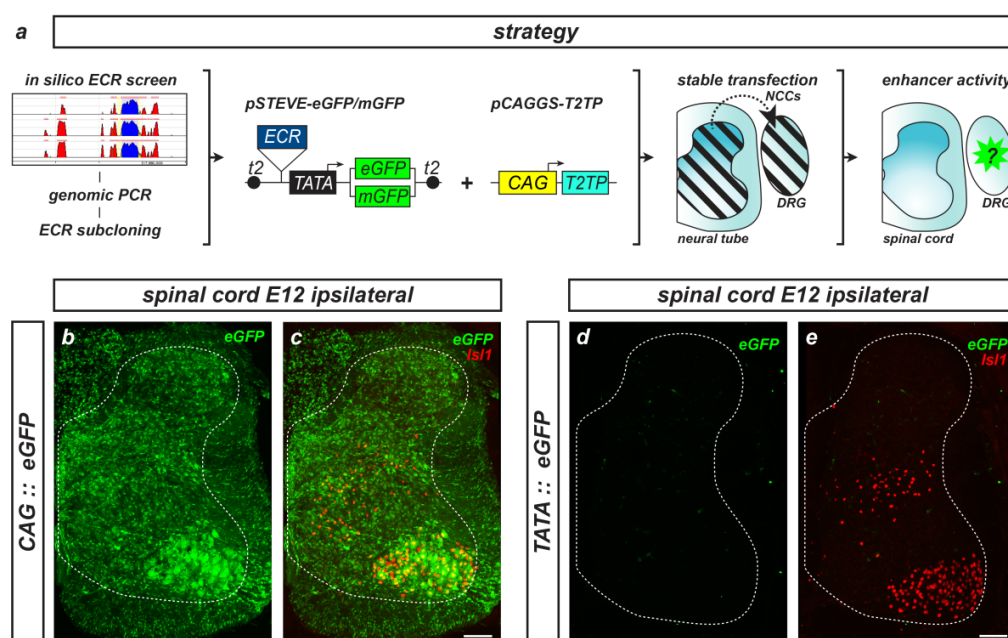


**Figure 3.1: Selective and stable genetic tagging of spinal and somatosensory neurons in chick**

**(a)** Strategy: Subcloning of *in silico* identified evolutionary conserved non-coding regions (ECRs) into transposon-based *pSTEVE-eGFP* or *mGFP*. Co-electroporation with transposase (*T2TP*) into the neural tube of a chick embryo HH stage 11-13 (E2 - 2.2) for stable transfection of neural crest cells (NCCs) before their emigration and formation of the dorsal root ganglia (DRGs). Analysis of putative enhancer activities in late-gestation embryos.

**(b-c)** The constitutive *CAG* promoter (*pCAG-STEVE-eGFP*) drives eGFP expression in virtually all cells on the transfected (ipsilateral) side of the chick spinal cord in E12 transverse sections. *Isl1* protein expression is restricted to motor neurons and dI3 interneurons. Dotted lines outline spinal cord gray matter. Scale bar: 100  $\mu$ m.

**(d-e)** No expression is detected in embryos transfected with enhancer-less constructs (*pSTEVE-eGFP*) in transverse sections at E12. Scale bar: 100  $\mu$ m.

Based on literature search and gene expression databases, a set of candidate genes with general and subtype-restricted expression in somatosensory neurons were selected for the *in silico-to-in vivo* screen and the identified ECRs were analyzed for their spatial and temporal expression pattern in the sensory lineage at both early and late stages of gestation (Table 3.1). The neuron type composition of NCC progeny tagged by stable reporter protein expression was investigated at different developmental stages spanning embryonic day (E) 5 to E15 for all examined ECRs.

**Table 3.1: *In silico-to-in vivo* ECR screen of sensory neuron-specific candidate genes**

literature		ECR screen			
sensory lineage	gene	ECR	genomic locus	ECR activity	ECR specificity
pan-sensory	<i>Islet1</i>	<i>Crest3</i>	<i>mm chr13</i> : 116,633,179-116,634,173 995 bps	all sensory neurons	yes
pan-sensory	<i>Advillin</i>	<i>Lucy1</i>	<i>mm chr10</i> : 127,000,229-127,000,828 600 bps	all sensory neurons	yes
nociceptive	<i>TrkA</i>	<i>ECR1</i>	<i>mm chr3</i> : 87,795,338-87,796,203 866 bps	not observed	no
proprioceptive	<i>Runx3</i>	<i>ECR1</i>	<i>mm chr4</i> : 135,025,698-135,026,347 650 bps	sensory neurons	no
		<i>ECR2</i>	<i>mm chr4</i> : 135,050,017-135,051,782 1766 bps	sensory neurons	no
		<i>ECR3</i>	<i>mm chr4</i> : 135,088,427-135,089,369 943 bps	not observed	no
subtype-specific ?	<i>NetrinG1</i>	<i>Mech1</i>	<i>galGal chr8</i> : 821,118-821,467 350 bps	mechanoreceptive neurons	yes

**Table 3.1: *In silico-to-in vivo* ECR screen of sensory neuron-specific candidate genes**

Candidate genes with general and subtype-restricted expression in somatosensory neurons were screened for evolutionary conserved non-coding regions (ECRs). The identified ECRs were analyzed via *in ovo* electroporation for their spatial and temporal expression activity in late-gestation sensory neurons and for their specificity for the endogenous gene expression of the corresponding genes.

As a general somatosensory marker and a proof of principle experiment, the *Islet1* (*Isl1*) gene was chosen, which at spinal levels is expressed at earliest stage of neural differentiation by all subtypes of somatosensory neurons, somatic and preganglionic motor neurons, as well as by dorsal (dl3) interneurons (Ericson *et al.*, 1992). The transcription factor *Isl1* is highly conserved during evolution and plays a central role in the transition from sensory neurogenesis to subtype specification, whereby gene expression is mediated by different subtype-specific enhancers (Tsuchida *et al.*, 1994;

Thaler *et al.*, 2004; Uemura *et al.*, 2005; Sun *et al.*, 2011). Herein, an ECR at around 323 kb upstream of the mouse *Isl1* gene transcription start site coincides with a genomic fragment previously been shown to drive expression in sensory neurons in zebrafish (Uemura *et al.*, 2005). This mouse genomic ECR, *Isl1*<sup>Crest3</sup>, was found to drive specific and robust reporter gene expression in sensory DRG neurons of transfected chick embryos (see chapter 3.2).

In order to establish a late-gestation and adult pan-sensory marker, the *Advillin* (*Avil*) gene locus was screened for a putative enhancer. The actin binding protein Avil, which is highly conserved between mammals but not yet identified in the chick genome, is specifically expressed in sensory neurons and implicated in regenerative neurite outgrowth (Hasegawa *et al.*, 2007; Lau *et al.*, 2011; Zurborg *et al.*, 2011). The identified ECR *Avil*<sup>Lucy1</sup> locates just upstream to the gene coding sequence. Upon isolation, subcloning into *STEVE* and *in ovo* electroporation, *Avil*<sup>Lucy1</sup> was able to drive a robust expression highly restricted to sensory DRG neurons, which was retained at least until hatching (see chapter 3.3).

The growth factor receptor Tropomyosin receptor kinase A (TrkA) is confined to be expressed in most pain-transmitting neurons and plays an important role in shaping the nociceptive phenotype (Martin-Zanca *et al.*, 1990; Smeyne *et al.*, 1994; Ma *et al.*, 2003). A core enhancer located upstream adjacent to the gene transcription start site was shown to drive somatosensory-specific expression in mouse (Ma *et al.*, 2000). This *TrkA*<sup>ECR1</sup>, which was not conserved in the chick genome, was tested for enhancer activity in the chick embryo. However, no reporter gene expression could be observed in DRG neurons at different developmental stages (data not shown; see chapter 4.2 for discussion).

Proprioceptive neurons highly express the Runt-related transcription factor 3 (Runx3) as a key factor in their specification and functional circuit formation (Inoue *et al.*, 2002; Levanon *et al.*, 2002; Chen AI *et al.*, 2006). Three ECR sequences with a conservation of around 80% between mouse and chicken were selected for enhancer analysis spanning a region from 95 kb to 31 kb upstream of the gene transcription start site. Both *Runx3*<sup>ECR1</sup> and *Runx3*<sup>ECR2</sup> were driving expression in sensory neurons which

appeared more wide-spread and not restricted to the proprioceptive subtype, whereas *Runx3*<sup>ECR3</sup> did not show a detectable expression in transfected cells at different developmental stages (data not shown). Therefore, the identified ECRs did not reflect the endogenous *Runx3* gene expression and were not characterized further (see chapter 4.2 for discussion).

*NetrinG1* (*Ntng1*) appears to be expressed by a subset of large-diameter sensory neurons in postnatal mouse DRGs and encodes a Glycosyl-phosphatidyl-inositol (GPI)-linked interaction partner of the transmembrane NetrinG1 ligand (NGL1), which is implicated in laminar neurite targeting and synaptogenesis (Yin *et al.*, 2002; [www.brain-map.org](http://www.brain-map.org)). Although the role of *Ntng1* in somatosensory neurons remains unknown, it might be involved in sensory connectivity (Nakashiba *et al.*, 2002; Nishimura-Akiyoshi *et al.*, 2007; Woo *et al.*, 2009). An identified ECR located 2.6 kb upstream of the gene coding sequence showed a specific expression in a subclass of large-diameter mechanoreceptive neurons (see chapter 3.5).

Alltogether, the designed strategy, including the *in silico*-to-*in vivo* ECR screen and the stable expression system *STEVE*, thus facilitates the detection of cis-regulatory activities and their subsequent use for the stable genetic tagging of somatosensory neurons in chick.

### 3.2. Analysis of the sensory neuron-specific enhancer *Isl1<sup>Crest3</sup>*

During early vertebrate embryogenesis, the transcription factor *Isl1* is expressed in a defined population of somatosensory neurons, somatic and preganglionic motor neurons, as well as dorsal (dl3) interneurons (Ericson *et al.*, 1992). Thereby, the evolutionary highly conserved factor has been shown to be critical in neuronal specification of both motor and sensory neurons (Tsuchida *et al.*, 1994; Thaler *et al.*, 2004; Sun *et al.*, 2011). The endogenous gene expression is mediated by distinct neuron type-specific enhancers (Uemura *et al.*, 2005). A through *in silico* screen identified ECR, *Isl1<sup>Crest3</sup>*, at around 323 kb upstream of the mouse *Isl1* coding sequence coincided with a genomic fragment previously been shown to predominantly drive expression in sensory neurons in zebrafish (Figure 3.2 a) (Uemura *et al.*, 2005). This mouse ECR with a length of 995 bps revealed 91% and 85% homologies with the human and chicken sequences, respectively, and included 94 putative conserved transcription factor binding sites (TFBS) (Figure 3.2 b).

Based on this information, *Isl1<sup>Crest3</sup>* was chosen as a putative early stage pan-sensory marker and analyzed for the spatial and temporal enhancer activity in the chick somatosensory lineage. When coupled to *STEVE Isl1<sup>Crest3</sup>* was specifically driving high-level GFP expression in transfected somatosensory neurons at all axial levels immediately after NCC emigration and coalescence into DRGs between E2.5 and E4 (Figure 3.3 a-b), in addition to labeling further NCC progeny at early developmental stages (Figure 3.3 c-f). The *Isl1<sup>Crest3</sup>*-driven GFP expression reflected the endogenous *Isl1* protein expression pattern in the sensory lineage, whereas none was found in *Isl1* expressing motor neurons or other locations of the neural tube. Fluorescence was also detected in sparse DRG neurons on the non-transfected (contralateral) side, consistent with the findings that NCCs can migrate to either side of the embryo (Figure 3.3 e-f) (Frank and Sanes, 1991). The analysis also verified that the endogenous gene expression pattern can be recapitulated by the use of mouse enhancers in the chick embryo. Additionally, it could have been shown that both orientations of the ECR sequence were capable of modulating gene expression with similar efficiency (data not shown).



**Figure 3.3: Genetic tagging of somatosensory neurons by  $Isl1^{Crest3}$  in early stage chick embryos**

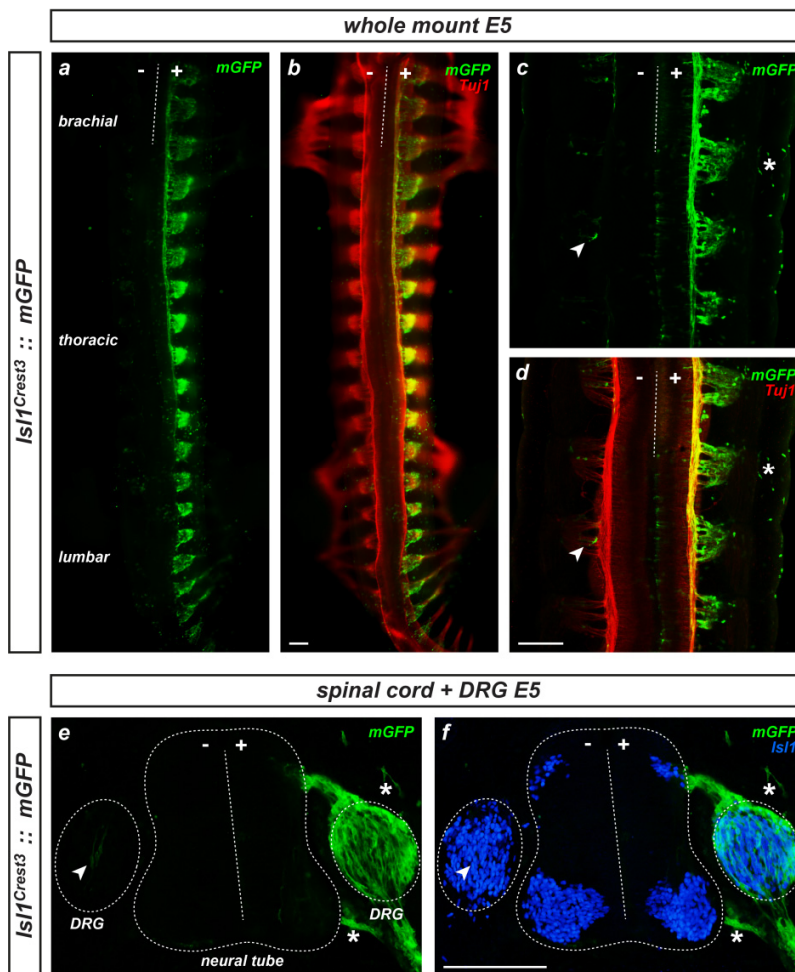


**Figure 3.3: Genetic tagging of somatosensory neurons by  $Isl1^{Crest3}$  in early stage chick embryos** (a-d) Whole mount of a chick embryo at E5 (dorsal view) shows specific dorsal root ganglion (DRG) labeling driven by  $Isl1^{Crest3}$  at all axial levels of the ipsilateral side of the neural tube (a-b). Motor and sensory axons are labeled by  $\beta$ III-tubulin (Tuj1). Detailed view of the whole mount (c-d). Scale bar: 200  $\mu$ m.

(e-f) Transverse sections at E5 reveal that  $Isl1^{Crest3}$ -driven GFP expression reflects the endogenous *Isl1* protein expression pattern in the sensory lineage, in addition to sparsely labeling contralaterally migrating DRG neurons (arrowheads) and further neural crest cell progeny (asterisks). *Isl1* protein expression is restricted to somatosensory neurons, motor neurons in the ventral horn and d13 interneurons. Scale bar: 200  $\mu$ m.

Due to the stable genomic integration of the ‘enhancer-promoter-reporter gene’ expression cassette, it became possible to overcome the limitations of plasmid-based transient transfection procedures in massively proliferating NCCs and to study the late development of NCC-derived lineages in chick embryos. In accordance with the early



pan-sensory expression pattern,  $Isl1^{Crest3}$  was driving reporter gene expression in both small and large-diameter somatosensory neurons in late-gestation DRGs and visualized the central afferent collateral projections in the spinal cord (Figure 3.4 a-d). Based on the central afferent termination zones in the dorsal and ventral horn of the spinal cord,  $Isl1^{Crest3}$  revealed an unbiased tagging of all three sensory subtypes: nociceptive, mechanoreceptive and proprioceptive neurons.

**Figure 3.4: Tagging of somatosensory neurons by  $Isl1^{Crest3}$  in late-gestation chick embryos**

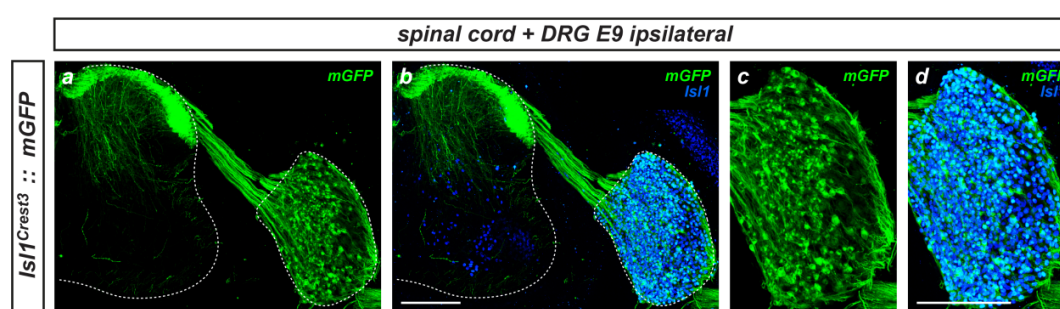


**Figure 3.4: Tagging of somatosensory neurons by  $Isl1^{Crest3}$  in late-gestation chick embryos**

(a-d)  $Isl1^{Crest3}$ -driven GFP expression shows specific enhancer activity in somatosensory neurons and visualizes central afferents projecting into the spinal cord in transverse sections at E9 (a-b).  $Isl1$  protein expression is restricted to somatosensory neurons, motor neurons in the ventral horn and d13 interneurons. Detailed view of the DRG reveals overlap of  $Isl1^{Crest3+}$  cells with  $Isl1^+$  somatosensory neurons (c-d). Scale bar: 200  $\mu$ m.

Consistently,  $Isl1^{Crest3}$  robustly labeled peripheral sensory projections terminating in glabrous skin, feathery skin and musculature (Figure 3.5 a-b). The central connectivity pattern was mirrored by the corresponding sensory end organ structures targeted by their  $Isl1^{Crest3+}$  peripheral collaterals, including nociceptive and mechanoreceptive endings in the dermis (Figure 3.5 c-d) and muscle spindle receptors on intrafusal muscle fibers (Figure 3.5 e-h).



**Figure 3.5: Analysis of  $Isl1^{Crest3+}$  peripheral collaterals in late-gestation chick embryos**

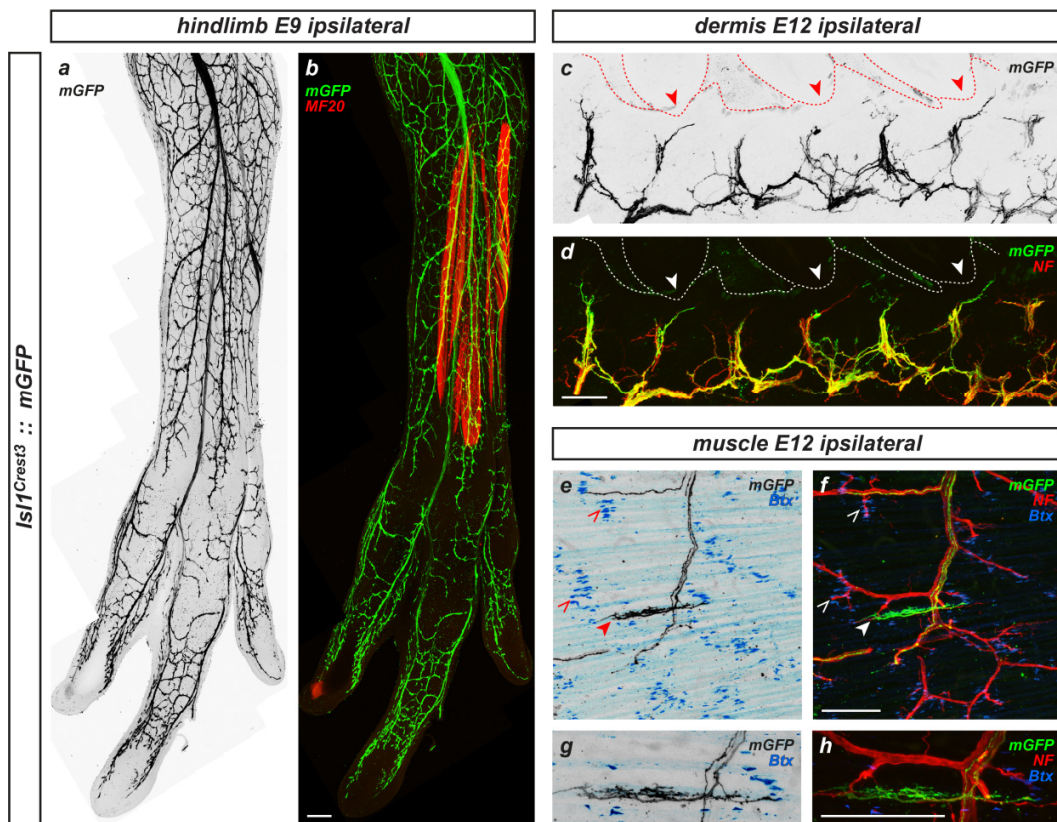


**Figure 3.5: Analysis of  $Isl1^{Crest3+}$  peripheral collaterals in late-gestation chick embryos**

(a-b)  $Isl1^{Crest3}$  labels peripheral sensory projections. Whole hindlimb at E9 shows  $Isl1^{Crest3+}$  peripheral collaterals projecting in glabrous skin, feathery skin and musculature (labeled by MF20). Scale bar: 200  $\mu\text{m}$ .

(c-d) Tagging of the skin innervation in E12 transverse sections illustrates complete overlap of  $Isl1^{Crest3+}$  axons with neurofilament (NF). Arrowheads indicate feather follicle shafts. Dotted lines demarcate outer side. Scale bar: 100  $\mu\text{m}$ .

(e-h)  $Isl1^{Crest3}$ -labeled peripheral projections terminate as muscle spindle receptors on intrafusal muscle fibers (closed arrowheads) in E12 longitudinal sections (e-f). No overlap between  $Isl1^{Crest3+}$  axons and motor end plates (open arrowheads), detected by Bungarotoxin (Btx), can be observed. NF labels both sensory and motor axons. Detailed view of an innervated muscle spindle (g-h). Scale bar: 100  $\mu\text{m}$ .

Using this approach,  $Isl1^{Crest3}$ -tagged central afferent projections of somatosensory neurons were mapped throughout gestation in chick. The  $Isl1^{Crest3}$  enhancer showed robust activity in the somatosensory lineage at least until E15. The labeled developing central afferents entered the spinal cord via the dorsal root entry zone and bifurcated into axon collaterals that extended rostrally and caudally within the dorsal funiculus, prior to penetrating the spinal cord gray matter (Figure 3.6 a-b).

Figure 3.6: Development of central afferent projections in chick I

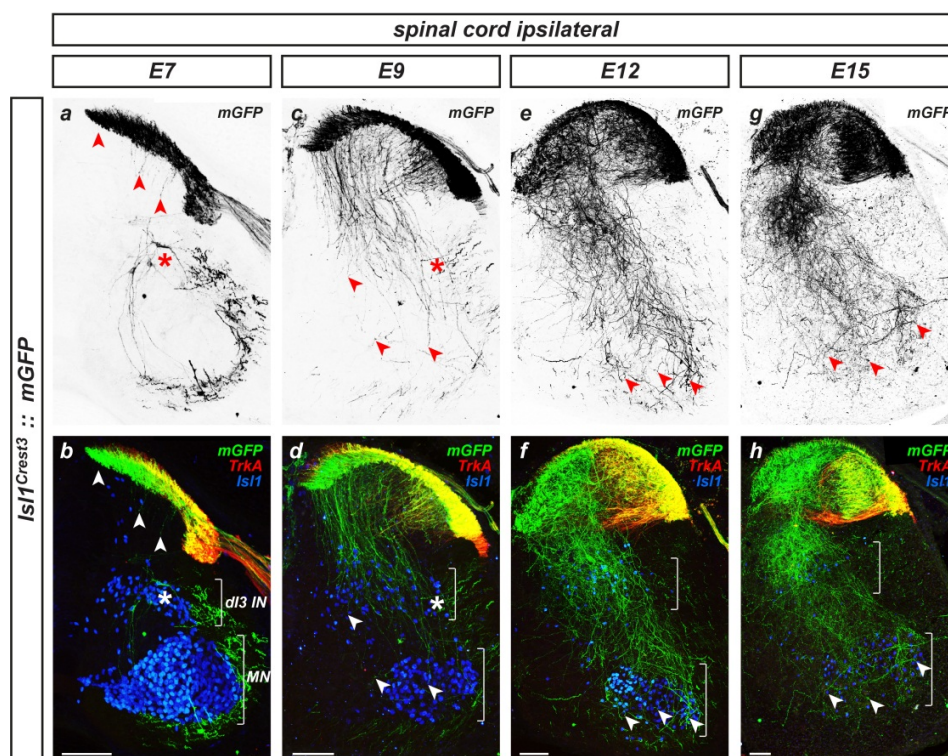


Figure 3.6: Development of central afferent projections in chick I

(a-h) Genetic tagging of developing ipsilateral central afferent projections by  $Isl1^{Crest3}$  throughout gestation in transverse sections from E7 to E15, in addition to labeling some spinal  $Isl1^+$  interneurons (dI3 IN) (asterisks). Proprioceptive afferents are indicated by arrowheads, nociceptive sensory axons are labeled by TrkA, motor neurons (MN) and dI3 IN by Isl1. Scale bar: 100  $\mu$ m.

The first  $Isl1^{Crest3+}$  somatosensory axons entered the spinal cord gray matter at around E7 (Figure 3.7 a-c). These axons were invariably negative for the nociceptive marker TrkA, while the first TrkA<sup>+</sup> axons began advancing into the dorsal horn gray matter between E8 and E9 (Figure 3.7 d-f). These observations were in consistency with previous transganglionic axon tracing experiments in chick (Davis *et al.*, 1989; Eide and Glover, 1997). At around the same developmental stage, the proprioceptive projections began reaching their targets in the intermediate and ventral spinal cord (Figure 3.6 c-d). In late-gestation embryos,  $Isl1^{Crest3}$ -tagged central afferents converged at their termination zones (Figure 3.6 e-h). Thus, the overall developmental sequence of proprioceptive/mechanoreceptive (TrkA<sup>-</sup>) and nociceptive (TrkA<sup>+</sup>) collateral extension into the gray matter in chick mirrored that observed in the mammalian spinal cord. However, the delay in the establishment of nociceptive

compared to proprioceptive afferent connectivity observed in mammals appeared temporally compressed in avians, likely reflecting an ontogenic adaptation in precocial birds (Fitzgerald, 1987; Mirnics and Koerber, 1995; Ozaki and Snider, 1997; Marmigère and Ernfors, 2007).

**Figure 3.7: Development of central afferent projections in chick II**

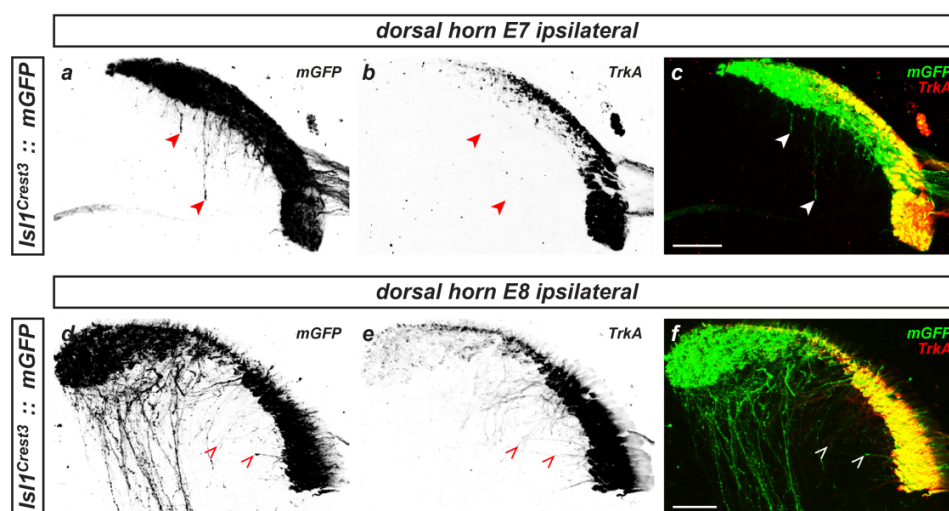


**Figure 3.7: Development of central afferent projections in chick II**

(a-f) Genetic tagging of ipsilateral central afferent projections by  $Isl1^{Crest3}$  in transverse sections. At E7 the first  $Isl1^{Crest3+} TrkA^-$  axons (closed arrowheads) enter the gray matter of the medial dorsal horn (a-c). First nociceptive projections, labeled by  $Isl1^{Crest3}$  and TrkA (open arrowheads), penetrate the gray matter of the lateral dorsal horn at E8 (d-f). Scale bar: 50  $\mu$ m.

These results therefore establish  $Isl1^{Crest3}$  as an early pan-sensory neuron gene regulatory element that can be used for driving a specific and robust reporter gene expression in somatosensory neurons. Furthermore, the analysis confirmed the suitability of the chosen strategy based on stable genetic tagging of DRG neurons in chick by the stable expression system STEVE.

### 3.3. Analysis of the sensory neuron-specific enhancer *Avil*<sup>Lucy1</sup>

Advillin (*Avil*), a member of the Gelsolin superfamily of actin binding proteins, has been shown to be exclusively expressed in peripheral sensory neurons and has been implicated in regenerative neurite outgrowth (Ravenall *et al.*, 2002; Hasegawa *et al.*, 2007; Lau *et al.*, 2011; Zurborg *et al.*, 2011). Transgenic mice expressing reporter genes under the control of the *Avil* promoter displayed robust and specific expression in postmitotic somatosensory neurons, from embryonic stages into adulthood, thus enabling the study of central and peripheral somatosensory target innervation (Hasegawa *et al.*, 2007; Zurborg *et al.*, 2011). The gene coding sequence of *Avil* showed high homology between mammals, but has not yet been identified in the chick genome. In order to establish a late-gestation and adult pan-sensory marker, the *Avil* gene locus was screened for putative enhancers via *in silico* ECR screen (Figure 3.8 a). An identified ECR, *Avil*<sup>Lucy1</sup>, which was located upstream adjacent to the gene coding sequence, was also included in the *Avil* promoter sequences chosen for transgenic mice. This ECR, with a length of 600 bps, showed 80% homology with the human sequence and included 26 putative conserved TFBS (Figure 3.8 b).

The identified ECR *Avil*<sup>Lucy1</sup> was inserted into the stable expression vector *STEVE* and analyzed for the spatial and temporal enhancer activity in the chick sensory lineage. *Avil*<sup>Lucy1</sup> was driving a robust reporter gene expression with high specificity in transfected sensory neurons, which retained at least until hatching (Figure 3.9 a-d). Therefore, the *Avil*<sup>Lucy1</sup>-mediated expression recapitulated the transgene-driven *Avil* expression pattern observed by other groups (Hasegawa *et al.*, 2007; Zurborg *et al.*, 2011). Compared to *Isl1*<sup>Crest3</sup>, *Avil*<sup>Lucy1</sup> displayed a later onset of enhancer activity at around E5. By the analysis of peripheral collaterals, *Avil*<sup>Lucy1</sup>-tagged projections innervated the dermis (Figure 3.9 e-f) and intrafusal, but not extrafusal muscle fibers (Figure 3.9 g-j). As for *Isl1*<sup>Crest3</sup>, *Avil*<sup>Lucy1+</sup> central afferent collateral projections were mapped throughout gestation in chick, which closely resembled the observations made by the pan-sensory marker *Isl1*<sup>Crest3</sup> (Figure 3.10). Herein, *Avil*<sup>Lucy1</sup>-labeled central afferents occupied all termination zones in the spinal cord of nociceptive, mechanoreceptive and proprioceptive axons, indicating that *Avil*<sup>Lucy1</sup>-driven expression was not biased towards a certain sensory subtype.





**Figure 3.9: Tagging of somatosensory neurons by *Avil<sup>Lucy1</sup>* in late-gestation chick embryos**

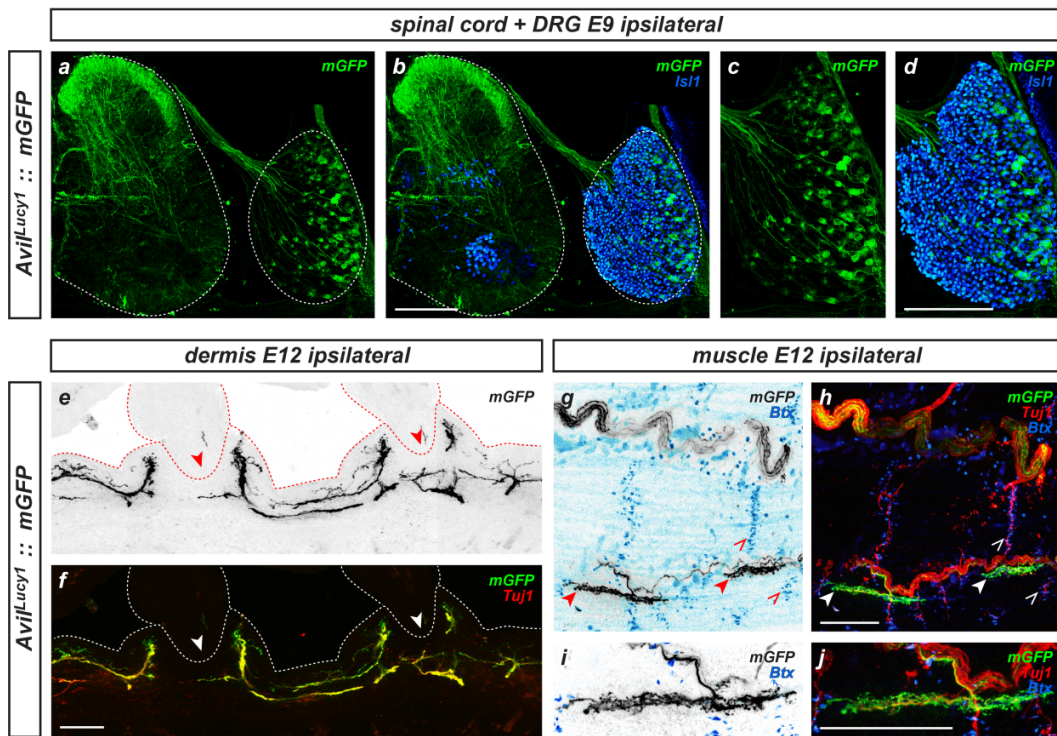


**Figure 3.9: Tagging of somatosensory neurons by *Avil<sup>Lucy1</sup>* in late-gestation chick embryos**  
**(a-d)** *Avil<sup>Lucy1</sup>*-driven reporter gene expression displays specific enhancer activity in somatosensory neurons, in addition to labeling their central afferents in transversal sections of the E9 spinal cord **(a-b)**. *Isl1* protein expression is restricted to somatosensory neurons, motor neurons located in the ventral horn and *dl3* interneurons. *Avil<sup>Lucy1+</sup>* cells overlap with *Isl1<sup>+</sup>* somatosensory neurons **(c-d)**. Scale bar: 200  $\mu$ m.  
**(e-f)** *Avil<sup>Lucy1</sup>* labels peripheral somatosensory projections innervating the feathery skin in E12 transverse sections. Nociceptive and mechanoreceptive axons are labeled by  $\beta$ III-tubulin (*Tuj1*). Arrowheads indicate feather follicle shafts. Dotted lines demarcate outer side. Scale bar: 100  $\mu$ m.  
**(g-j)** *Avil<sup>Lucy1+</sup>* muscle spindle receptors terminating on intrafusal muscle fibers (closed arrowheads) show no overlap with motor end plates (open arrowheads), detected by Bungarotoxin (*Btx*), in E12 longitudinal sections **(g-h)**. *Tuj1* labels both sensory and motor axons. Detailed view of an innervated muscle spindle **(h-j)**. Scale bar: 100  $\mu$ m.

**Figure 3.10: Mapping of central afferent projections by *Avil<sup>Lucy1</sup>* throughout gestation in chick**

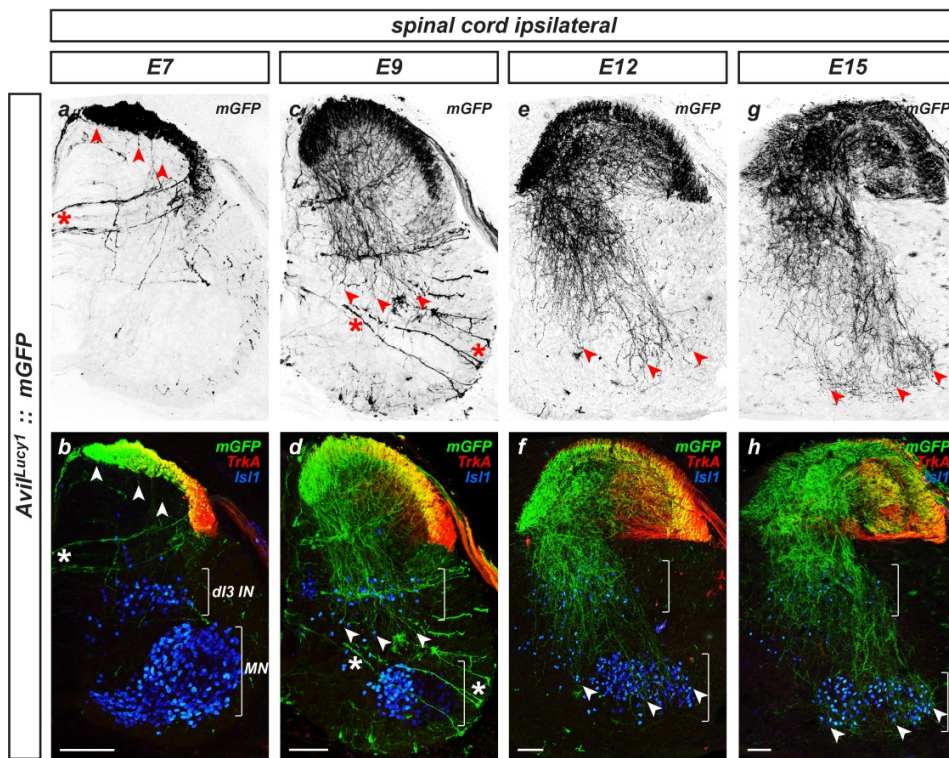


**Figure 3.10: Mapping of central afferent projections by *Avil<sup>Lucy1</sup>* throughout gestation in chick**  
**(a-h)** Genetic tagging of developing ipsilateral central afferent projections by *Avil<sup>Lucy1</sup>* throughout gestation in transverse sections from E7 to E15. At early stages, *Avil<sup>Lucy1</sup>* displays ectopic expression in premitotic interneurons (asterisks). Proprioceptive afferents are indicated by arrowheads, nociceptive sensory axons are labeled by TrkA, motor neurons (MN) and dorsal interneurons (dl3 IN) by Isl1. Scale bar: 100  $\mu$ m.

These results demonstrate that the newly identified enhancer *Avil<sup>Lucy1</sup>* can be used as a pan-sensory neuron marker from mid-embryonic stages at least into late-gestation, by driving specific and strong reporter gene expression in the somatosensory neuron lineage in chick.

### 3.4. Analysis of ipsilaterally and contralaterally migrating neural crest cells

During early vertebrate development, a vast range of peripheral cell types, including autonomic and somatosensory ganglion neurons and further non-neuronal cells, are generated from NCCs, which arise from the roof plate of the dorsal neural tube and emigrate towards their respective peripheral targets (Bronner-Fraser and Fraser, 1988; Frank and Sanes, 1991; Le Douarin and Kalcheim, 1999; Kim *et al.*, 2003; Squire *et al.*, 2008). The adoption of specific cell fates by NCCs is a multistep process involving extensive interaction with the peripheral locales they colonize and is further influenced by the time window of emigration (Harris and Erickson, 2007; Marmigère and Ernfors, 2007). The extent to which the fate of premigratory or early migratory NCCs is predetermined remains less clear, however (Hari *et al.*, 2012). The initial pattern of NCC emigration appears to be determined by homotypic interactions, during which some NCCs enter trajectories that cause them to cross the neural tube midline and to contribute to the contralateral NCC migratory stream (Figure 3.11 a) (Frank and Sanes, 1991; Carmona-Fontaine *et al.*, 2008).

**Figure 3.11: Scenarios of ipsilaterally and contralaterally migrating NCC progeny in chick**

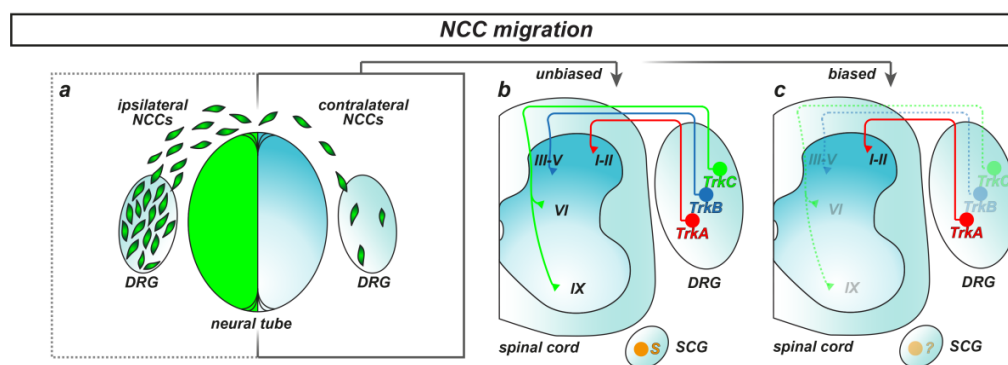


**Figure 3.11: Scenarios of ipsilaterally and contralaterally migrating NCC progeny in chick**  
**(a-c)** Schematic of a unilaterally transfected neural tube (green label) depicts ipsilateral and contralateral neural crest cell (NCC) streams colonizing dorsal root ganglia (DRGs) **(a)**. Two scenarios of contralaterally migrating NCCs contributing to peripheral neurons and circuits: unbiased, giving rise to all neuron classes **(b)**, or biased to a certain neuron class **(c)**. Numbers: preferential spinal cord laminar targets of nociceptive (TrkA), mechanoreceptive (TrkB) and proprioceptive (TrkC) DRG neuron axon collaterals. S, sympathetic neuron; SCG, sympathetic chain ganglion.



**Figure 3.12: Direct fate-tracking of ipsilaterally and contralaterally migrating NCCs in chick**

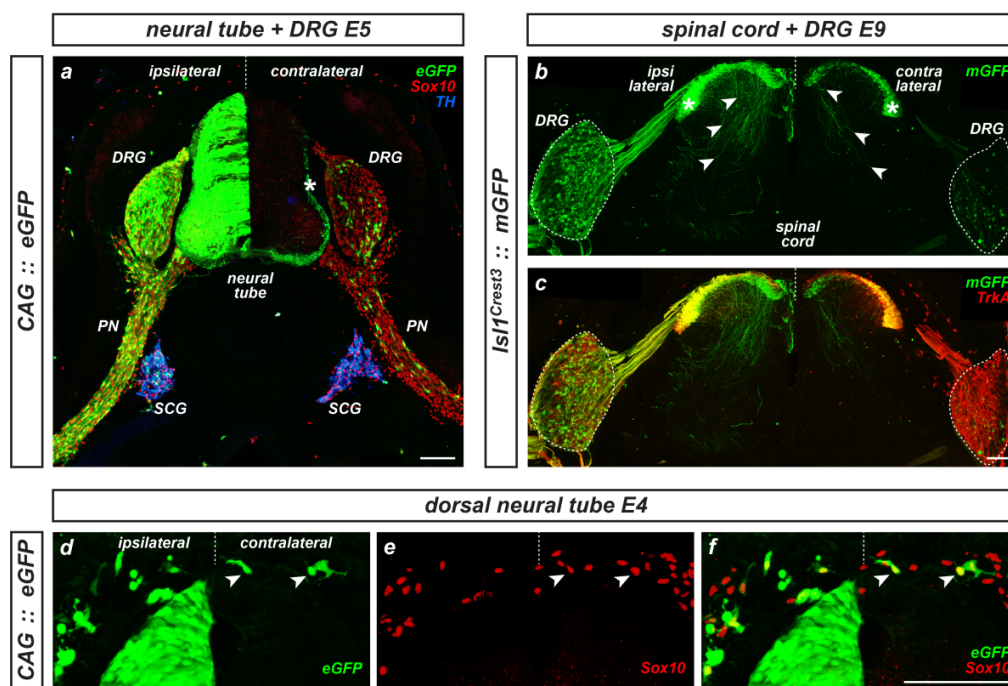


**Figure 3.12: Direct fate-tracking of ipsilaterally and contralaterally migrating NCCs in chick**

(a) Based on unilateral transfection of the neural tube, the constitutive *CAG* promoter (*pCAG-STEVE-eGFP*) stably tracks ipsilateral and contralateral NCCs in transverse sections at E5. DRGs, SCGs and peripheral nerves (PNs) reveal bilateral labeling of NCC streams, colabeled for NCC marker *Sox10* and SCG neuron marker tyrosine hydroxylase (*TH*). *eGFP*<sup>+</sup> ipsilateral commissural projections extend into contralateral neural tube (asterisk). Scale bar: 100  $\mu$ m.

(b-c) Stably transfected *Isl1*<sup>Crest3</sup>-tagged ipsilateral and contralateral NCC-derived neurons and central collateral projections (arrowheads) in E9 transverse sections. *TrkA* labels nociceptive neurons. Asterisks, dorsal root entry zone and Lissauer's tract. Scale bar: 100  $\mu$ m.

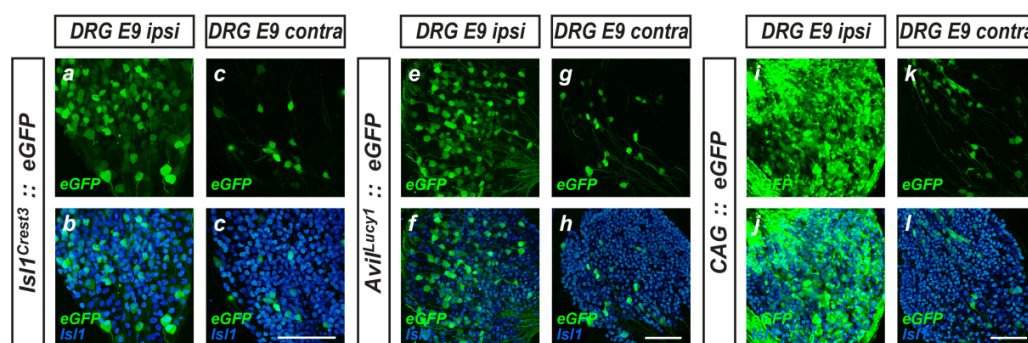
(d-f) Transverse section of unilaterally *CAG*-labeled E4 dorsal neural tube with ipsilaterally and contralaterally (arrowheads) emigrating NCCs expressing *Sox10*. Scale bar: 100  $\mu$ m.

George and colleagues raised the possibility that NCCs diverge into discrete lineage-restricted pools of NCCs choosing diametrically opposed (ipsilateral and contralateral) migratory streams, such that contralateral NCCs are biased to generate pain-sensing nociceptive somatosensory neurons within DRGs (Figure 3.11 c) (George *et al.*, 2007; Lefcort and George, 2007; George *et al.*, 2010). The author's conclusions were inferred from three principle observations: first, the correlated timing of contralateral NCC and nociceptive DRG neuron differentiation, second, an indirectly estimated bias in the contribution of contralateral NCCs to nociceptive DRG neurons and third, a

reduction of nociceptive or total DRG neuron numbers upon surgically cutting off the contralateral NCC stream at the neural tube midline (George *et al.*, 2007).

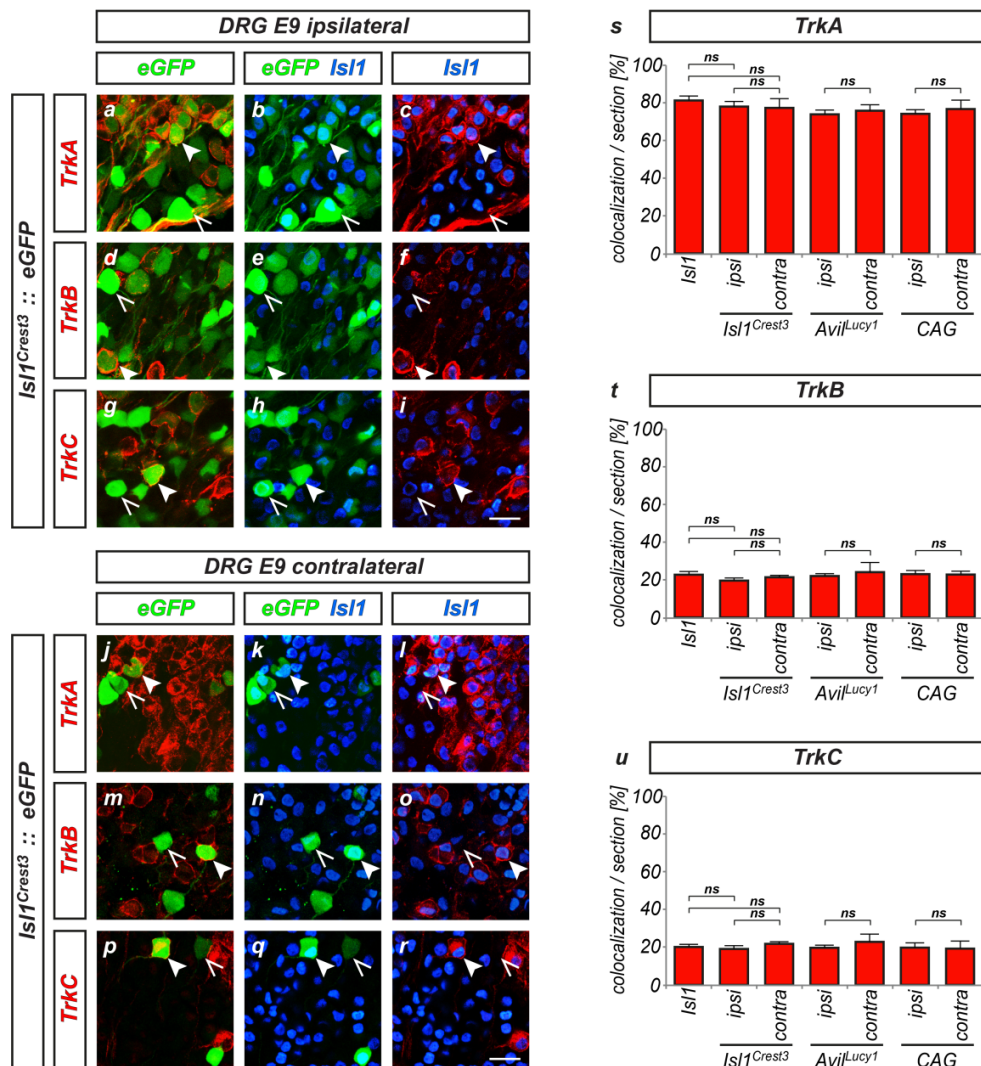
This hypothesis was investigated by *STEVE*-based direct lineage-tracking upon unilateral *in ovo* transfection, followed by neuron type composition analysis in the tagged NCC progeny. Therefore, any lineage-restriction of contralaterally migrating NCCs would consequently be reflected in a bias in the proportion of neuronal classes transfected in contralateral DRGs, compared to those in the ipsilateral DRGs (Figure 3.11 b-c). Upon unilateral neural tube transfection of constitutive (*CAG*) and somatosensory-specific (*Isl1<sup>Crest3</sup>*) constructs, both ipsilateral and contralateral migrating NCC derivatives were indeed labeled at early and late stages of gestation (Figure 3.12 a-c). Furthermore, the method allowed detailed observation of NCC delamination and migration along distinct pathways (Figure 3.12 d-f). The three major DRG neuron classes form stereotypic laminar connections in the spinal cord via central axon collaterals, reflecting their incorporation into discrete somatosensory circuits (Brown, 1982; Lallemand and Ernfors, 2012). However, in neither the ipsilateral nor the contralateral spinal cord the *Isl1<sup>Crest3+</sup>* central collaterals displayed an obvious bias towards specific termination zones in the dorsal or ventral horn of the spinal cord (Figure 3.12 b-c).

**Figure 3.13: Genetic tagging of ipsilateral and contralateral somatosensory neurons in chick**



**Figure 3.13: Genetic tagging of ipsilateral and contralateral somatosensory neurons in chick**  
**(a-l)** Genetic tagging of ipsilateral and contralateral NCC-derived DRG neurons by somatosensory-specific *Isl1<sup>Crest3</sup>* **(a-d)** and *Avil<sup>Lucy1</sup>* **(e-h)** and by ubiquitous *CAG* **(i-l)** in transverse sections at E9. *Isl1*, pan-DRG neuron marker. Scale bar: 100  $\mu$ m.

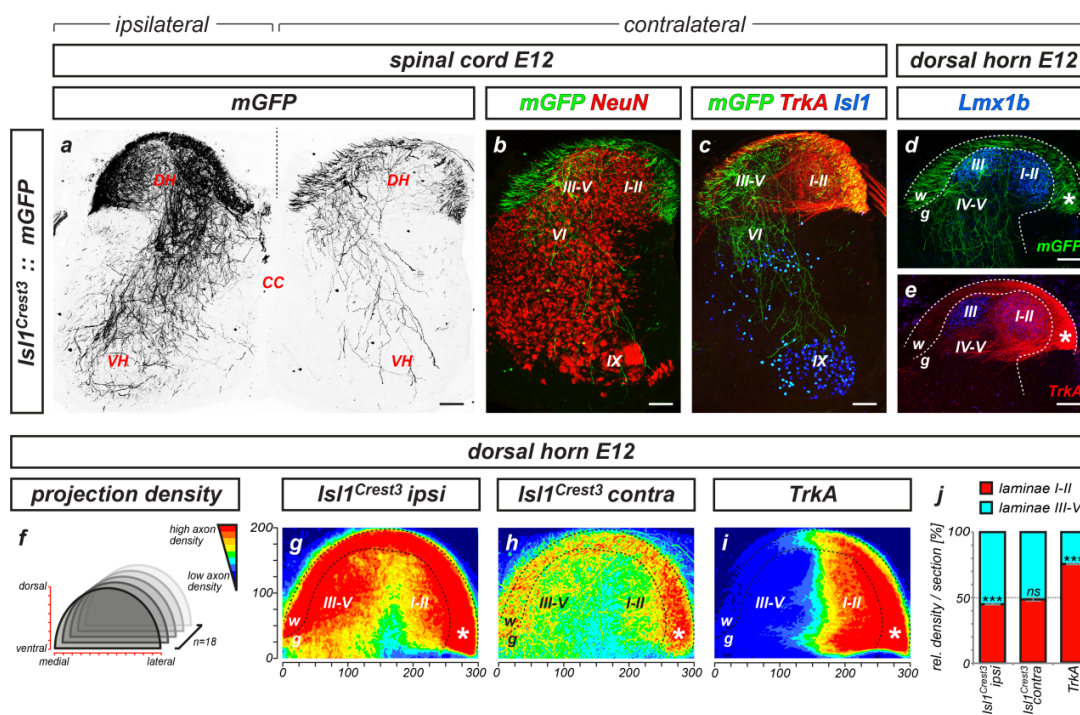
Figure 3.14: DRG neuron type composition of ipsilateral and contralateral NCC progeny in chick



**Figure 3.14: DRG neuron type composition of ipsilateral and contralateral NCC progeny in chick** (a-r) E9 transverse sections of Neurotrophin receptor (Trk) class expression in ipsilaterally-derived (a-i) and contralaterally-derived (j-r) DRG neurons tagged by *Isl1<sup>Crest3</sup>*. Major DRG neuron classes: nociceptive (TrkA), mechanoreceptive (TrkB) and proprioceptive (TrkC) neurons. Closed arrowheads: co-expression. Open arrowheads: no co-expression. Isl1, pan-DRG neuron marker. Scale bar: 25  $\mu$ m. (s-u) Quantitative analysis: proportion of ipsilateral and contralateral NCC-derived E9 DRG neurons expressing TrkA, TrkB or TrkC separately traced by three independent transgenes: *Isl1<sup>Crest3</sup>*, *Avil<sup>Lucy1</sup>* or CAG, compared to *Isl1<sup>+</sup>* total DRG neurons. No significant differences in the proportion of TrkA<sup>+</sup> (s), TrkB<sup>+</sup> (t) or TrkC<sup>+</sup> (u) eGFP-tagged neurons were observed between ipsilateral, contralateral or *Isl1<sup>+</sup>* total DRG neurons. Note: a substantial portion of DRG neurons express more than one Trk receptor class at E9. Data are presented as mean  $\pm$  SEM (two-tailed Student's *t* test with two samples and unequal variance). ns, not significant,  $p > 0.05$ ; see Table 3.2 for statistical analysis.

For a more detailed analysis, the relative proportions of the three major classes of DRG neurons, respectively expressing the Neurotrophin receptors TrkA (corresponding to nociceptive neurons), TrkB ( $\approx$ low-threshold mechanoreceptive neurons) or TrkC ( $\approx$ proprioceptive neurons), derived from ipsilaterally versus contralaterally migrating NCCs were compared (Lewin and Moshourab, 2004; Marmigère and Ernfors, 2007). Thereby, NCC progeny were labeled upon selectively tracking neuronal or both neuronal and non-neuronal cells with three distinct transgene vectors facilitating DRG neuron-restricted (*Isl1<sup>Crest3</sup>*, *Avi<sup>Lucy1</sup>*) or generalized (CAG) reporter expression (Figure 3.13). Throughout this analysis, the relative proportions of TrkA<sup>+</sup>, TrkB<sup>+</sup> or TrkC<sup>+</sup> DRG neurons derived from contralateral NCCs (Figure 3.14 j-r) were indistinguishable from those derived from ipsilateral NCCs (Figure 3.14 a-i). The same principal results were consistently obtained by all three constructs (Figure 3.14 s-u). Furthermore, the neuron class composition of both ipsilaterally- and contralaterally-derived NCC progeny matched that characteristically found for *Isl1*<sup>+</sup> DRG neurons (Figure 3.14 s-u), together suggesting that contralaterally migrating NCCs lack a measurable bias towards generating particular DRG neuron classes.

In late-gestation embryos, DRG neurons of both ipsilateral and contralateral migratory streams would establish stereotypic laminar connectivity patterns according to their phenotypic profiles. In accordance to the Neurotrophin receptor quantification, the overall connectivity patterns established by contralaterally-derived *Isl1*<sup>Crest3+</sup> DRG neurons invariably matched those formed by ipsilaterally-derived *Isl1*<sup>Crest3+</sup> DRG neurons, with collaterals projecting to the dorsal horn, intermediate gray matter and the ventral horn of the spinal cord (Figure 3.15 a-b). Contralaterally-derived central afferents were terminating in laminae I-II predominantly targeted by the collaterals of nociceptive DRG neurons, laminae III-V preferentially targeted by low-threshold mechanoreceptive neurons, and laminae VI and IX targeted by proprioceptive neurons (Figure 3.15 c-e) (Brown, 1982; Lallemand and Ernfors, 2012).

**Figure 3.15: Central connectivity pattern of ipsilateral and contralateral NCC progeny in chick****Figure 3.15: Central connectivity pattern of ipsilateral and contralateral NCC progeny in chick**

(a-e) Central collateral projections established by ipsilaterally- and contralaterally-derived  $Isl1^{Crest3}$ -tagged DRG neurons in transverse spinal cord sections at E12. Overlay of  $Isl1^{Crest3}$ -driven mGFP in contralateral collaterals with pan-neuronal marker NeuN<sup>+</sup> neurons (b), TrkA<sup>+</sup> nociceptive collaterals and  $Isl1^{+}$  motor neurons in lamina IX and d3 interneurons (c) and with Lmx1b<sup>+</sup> laminae I-III neurons (d). TrkA<sup>+</sup> (e), but not mGFP<sup>+</sup> contralateral collaterals are biased to laminae I-II. Numbers indicate respective laminae. Note: compared to mammals, dorsal horn lamination in chick exhibits a mediolaterally rotated appearance. Dotted lines demarcate white (w) and gray (g) matter. DH, dorsal horn; VH, ventral horn; CC, central canal; asterisks, dorsal root entry zone and Lissauer's tract. Scale bar: 100  $\mu$ m.

(f-i) Comparative projection density maps of  $Isl1^{Crest3}$ -tagged ipsilaterally-derived (g), contralaterally-derived (h) or TrkA<sup>+</sup> nociceptive (i) axon collateral projections in the E12 dorsal horn. Average axon densities were established in serial transverse sections (n=18/8 sections/embryos), normalized and plotted as heat maps (red-blue: high-low axon density) (f). Ipsilateral and contralateral projections (g-h) are distributed among all laminae, whereas TrkA<sup>+</sup> projections (i) converge on laminae I-II. See Figure 3.18-3.20 for details on projection density map compositions.

(j) Comparative quantitative analysis of axon densities in laminae I-II versus laminae III-V. Slight bias of ipsilateral and contralateral mGFP<sup>+</sup> axons towards laminae III-V; marked bias of TrkA<sup>+</sup> projections towards laminae I-II. Data are presented as mean  $\pm$  SEM (two-tailed Student's *t* test with two samples and unequal variance). \*\*\*,  $p < 0.001$ ; ns, not significant,  $p > 0.05$ ; see Table 3.2 for statistical analysis.

In order to detect a small, but significant laminar bias of the overall connectivity patterns, projection density maps were performed (Figure 3.15 f). Herein, the amount of projections converging onto laminae I-II versus laminae III-V that extended from



ipsilaterally-derived  $Isl1^{Crest3+}$  DRG neurons (Figure 3.15 g and Figure 3.18), compared to those extending from contralaterally-derived  $Isl1^{Crest3+}$  neurons (Figure 3.15 h and Figure 3.19) or  $TrkA^+$  nociceptive neurons (Figure 3.15 i and Figure 3.20) was measured. Whereas the vast majority of  $TrkA^+$  collaterals exclusively targeted laminae I-II, both contralateral and ipsilaterally-derived  $Isl1^{Crest3}$ -tagged DRG neurons exhibited a slight bias towards laminae III-V (Figure 3.15 j).

**Figure 3.16: Peripheral collaterals of ipsilateral and contralateral NCC progeny in chick**

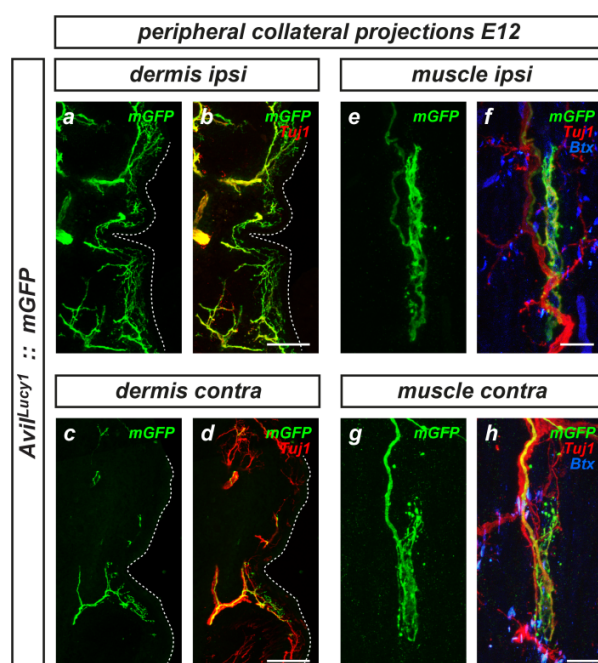


**Figure 3.16: Peripheral collaterals of ipsilateral and contralateral NCC progeny in chick**

(a-d) Peripheral projections established by ipsilaterally- and contralaterally-derived  $Avil^{Lucy1}$ -tagged DRG neurons form nociceptive and mechanoreceptive  $Tuj1^+$  ( $\beta$ III-tubulin) endings in transverse E12 skin sections. Dotted lines demarcate outer side. Scale bar: 100  $\mu$ m.

(e-h) Ipsilateral and contralateral  $Avil^{Lucy1}$ -tagged proprioceptive axons terminate in spindle receptor organs in longitudinal muscle sections at E12. Motor end plates are detected by Bungarotoxin (Btx).  $Tuj1$  labels both sensory and motor axons. Scale bar: 50  $\mu$ m.

In addition, the central connectivity patterns established by ipsilaterally- and contralaterally-derived DRG neurons were mirrored by the corresponding sensory end organ structures targeted by their  $Avil^{Lucy1+}$  peripheral collaterals, including presumptive nociceptive and mechanoreceptive endings in the skin (Figure 3.16 a-d) and muscle spindle receptors on intrafusal muscle fibers (Figure 3.16 e-h). Moreover, ipsilaterally and contralaterally migrating CAG-tagged NCCs contributed to several

other neuronal and non-neuronal NCC derivatives, including Schwann cells (Figure 3.17 a-d), skin melanocytes (Figure 3.17 e-h) and sympathetic ganglion neurons (Figure 3.17 i-l). Ipsilaterally and contralaterally migrating NCCs thus appear to give rise to an equivalent range of neuronal and non-neuronal derivatives.

**Figure 3.17: Ipsilateral and contralateral NCC derivatives in the periphery of chick embryos**

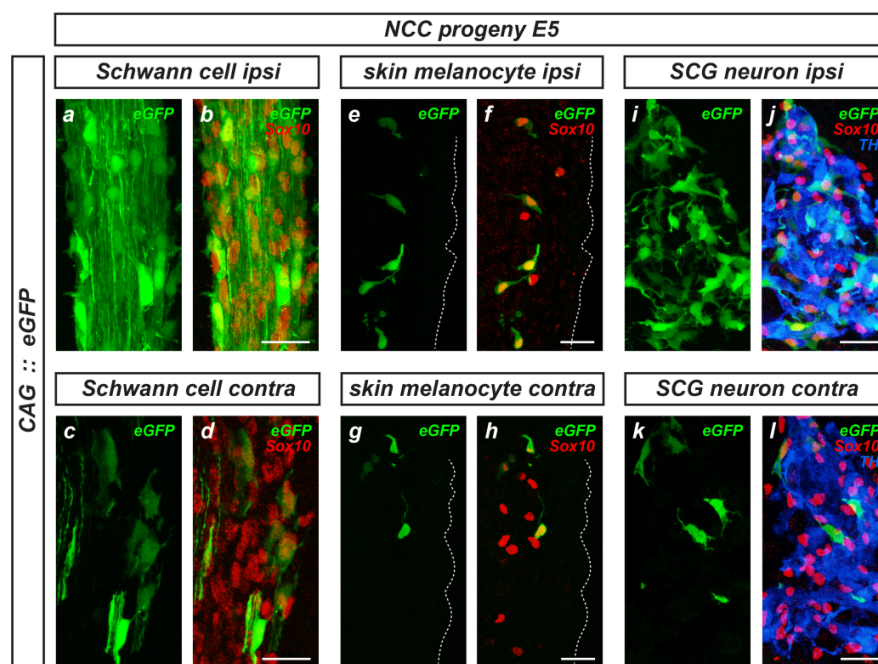


**Figure 3.17: Ipsilateral and contralateral NCC derivatives in the periphery of chick embryos**  
 (a-l) Ipsilateral and contralateral CAG-tagged NCC progeny include Sox10<sup>+</sup> Schwann cells (a-d), Sox10<sup>+</sup> skin melanocytes (e-h) and Sox10<sup>+</sup> TH<sup>+</sup> (tyrosine hydroxylase) sympathetic ganglion neurons (i-l) in transverse sections at E5. Dotted lines demarcate outer side. Scale bar: 25  $\mu$ m.

Using *STEVE*-based direct lineage-tracking and systematic analysis of NCC progeny and their connections in chick, the results provide conclusive evidence that primary somatosensory neurons derive from neurogenically equivalent ipsilaterally and contralaterally migrating NCCs.

**Figure 3.18: Projection density map of ipsilaterally-derived  $Isl1^{Crest3+}$  central collaterals in chick**

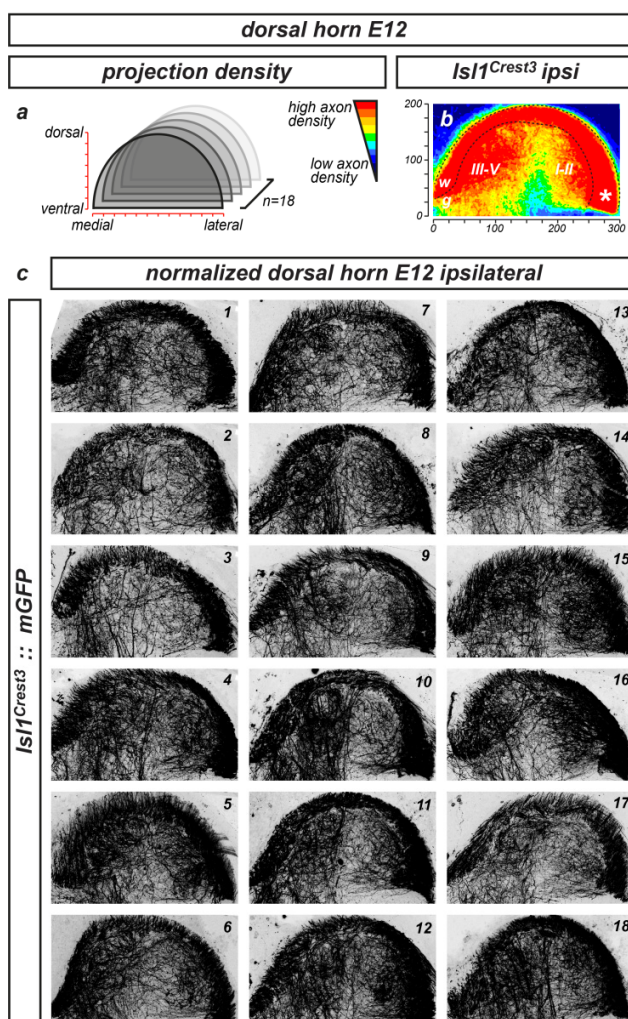


**Figure 3.18: Projection density map of ipsilaterally-derived  $Isl1^{Crest3+}$  central collaterals in chick**

**(a)** Average axon densities were established in serial transverse sections ( $n=18/8$  sections/embryos), normalized and plotted as heat maps (red-blue: high-low axon density).

**(b)** Heat map of  $mGFP^+$  central collaterals labeled by  $Isl1^{Crest3}$  transgene in ipsilateral E12 dorsal horn. Inner and outer dotted lines respectively delineate white (w) and gray (g) matter. Numbers indicate respective laminae. Asterisk, dorsal root entry zone and Lissauer's tract.

**(c)** Normalized raw image files of  $Isl1^{Crest3}$ -tagged central collaterals in ipsilateral E12 dorsal horn sections (1-18).



**Figure 3.19: Projection density map of contralaterally-derived  $Isl1^{Crest3+}$  central collaterals in chick**

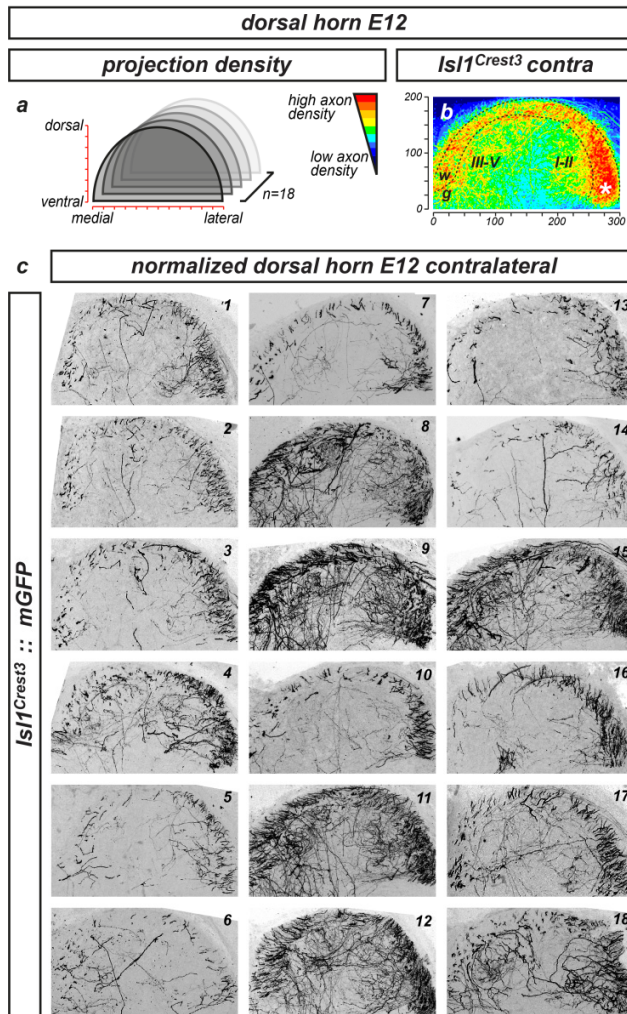


**Figure 3.19: Projection density map of contralaterally-derived  $Isl1^{Crest3+}$  central collaterals in chick**

(a) Average axon densities were established in serial transverse sections ( $n=18/8$  sections/embryos), normalized and plotted as heat maps (red-blue: high-low axon density).

(b) Heat map of  $mGFP^+$  central collaterals labeled by  $Isl1^{Crest3}$  transgene in contralateral E12 dorsal horn. Inner and outer dotted lines respectively delineate white (w) and gray (g) matter. Numbers indicate respective laminae. Asterisk, dorsal root entry zone and Lissauer's tract.

(c) Normalized raw image files of  $Isl1^{Crest3}$ -tagged central collaterals in contralateral E12 dorsal horn sections (1-18).

**Figure 3.20: Projection density map of TrkA<sup>+</sup> central collaterals in chick**

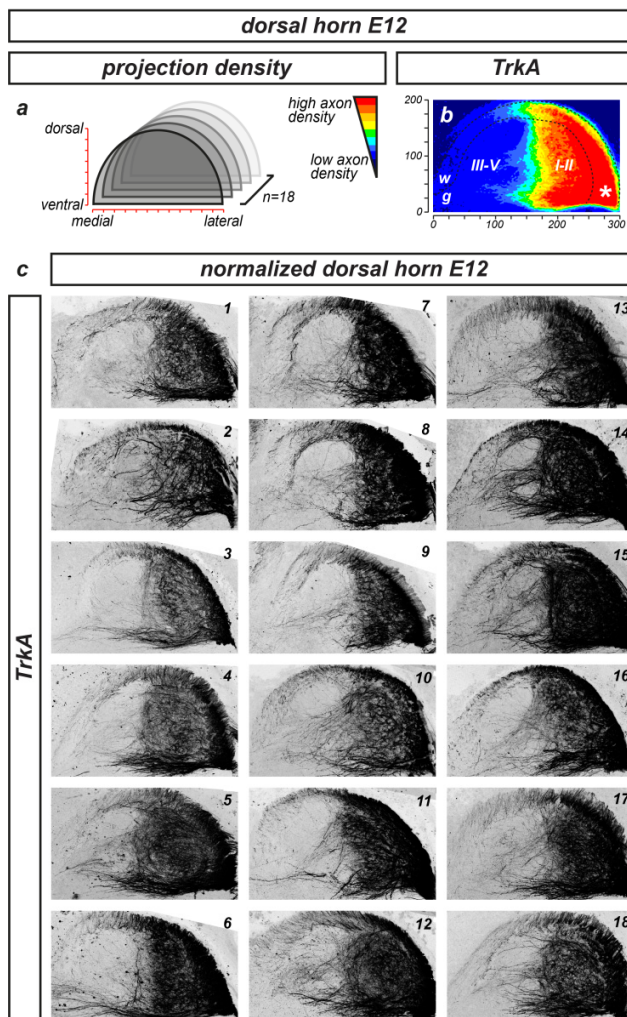


**Figure 3.20: Projection density map of TrkA<sup>+</sup> central collaterals in chick**

(a) Average axon densities were established in serial transverse sections (n=18/8 sections/embryos), normalized and plotted as heat maps (red-blue: high-low axon density).

(b) Heat map of TrkA<sup>+</sup> central collaterals in E12 dorsal horn. Inner and outer dotted lines respectively delineate white (w) and gray (g) matter. Numbers indicate respective laminae. Asterisk, dorsal root entry zone and Lissauer's tract.

(c) Normalized raw image files of TrkA<sup>+</sup> central collaterals in E12 dorsal horn sections (1-18).

**Table 3.2: Statistical analysis of ipsilateral and contralateral NCC progeny experiments**

DRG E9 colocalization analysis						
sensory lineage	mean [%]	SEM [%]	sections	cells	p value to Isl1	p value to contra
<i>TrkA colocalization / section</i>						
<i>Isl1</i>	81.26	2.39	10	2060		
<i>Isl1<sup>Crest3</sup> ipsi</i>	78.05	2.68	15	959	0.3801	0.8794
<i>Isl1<sup>Crest3</sup> contra</i>	77.35	4.89	22	514	0.3951	
<i>Avil<sup>Lucy1</sup> ipsi</i>	73.91	2.29	10	1097		0.6362
<i>Avil<sup>Lucy1</sup> contra</i>	75.80	3.18	10	204		
<i>CAG ipsi</i>	74.17	2.15	10	1089		0.6357
<i>CAG contra</i>	76.69	4.75	12	342		
<i>TrkB colocalization / section</i>						
<i>Isl1</i>	22.97	1.53	10	1698		
<i>Isl1<sup>Crest3</sup> ipsi</i>	19.80	1.21	19	898	0.1202	0.2491
<i>Isl1<sup>Crest3</sup> contra</i>	21.57	0.90	27	744	0.4417	
<i>Avil<sup>Lucy1</sup> ipsi</i>	22.25	1.07	10	694		0.6890
<i>Avil<sup>Lucy1</sup> contra</i>	24.28	4.84	12	180		
<i>CAG ipsi</i>	23.24	1.73	10	1335		0.9429
<i>CAG contra</i>	23.07	1.54	15	632		
<i>TrkC colocalization / section</i>						
<i>Isl1</i>	20.14	1.42	10	1981		
<i>Isl1<sup>Crest3</sup> ipsi</i>	19.07	1.78	13	502	0.6450	0.2035
<i>Isl1<sup>Crest3</sup> contra</i>	21.83	1.12	31	731	0.3594	
<i>Avil<sup>Lucy1</sup> ipsi</i>	19.71	1.45	10	975		0.4792
<i>Avil<sup>Lucy1</sup> contra</i>	22.88	4.13	14	272		
<i>CAG ipsi</i>	19.80	2.54	10	1094		0.9125
<i>CAG contra</i>	19.27	4.02	12	436		
dorsal horn E12 projection density analysis						
sensory lineage	mean [%]	SEM [%]	sections	p value laminae I-II / III-V		
<i>laminae I-II versus I-V projection density / section</i>						
<i>Isl1<sup>Crest3</sup> ipsi</i>	44.85	0.65	18	5.46 • 10 <sup>-13</sup>		
<i>Isl1<sup>Crest3</sup> contra</i>	48.10	1.37	18	0.057		
<i>TrkA</i>	75.07	0.58	18	2.12 • 10 <sup>-36</sup>		

**Table 3.2: Statistical analysis of ipsilateral and contralateral NCC progeny experiments**

Data of colocalization and projection density analysis are presented as the mean ± standard error of the mean (SEM). Statistical comparisons were established using a two-tailed Student's *t* test with two samples and unequal variance.



Although the role of *Ntng1* in sensory neurons remains unknown, one might speculate, based on previous observations in the brain, that *Ntng1*-NGL1 interactions could also have an impact on the establishment of somatosensory circuits (Woo *et al.*, 2009). The *Ntng1* gene locus was screened via *in silico* ECR analysis for a putative enhancer driving the sensory subtype-specific gene expression (Figure 3.21 a). One of the ECRs identified, *Ntng1<sup>Mech1</sup>*, located 2.6 kb upstream of the gene coding sequence in the chick, showed 86% and 83% homologies with the human and mouse sequences, respectively, and included 26 putative TFBS (Figure 3.21 b). In the human and the mouse genome the evolutionary conserved *Ntng1<sup>Mech1</sup>* was detected in the first intron region.

In order to analyze the potential enhancer activity of *Ntng1<sup>Mech1</sup>*, the ECR was coupled to *STEVE* and tested for the spatial and temporal expression pattern in both early and late stages of the somatosensory lineage. *Ntng1<sup>Mech1</sup>* consistently labeled a population of large-diameter sensory neurons confined to the ventrolateral portion of the DRGs (Figure 3.22 a-b), in contrast to the pan-sensory reporter gene expression driven by *Isl1<sup>Crest3</sup>* (Figure 3.22 c-d). Thereby, *Ntng1<sup>Mech1</sup>* appeared to reflect the endogenous *Ntng1* expression pattern in somatosensory neurons observed by other groups (Yin *et al.*, 2002; [www.brain-map.org](http://www.brain-map.org)). The earliest activity of *Ntng1<sup>Mech1</sup>* in somatosensory neurons could be detected after E6, while high-level expression persisted from E9 to at least until hatching. An additional activity was observed in a small subset of ventral interneurons in the spinal cord after E5. The central afferents of *Ntng1<sup>Mech1</sup>*-labeled sensory neurons displayed a highly restricted projection pattern confined to the medial dorsal horn of the spinal cord (Figure 3.22 e-f), in contrast to *Isl1<sup>Crest3+</sup>* central collaterals occupying all laminae of the dorsal horn, as well as the intermediate and ventral spinal cord (Figure 3.22 g-h). At E7, the first detectable *Ntng1<sup>Mech1+</sup>* centrally projecting axons assumed a medial position within the dorsal funiculus and segregated from laterally positioned *TrkA<sup>+</sup>* nociceptive projections prior to entering the spinal cord gray matter (compare Figure 3.23 a-b and i-j). By E9, *Ntng1<sup>Mech1+</sup>* axons penetrated the dorsal gray matter, but remained confined within the medioventral quadrant of the dorsal horn, while *TrkA<sup>+</sup>* nociceptive afferents began occupying most of the lateral portion of the dorsal horn gray matter (Figure 3.23 c-d). At the same time, *Isl1<sup>Crest3+</sup>* nociceptive and mechanoreceptive afferents projected throughout the dorsal horn,



whereas *Isl1<sup>Crest3</sup>*-labeled proprioceptive collaterals occupied the intermediate and ventral spinal cord (Figure 3.23 k-l and Figure 3.6 c-d).

**Figure 3.22: Selective tagging of a somatosensory neuron subtype by *Ntng1<sup>Mech1</sup>* in chick**

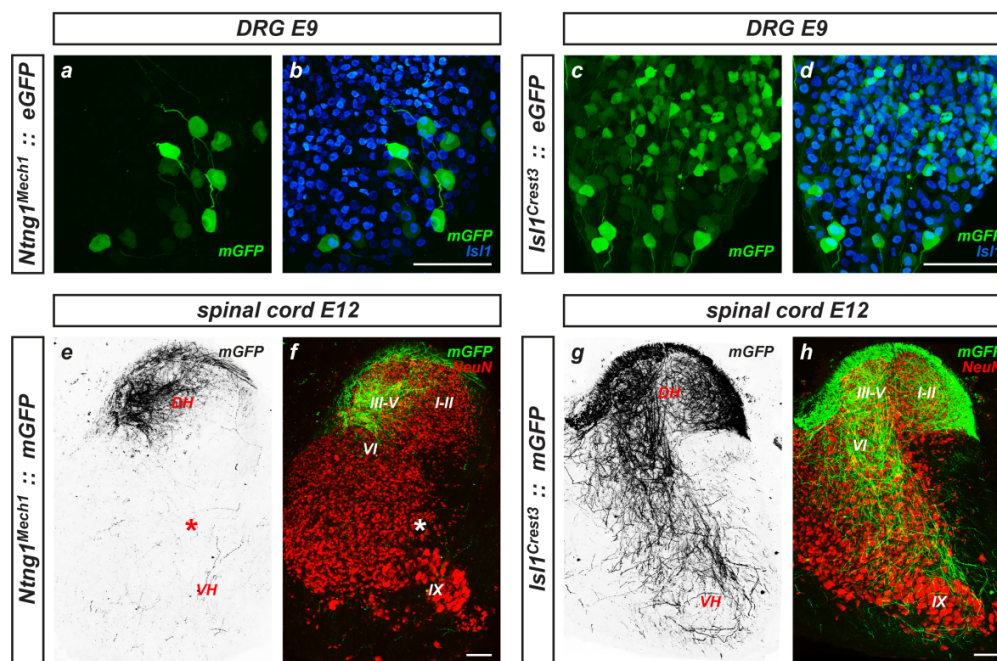
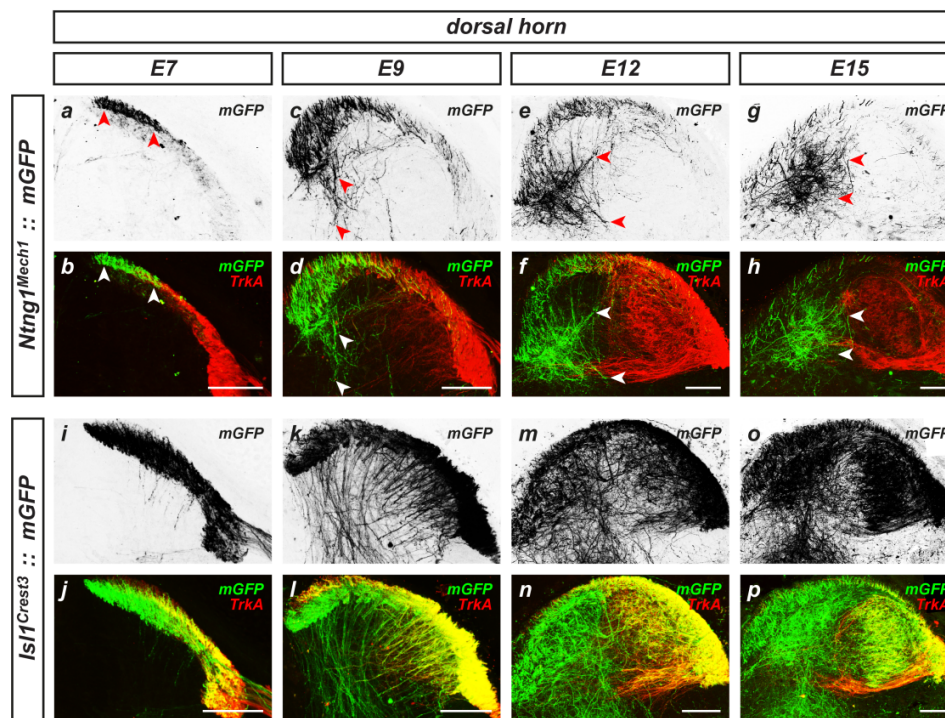


**Figure 3.22: Selective tagging of a somatosensory neuron subtype by *Ntng1<sup>Mech1</sup>* in chick**  
**(a-d)** *Ntng1<sup>Mech1</sup>* enhancer activity selectively drives reporter gene expression in large-diameter ventrolateral dorsal root ganglion (DRG) neurons **(a-b)**, compared to *Isl1<sup>Crest3</sup>*-driven GFP expression in all somatosensory neuron types **(c-d)** in transverse sections at E9. *Isl1*, pan-DRG neuron marker. Scale bar: 100  $\mu$ m.  
**(e-g)** *Ntng1<sup>Mech1+</sup>* central collaterals project to the medioventral dorsal horn in transverse sections at E12 **(e-f)**. Additional low *Ntng1<sup>Mech1</sup>* activity is detected in ventral interneurons (asterisks). In contrast, *Isl1<sup>Crest3+</sup>* central collaterals occupy all laminae of the dorsal horn, as well as the intermediate and ventral spinal cord **(g-h)**. *NeuN<sup>+</sup>* neurons outline spinal cord gray matter. Numbers indicate respective laminae. DH, dorsal horn; VH, ventral horn. Scale bar: 100  $\mu$ m.

Between E12 and E15, *Ntng1<sup>Mech1+</sup>* axons converged onto an increasingly condensed zone within the medioventral quadrant of the dorsal horn, which remained largely unoccupied by *TrkA<sup>+</sup>* nociceptive projections (compare Figure 3.23 e-h and m-p). The identified *Ntng1<sup>Mech1</sup>* thus has been shown to drive specific expression in a subset of somatosensory neurons, whose central collaterals occupied a central termination zone distinct from that occupied by nociceptive or proprioceptive afferents. Based on their large soma size, their defined ventrolateral position in the DRG, and their discrete

central afferent termination pattern in the dorsal horn,  $Ntng1^{Mech1+}$  neurons showed initial characteristics of low-threshold mechanoreceptors (LTMRs).

**Figure 3.23: Development of  $Ntng1^{Mech1+}$  central afferent projections in chick**

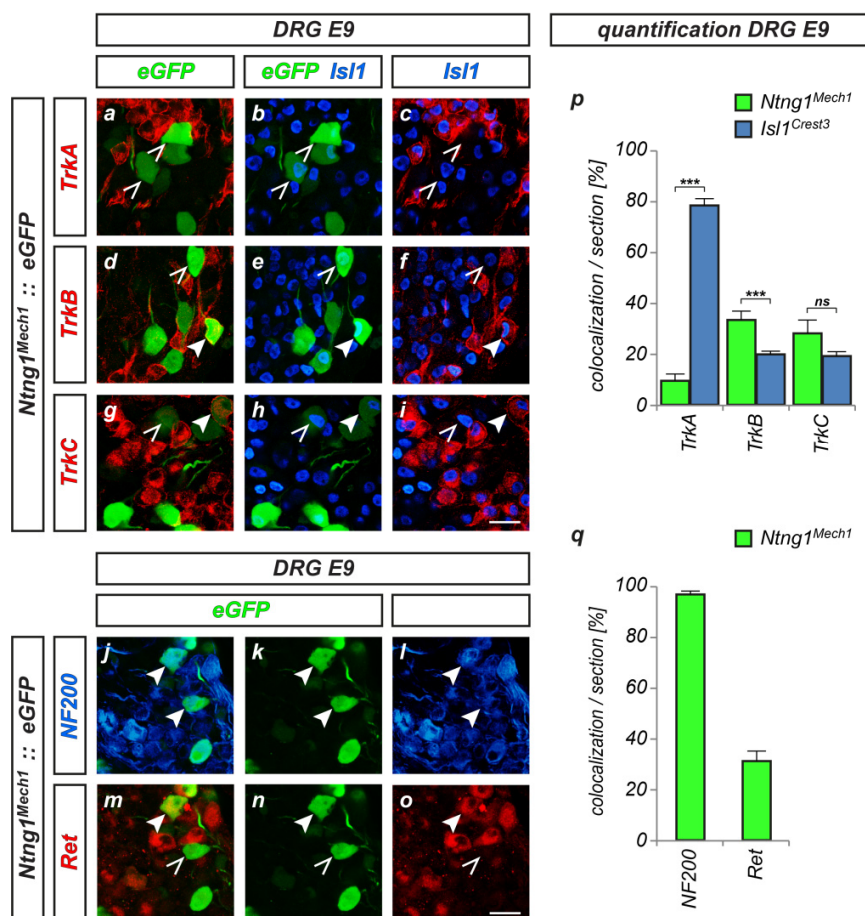


**Figure 3.23: Development of  $Ntng1^{Mech1+}$  central afferent projections in chick**

(a-h) Development of  $Ntng1^{Mech1+}$  central collaterals throughout gestation in transverse dorsal horn sections from E7 to E15.  $Ntng1^{Mech1+}$  projections (arrowheads) segregate from  $TrkA^+$  nociceptive afferents and remain confined in the medioventral quadrant of the dorsal horn. Scale bar: 100  $\mu$ m.

(i-p) Development of  $Isl1^{Crest3+}$  central collaterals throughout gestation in transverse dorsal horn sections from E7 to E15.  $Isl1^{Crest3+}$  collaterals project throughout the dorsal horn including nociceptive, mechanoreceptive and proprioceptive trajectories.  $TrkA^+$  nociceptive sensory axons overlap with  $Isl1^{Crest3+}$  axons. Scale bar: 100  $\mu$ m.

For a more detailed analysis, the relative proportions of Neurotrophin receptors expressing neurons tagged by  $Ntng1^{Mech1}$  compared to  $Isl1^{Crest3}$ -tagged neurons were scored. Herein, the three major classes of DRG neurons expressing  $TrkA$ ,  $TrkB$  and  $TrkC$  mainly correspond to nociceptive neurons, subtypes of LTMR neurons and proprioceptive neurons, respectively (Figure 3.24 a-i) (Lewin and Moshourab, 2004; Marmigère and Ernfor, 2007).

Figure 3.24: Molecular analysis of *Ntng1<sup>Mech1+</sup>* somatosensory neurons in chickFigure 3.24: Molecular analysis of *Ntng1<sup>Mech1+</sup>* somatosensory neurons in chick

(a-h) E9 transverse sections of Neurotrophin receptor (Trk) class expression in *Ntng1<sup>Mech1+</sup>* DRG neurons. Closed arrowheads: co-expression. Open arrowheads: no co-expression. *Isl1*, pan-DRG neuron marker. Scale bar: 25  $\mu$ m.

(j-o) Co-expression analysis of *Ntng1<sup>Mech1+</sup>* DRG neurons with myelination marker NF200 and Ret in E9 transverse sections. Scale bar: 25  $\mu$ m.

(p) Quantitative analysis: proportions of *Ntng1<sup>Mech1+</sup>* and *Isl1<sup>Crest3+</sup>* E9 DRG neurons expressing TrkA, TrkB or TrkC display significant differences. Data are presented as mean  $\pm$  SEM (two-tailed Student's *t* test with two samples and unequal variance). \*\*\*,  $p < 0.001$ ; ns, not significant,  $p > 0.05$ ; see Table 3.3 for statistical analysis.

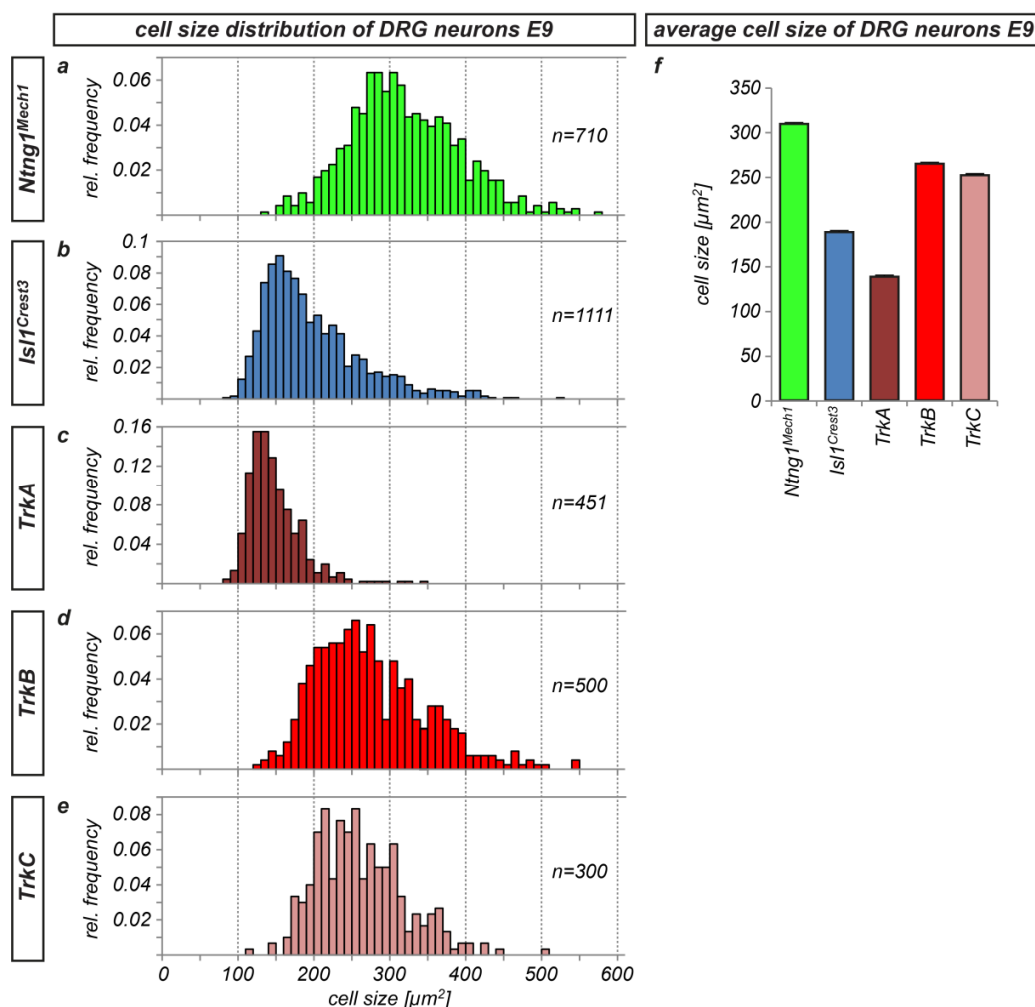
(q) Quantitative analysis: proportions of *Ntng1<sup>Mech1+</sup>* E9 DRG neurons expressing NF200 and Ret. Data are presented as mean  $\pm$  SEM. See Table 3.3 for statistical analysis.

Around  $78.05 \pm 2.68$  % of *Isl1<sup>Crest3</sup>*-tagged DRG neurons were *TrkA<sup>+</sup>* (Figure 3.24 p), which matches the proportion of *TrkA<sup>+</sup>* neurons in total *Isl1<sup>+</sup>* DRG neurons (Figure 3.14 s), and that typically found in the DRGs of adult mammals (Fariñas *et al.*, 1998; Marmigère and Ernfors, 2007). In contrast, only  $9.44 \pm 2.67$  % of *Ntng1<sup>Mech1+</sup>*



DRG neurons expressed the nociceptive marker TrkA (Figure 3.24 p). At the same time,  $Ntng1^{Mech1+}$  neurons contained markedly higher proportions of  $TrkB^+$  and  $TrkC^+$  neurons with  $33.24 \pm 3.45 \%$  and  $27.98 \pm 5.22 \%$ , respectively, compared to  $Isl1^{Crest3+}$ -tagged sensory neurons with  $19.80 \pm 1.21 \%$  and  $19.07 \pm 1.78 \%$ , respectively (Figure 3.24 p). In agreement with previous data, the cumulative proportion of  $TrkA^+$ ,  $TrkB^+$  and  $TrkC^+$  neurons scored in total or  $Isl1^{Crest3+}$  DRG neurons amounted to more than 100%, reflecting the presence of sensory neurons co-expressing more than one class of Trk receptors (Fariñas *et al.*, 1998). Taking this into account, a considerable portion of  $Ntng1^{Mech1+}$  neurons appeared to express neither Trk receptor class, which would be in congruence with the molecularly identified  $earlyRet^+$  population of LTMR neurons in mouse (Bourane *et al.*, 2009; Luo *et al.*, 2009). Therefore, the  $Ntng1^{Mech1+}$ -tagged DRG neurons were analyzed for co-expression with the myelination marker NF200, as well as with Ret, a newly identified marker predominantly labeling rapidly adapting LTMRs and subtypes of nociceptive neurons (Figure 3.24 j-o) (Bourane *et al.*, 2009; Luo *et al.*, 2009). The vast majority of  $Ntng1^{Mech1+}$  sensory neurons were  $NF200^+$  ( $96.42 \pm 1.35 \%$ ), whereas only  $31.04 \pm 3.95 \%$  co-expressed Ret (Figure 3.24 q). According to the obtained molecular marker profile,  $Ntng1^{Mech1+}$  neurons thus partially separate from  $Ret^+$  and  $Trk^+$  mechanoreceptive populations, and appear to selectively tag a molecularly not-yet-identified subtype of A $\beta$ -LTMRs.

Since the specification of sensory neuron classes is associated with characteristic differences in their cell soma sizes, the distribution of soma sizes of  $Ntng1^{Mech1+}$  neurons, compared to  $Isl1^{Crest3+}$  neurons, as well as those of  $TrkA^+$ ,  $TrkB^+$  and  $TrkC^+$  neurons were measured (Figure 3.25).  $Ntng1^{Mech1+}$  neurons showed a marked bias towards the largest DRG neuron sizes with an average soma size area of  $309.09 \pm 2.72 \mu m^2$  (Figure 3.25 a, f). Furthermore, the distribution of  $Ntng1^{Mech1+}$  cell sizes clearly segregated from the overall distribution of  $Isl1^{Crest3+}$  soma sizes with an average of  $188.27 \pm 1.98 \mu m^2$  (Figure 3.25 b, f), and from that of the small-diameter  $TrkA^+$  neurons with an average of  $138.43 \pm 1.65 \mu m^2$  (Figure 3.25 c, f). In contrast,  $Ntng1^{Mech1+}$  neuron soma sizes partially overlapped with those of  $TrkB^+$  and  $TrkC^+$  neurons with  $264.54 \pm 3.24 \mu m^2$  and  $251.54 \pm 3.36 \mu m^2$ , respectively (Figure 3.25 d-f). The large soma size of DRG neurons tagged by  $Ntng1^{Mech1+}$  was thus in congruence with their A $\beta$ -LTMR-specific molecular marker profile.

Figure 3.25: Morphological analysis of *Ntng1<sup>Mech1+</sup>* somatosensory neurons in chickFigure 3.25: Morphological analysis of *Ntng1<sup>Mech1+</sup>* somatosensory neurons in chick

(a-e) Cell size distribution of *Ntng1<sup>Mech1+</sup>* DRG neurons displays a bias towards the largest cell soma sizes (n=710) (a), compared to *Isl1<sup>Crest3+</sup>* (n=1111) (b), *TrkA<sup>+</sup>* (n=451) (c), and partial similarity with large-size *TrkB<sup>+</sup>* (n=500) (d), and *TrkC<sup>+</sup>* neurons (n=300) (e). Cell size area was obtained by cell border determination of neurons with clear morphology and visible nucleus in transverse section of E9 DRGs. (f) Corresponding average cell sizes of GFP- and Trk-labeled E9 DRG neuron populations. Data are presented as mean ± SEM. See Table 3.3 for statistical analysis.

Both adult and embryonic nociceptive and mechanoreceptive sensory neurons can be distinguished by their electrophysiological properties, including characteristic action potential waveforms (Koerber *et al.*, 1988; Djouhri *et al.*, 1998; Fang *et al.*, 2005). Mechanoreceptors typically fire narrow uninflected spikes with short half peak durations (HPDs) and short afterhyperpolarization (AHP) durations (Figure 3.26 a), whereas nociceptors fire action potentials that exhibit a ‘hump’ on the falling phase

and have very long HPDs and AHP durations (Figure 3.26 b) (Lechner *et al.*, 2009). Via whole cell patch clamp recordings in dissociated E9 DRG neurons, which were performed in collaboration with Stefan G. Lechner and Gary R. Lewin at the 'Max-Delbrück-Center for Molecular Medicine' in Berlin, the firing properties of  $Ntng1^{Mech1+}$  compared to  $Isl1^{Crest3+}$  sensory neurons were monitored. Action potentials evoked by current injection of patched  $Ntng1^{Mech1+}$  neurons displayed short HPDs ( $1.55 \pm 0.11$  ms) and AHPs ( $3.92 \pm 0.25$  ms) (Figure 3.26 e-f, h), which were characteristic for mechanoreceptors.  $Isl1^{Crest3+}$  neurons, marking all sensory neuron subtypes, displayed a considerably wider range of HPD and AHP values, including both nociceptor- and mechanoreceptor-specific types of action potentials (Figure 3.26 e-f). Herein, the average HPD of  $2.50 \pm 0.18$  ms and average AHP duration of  $6.74 \pm 0.84$  ms evoked from  $Isl1^{Crest3+}$  neurons was significantly higher than from  $Ntng1^{Mech1+}$ -tagged neurons (Figure 3.26 h).  $Ntng1^{Mech1+}$  neurons therefore represent a discrete population of sensory neurons with spike characteristics typical of embryonic mechanoreceptors.

LTMRs can be further distinguished by the feature of a rapid and highly sensitive mechanosensitive current, which appears as soon as they innervate their peripheral targets (Lechner *et al.*, 2009). Adult and embryonic LTMRs possess a so-called RA-mechanosensitive current, which is a mechanically activated inward current that activates and inactivates within a few milliseconds (Figure 3.26 c) (Drew *et al.*, 2002; Hu and Lewin, 2006; Lechner *et al.*, 2009). RA-mechanosensitive currents are also found in nociceptors, but the majority of nociceptors exhibit much slower inactivating IA and SA-currents (Figure 3.26 d). By investigating mechanosensitive currents  $Ntng1^{Mech1+}$  neurons exclusively displayed RA-currents with an average inactivation time of  $1.28 \pm 0.32$  ms, whereas  $Isl1^{Crest3+}$  neurons exhibited both RA- and IA-currents with an average inactivation time of  $7.36 \pm 1.46$  ms (Figure 3.26 g-h). Consistent with previous observations showing that SA-currents appear very late in mouse DRG, SA-currents were absent from chick E9 nociceptors (Lechner *et al.*, 2009).

**Figure 3.26: Electrophysiological analysis of *Ntng1*<sup>Mech1+</sup> somatosensory neurons in chick I**

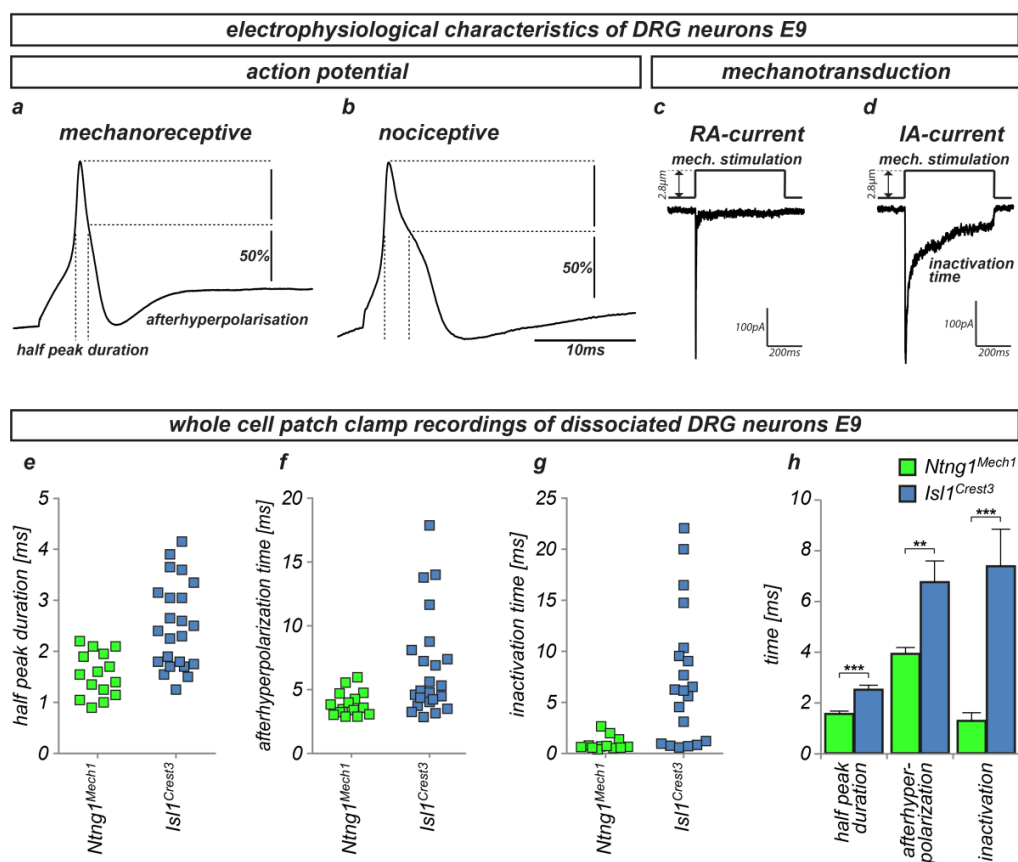


**Figure 3.26: Electrophysiological analysis of *Ntng1*<sup>Mech1+</sup> somatosensory neurons in chick I**

(a-d) Examples of mechanoreceptive (a) and nociceptive (b) action potentials show characteristic differences in action potential shape, half peak duration, and afterhyperpolarization. Examples of mechanotransduction currents typically elicited in mechanoreceptors (RA current) (c) and nociceptors (IA current) (d) display differences in the inactivation time after mechanical stimulation. Examples are obtained from whole cell patch clamp recordings in dissociated E9 DRG neurons in chick.

(e-g) Whole cell patch clamp recordings in *Ntng1*<sup>Mech1+</sup> and *Isl1*<sup>Crest3</sup>-labeled dissociated E9 DRG neurons. *Ntng1*<sup>Mech1+</sup> E9 sensory neurons display a narrow range of short half peak duration (e), short afterhyperpolarization time (f) and fast inactivation time (g), compared to the wide range of *Isl1*<sup>Crest3</sup>-tagged sensory neurons.

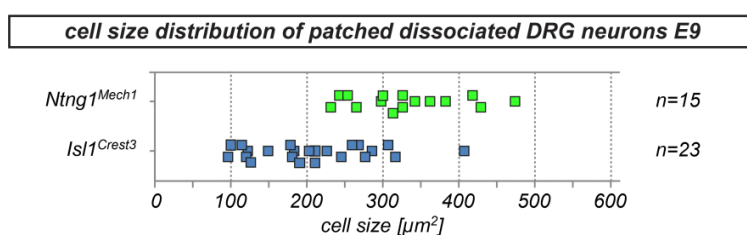
(h) Average of half peak duration, afterhyperpolarization time and inactivation time display significant differences between *Ntng1*<sup>Mech1+</sup> and *Isl1*<sup>Crest3+</sup> sensory neurons. Data are presented as mean ± SEM (two-tailed Student's *t* test with two samples and unequal variance). \*\*\*, *p*<0.001; \*\*, *p*<0.005; see Table 3.4 for statistical analysis.

Electrophysiological measurements were performed in collaboration with Stefan G. Lechner and Gary R. Lewin at the 'Max-Delbrück-Center for Molecular Medicine' in Berlin.

For electrophysiological measurements, *Ntng1*<sup>Mech1+</sup> and *Isl1*<sup>Crest3+</sup> neurons spanning the whole range of their cell size distribution were selected (compare Figure 3.27 and

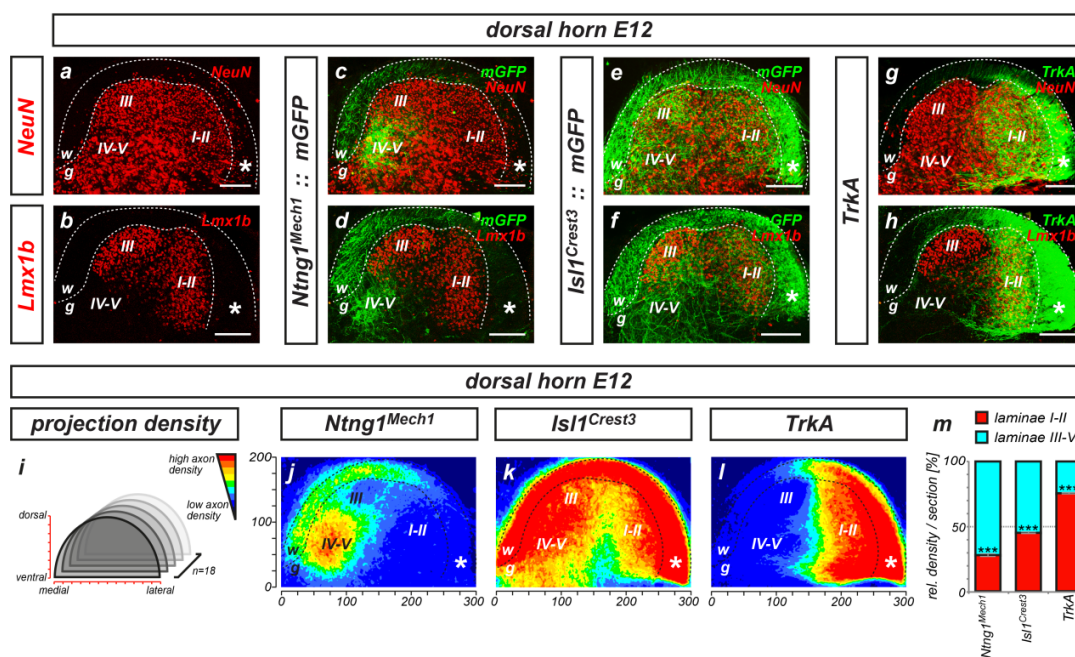
Figure 3.25 a-b).  $Ntng1^{Mech1+}$  neurons thus represent a discrete population of somatosensory neurons with functional properties characteristic for LTMRs, including narrow uninflected action potentials with short HPDs, short AHPs and RA-mechanosensitive currents.

**Figure 3.27: Electrophysiological analysis of  $Ntng1^{Mech1+}$  somatosensory neurons in chick II**



**Figure 3.27: Electrophysiological analysis of  $Ntng1^{Mech1+}$  somatosensory neurons in chick II**  
 Selected  $Ntng1^{Mech1+}$  neurons (n=15) and  $Isl1^{Crest3+}$  neurons (n=23) for electrophysiological measurements span the whole range of their cell size distribution (compare with Figure 3.25 a-b). Electrophysiological measurements were performed in collaboration with Stefan G. Lechner and Gary R. Lewin at the 'Max-Delbrück-Center for Molecular Medicine' in Berlin.

In mammals, the majority of nociceptive afferents connect to relay neurons within the most superficial laminae I and II of the dorsal horn, while LTMRs mainly terminate throughout the successively deeper laminae II (inner) and V, and proprioceptive afferents extend their axons in laminae VI and XI of the intermediate and ventrolateral gray matter (Brown, 1982; Lallemand and Ernfor, 2012). Unlike in mammals, the dorsal horn in chick displays a mediolaterally rotated appearance, with neurons expressing the laminae I-III marker  $Lmx1b$  respectively clustering into a lateral (laminae I-II) and a smaller mediodorsal crescent-shaped domain (lamina III) in the dorsal horn (Figure 3.28 a-b) (Rebelo *et al.*, 2010; Wild *et al.*, 2010). In order to obtain more precise information, the stereotypic laminar connectivity pattern established by  $Ntng1^{Mech1+}$  DRG neurons was compared with  $Isl1^{Crest3+}$  and  $TrkA^+$  central afferent projections. The vast majority of  $TrkA^+$  nociceptive projections into the dorsal horn gray matter concentrated within the lateral  $Lmx1b^+$  domain, while excluding the mediodorsal  $Lmx1b^+$  crescent (Figure 3.28 g-h), suggesting that the latter corresponds to lamina III, while the former corresponds to laminae I-II (Eide and Glover, 1997; Wild *et al.*, 2010).

Figure 3.28: Central connectivity pattern of  $Ntng1^{Mech1+}$  somatosensory neurons in chickFigure 3.28: Central connectivity pattern of  $Ntng1^{Mech1+}$  somatosensory neurons in chick

(a-h) Central collateral projections established by  $Ntng1^{Mech1+}$ ,  $Isl1^{Crest3+}$  and  $TrkA^+$  DRG neurons in transverse dorsal horn sections at E12. The discrete laminae in the chick dorsal horn can be distinguished by  $Lmx1b$  which labels laminae I-II on the lateral site and lamina III on the mediodorsal site (a-b).  $Ntng1^{Mech1+}$  afferents terminate in a definite domain ventrally of lamina III, presumably in laminae IV-V (c-d), compared to  $Isl1^{Crest3+}$  projections occupying all termination zones in the dorsal horn (e-f). Nociceptive  $TrkA^+$  projections converge in laminae I-II (g-h). NeuN labels all neurons of the dorsal horn gray matter. Note: compared to mammals, dorsal horn lamination in chick exhibits a mediolaterally rotated appearance. Numbers indicate respective laminae. Dotted lines demarcate white (w) and gray (g) matter. Asterisks, dorsal root entry zone and Lissauer's tract. Scale bar: 100  $\mu$ m.

(i-l) Comparative projection density maps of  $Ntng1^{Mech1+}$  (j),  $Isl1^{Crest3+}$  (k) or  $TrkA^+$  nociceptive (l) axon collateral projections in the E12 dorsal horn. Average axon densities were established in serial transverse sections ( $n=18/8$  sections/embryos), normalized and plotted as heat maps (red-blue: high-low axon density) (i).  $Ntng1^{Mech1+}$  projections (j) converge within a medioventral quadrant of the dorsal horn (laminae IV-V), whereas  $Isl1^{Crest3+}$  projections (k) are distributed among all laminae and  $TrkA^+$  projections (l) on laminae I-II. See Figure 3.18, 3.20 and 3.29 for details on projection density map compositions.

(m) Comparative quantitative analysis of axon densities in laminae I-II versus laminae III-V. Marked bias of  $Ntng1^{Mech1+}$  axons towards laminae III-V, in contrast to slight bias of  $Isl1^{Crest3+}$  axons towards laminae III-V and marked bias of  $TrkA^+$  projections towards laminae I-II. Data are presented as mean  $\pm$  SEM (two-tailed Student's  $t$  test with two samples and unequal variance). \*\*\*,  $p < 0.001$ ; see Table 3.4 for statistical analysis.

In accordance to previous obtained observations,  $Isl1^{Crest3+}$  axons projected throughout the dorsal horn (Figure 3.28 e-f), while  $Ntng1^{Mech1+}$  afferents converged within an oval shaped domain in the medioventral quadrant of the dorsal horn that excluded the mediodorsal  $Lmx1b^+$  crescent (Figure 3.28 c-d). Therefore,  $Ntng1^{Mech1+}$  afferents are suggested to terminate mainly in laminae IV-V, as there are currently no markers available in chick to discriminate these laminae further. The significant laminar bias towards laminae IV-V of  $Ntng1^{Mech1}$ -tagged central collaterals was further confirmed by projection density maps of the overall connectivity pattern (Figure 3.28 j, m and Figure 3.29). In contrast, only a slight bias of  $Isl1^{Crest3+}$  axons towards laminae III-V (Figure 3.28 k, m and Figure 3.18), and a marked bias of  $TrkA^+$  nociceptive projections towards laminae I-II was detected (Figure 3.28 l-m and Figure 3.20). Thus,  $Ntng1^{Mech1}$  defines a novel subtype of LTMRs whose central collaterals exclude laminae III and selectively terminate within a medioventral domain of the dorsal horn presumably corresponding to laminae IV-V.

The *in silico*-to-*in vivo* ECR screen in combination with the stable expression system *STEVE* facilitates identification and comprehensive analysis of late-onset somatosensory-specific genetic markers inaccessible to previous methods. Thereby, a novel molecularly defined subset of somatosensory neurons labeled by  $Ntng1^{Mech1}$  was uncovered, whose molecular (Trk, Ret, NF200 expression), morphological (soma size), electrophysiological (action potential wave form), functional (mechanotransduction current) and anatomical (central connectivity) characteristics correspond to a discrete subclass of A $\beta$ -LTMRs.

**Figure 3.29: Projection density map of  $Ntng1^{Mech1+}$  central collaterals in chick**

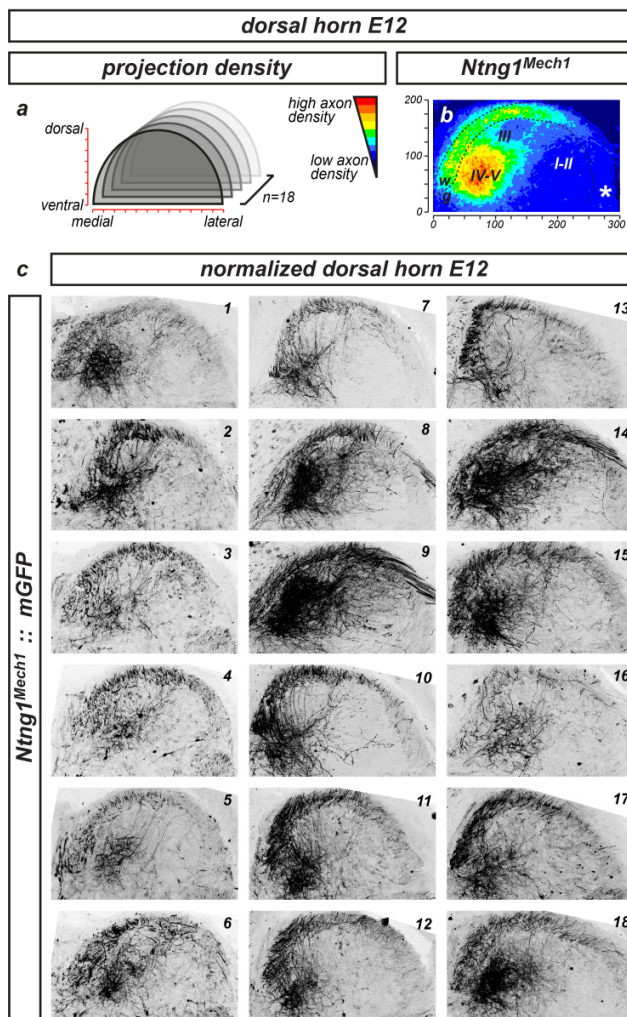


**Figure 3.29: Projection density map of  $Ntng1^{Mech1+}$  central collaterals in chick**

(a) Average axon densities were established in serial transverse sections ( $n=18/8$  sections/embryos), normalized and plotted as heat maps (red-blue: high-low axon density).

(b) Heat map of  $mGFP^+$  central collaterals labeled by  $Ntng1^{Mech1}$  transgene in E12 dorsal horn. Inner and outer dotted lines respectively delineate white (w) and gray (g) matter. Numbers indicate respective laminae. Asterisk, dorsal root entry zone and Lissauer's tract.

(c) Normalized raw image files of  $Ntng1^{Mech1+}$ -tagged central collaterals in E12 dorsal horn sections (1-18).



**Table 3.3: Statistical analysis of *Ntng1<sup>Mech1</sup>* colocalization and cell size experiments**

DRG E9 colocalization analysis					
sensory lineage	mean [%]	SEM [%]	sections	cells	p value to <i>Isl1<sup>Crest3</sup></i>
<i>TrkA</i> colocalization / section					
<i>Ntng1<sup>Mech1</sup></i>	9.44	2.67	19	192	$1.33 \cdot 10^{-6}$
<i>Isl1<sup>Crest3</sup></i>	78.05	2.68	15	959	
<i>TrkB</i> colocalization / section					
<i>Ntng1<sup>Mech1</sup></i>	33.24	3.45	40	340	0.0006
<i>Isl1<sup>Crest3</sup></i>	19.80	1.21	19	898	
<i>TrkC</i> colocalization / section					
<i>Ntng1<sup>Mech1</sup></i>	27.98	5.22	19	178	0.1208
<i>Isl1<sup>Crest3</sup></i>	19.07	1.78	13	502	
<i>NF200</i> colocalization / section					
<i>Ntng1<sup>Mech1</sup></i>	96.42	1.35	11	276	
<i>Ret</i> colocalization / section					
<i>Ntng1<sup>Mech1</sup></i>	31.04	3.95	11	276	
DRG E9 cell size analysis					
sensory lineage	mean [ $\mu\text{m}^2$ ]	SEM [ $\mu\text{m}^2$ ]	cells		
cell size average					
<i>Ntng1<sup>Mech1</sup></i>	309.09	2.72	710		
<i>Isl1<sup>Crest3</sup></i>	188.27	1.98	1111		
<i>TrkA</i>	138.43	1.65	451		
<i>TrkB</i>	264.54	3.24	500		
<i>TrkC</i>	251.75	3.36	300		

**Table 3.3: Statistical analysis of *Ntng1<sup>Mech1</sup>* colocalization and cell size experiments**

Data of colocalization and cell size analysis are presented as the mean  $\pm$  standard error of the mean (SEM). Statistical comparisons were established using a two-tailed Student's *t* test with two samples and unequal variance.

**Table 3.4: Statistical analysis of *Ntng1<sup>Mech1</sup>* electrophysiology and projection density experiments**

DRG E9 electrophysiology analysis				
sensory lineage	mean [ms]	SEM [ms]	cells	p value to <i>Isl1<sup>Crest3</sup></i>
<i>half peak duration</i>				
<i>Ntng1<sup>Mech1</sup></i>	1.55	0.11	15	$1.33 \cdot 10^{-6}$
<i>Isl1<sup>Crest3</sup></i>	2.50	0.18	23	
<i>afterhyperpolarization time</i>				
<i>Ntng1<sup>Mech1</sup></i>	3.92	0.25	15	0.0034
<i>Isl1<sup>Crest3</sup></i>	6.74	0.84	23	
<i>inactivation time</i>				
<i>Ntng1<sup>Mech1</sup></i>	1.28	0.32	12	0.0006
<i>Isl1<sup>Crest3</sup></i>	7.36	1.46	20	
dorsal horn E12 projection density analysis				
sensory lineage	mean [%]	SEM [%]	sections	p value laminae I-II / III-V
<i>laminae I-II versus I-V projection density / section</i>				
<i>Ntng1<sup>Mech1</sup></i>	27.84	1.12	18	$1.33 \cdot 10^{-6}$
<i>Isl1<sup>Crest3</sup></i>	44.85	0.65	18	$5.46 \cdot 10^{-13}$
<i>TrkA</i>	75.07	0.58	18	$2.12 \cdot 10^{-36}$

**Table 3.4: Statistical analysis of *Ntng1<sup>Mech1</sup>* electrophysiology and projection density experiments**

Data of electrophysiology and projection density analysis are presented as the mean  $\pm$  standard error of the mean (SEM). Statistical comparisons were established using a two-tailed Student's *t* test with two samples and unequal variance.

### 3.6. Overall organization of somatosensory central collaterals in chick

The combination of *STEVE*-mediated somatosensory-specific genetic markers with unbiased tagging of contralateral somatosensory neurons affords selective tracing of central afferent projections throughout the whole embryonic development, unobstructed by additional sites of labeling in the spinal cord. A further benefit is the comparatively sparse axonal labeling originating from small numbers of contralaterally transfected sensory neurons, which can be tuned to allow visualization of individual axon collaterals – a highly useful feature for the development of single neuron connectivity (Chen AI *et al.*, 2006; Jefferis and Livet, 2012). In order to establish the overall central connectivity pattern in chick, trajectories of individual afferent collaterals originating from sparsely labeled  $Isl1^{Crest3+}$ ,  $Avil^{Lucy1+}$  and  $Ntng1^{Mech1+}$  contralateral somatosensory neurons were traced and analyzed in detail.

Central afferents were categorized as following: nociceptive ( $Isl1^{Crest3+} TrkA^+$  collaterals), mechanoreceptive ( $Isl1^{Crest3+} TrkA^-$  collaterals terminating in the dorsal horn), ‘laminae IV-V’ mechanoreceptive ( $Ntng1^{Mech1+}$  collaterals) and proprioceptive ( $Isl1^{Crest3+} TrkA^-$  collaterals terminating in the intermediate and ventrolateral gray matter) (Figure 3.30 a-f). In agreement with previous observations, the dorsal horn in chick displays a mediolateral rotation, compared to the mammalian dorsal horn organization (Figure 3.30 g-h) (Brown, 1982; Rebelo *et al.*, 2010; Wild *et al.*, 2010). The majority of nociceptive collaterals appeared to directly terminate within laminae I-II upon entering the gray matter via the lateral funiculus/Lissauer’s tract (Figure 3.30 a and Figure 3.31 e-g). In addition, subsets of  $TrkA^+$  afferents projected medially along the ventral border of the dorsal horn before veering dorsally along the medial border of laminae I-II, or further medially towards the dorsal funiculus (Figure 3.30 b and Figure 3.31 h-j). This consistent observation apparently revealed a part of a yet uncharted ‘nociceptive tract’ (Figure 3.31 a-d) (Davis *et al.*, 1989; Guo *et al.*, 2011). Both mechanoreceptive and proprioceptive projections entered the medial dorsal horn through the dorsal funiculus, while avoiding laminae I-II (Figure 3.30 c-f). Thereby, most of mechanoreceptor collaterals directly terminated in laminae III-V proximal to their funicular point of entry (Figure 3.30 c and Figure 3.32 a-c).

Figure 3.30: Trajectories of individual molecularly defined central collaterals in chick

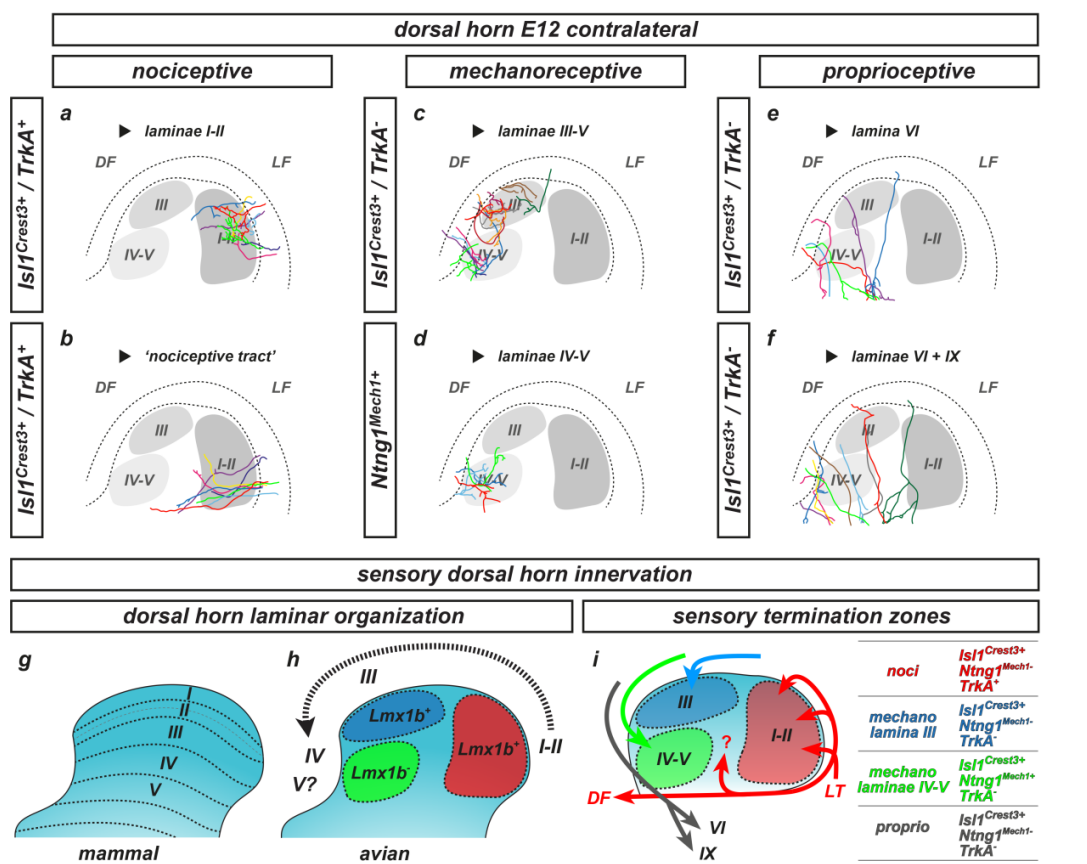


Figure 3.30: Trajectories of individual molecularly defined central collaterals in chick

(a-f) Reconstructed collaterals of individually traced contralateral somatosensory neurons by combinatorial labeling with  $Isl1^{Crest3+}$ ,  $Ntng1^{Mech1}$  and TrkA are superimposed on relative positions of laminae I-V in E12 dorsal horn. The majority of nociceptive ( $Isl1^{Crest3+} TrkA^+$  to laminae I-II) (a), mechanoreceptive ( $Isl1^{Crest3+} TrkA^+$  to laminae III-V) (c), 'laminae IV-V' mechanoreceptive ( $Ntng1^{Mech1+}$  to laminae IV-V) (d) and proprioceptive ( $Isl1^{Crest3+} TrkA^+$  to laminae VI and IX) (e-f) collaterals chose direct trajectories to target laminae. Dotted lines demarcate white and gray matter. Numbers indicate respective laminae. DF, dorsal funiculus; LF, lateral funiculus.

(g-i) Compared to dorsal horn laminar organization in mammals (g), the dorsal horn in avians displays a mediolaterally rotated appearance of distinct laminae (h), confirmed by laminae I-III marker  $Lmx1b$ . Summary of sensory trajectories displays direct laminae targeting in the chick dorsal horn of individual molecularly defined central collaterals in subtype-specific termination zones (i). Numbers indicate respective laminae. LT, Lissauer's tract; interrogation mark, unknown termination.

Consistently, the majority of 'laminae IV-V' mechanoreceptor afferents directly projected to their termination zone ventral to lamina III in the dorsal horn, while collaterals branching to both laminae III and IV-V was rarely observed (Figure 3.30 d and Figure 3.32 d-f).

Figure 3.31: Trajectory tracings of nociceptive central afferents in chick

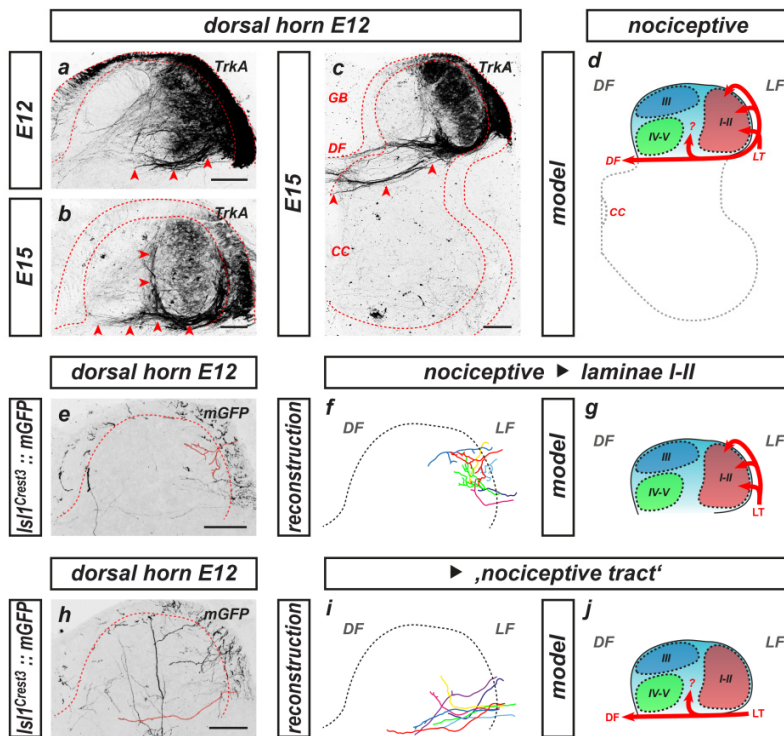
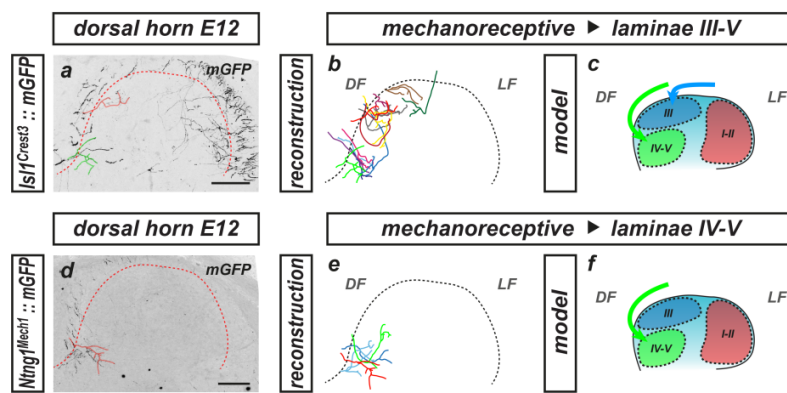


Figure 3.31: Trajectory tracings of nociceptive central afferents in chick

(a-d)  $TrkA^+$  nociceptive axons enter the gray matter of the dorsal horn via the lateral funiculus (LF) and target directly within laminae I-II in transverse dorsal horn sections at E12 and E15. A subset of these collaterals project medially along the ventral border of the dorsal horn (arrowheads) (a), or further towards the dorsal funiculus (DF), as part of a 'nociceptive tract' (arrowheads) (b-c). A summarized model of nociceptive afferents is shown in (d). Inner and outer dotted lines respectively delineate white and gray matter. Numbers indicate respective laminae. LT, Lissauer's tract, GB, glycogen body; CC, central canal; interrogation mark, unknown termination. Scale bar: 100  $\mu$ m.

(e-g) Example of an individual nociceptive afferent by contralaterally-derived  $Isl1^{Crest3+}$  sensory neurons in transverse E12 dorsal horn sections (e), a trajectory reconstruction of different sections (f) and a summarized model of nociceptive afferents entering the dorsal horn via the LF and terminating in laminae I-II (g). Dotted lines differentiate white and gray matter. Scale bar: 100  $\mu$ m.

(h-j) Example of an individual nociceptive afferent by contralaterally-derived  $Isl1^{Crest3+}$  sensory neurons in transverse E12 dorsal horn sections (h), a trajectory reconstruction of different sections (i) and a summarized model of nociceptive afferents projecting from the LF along the 'nociceptive tract' (j). Scale bar: 100  $\mu$ m.

**Figure 3.32: Trajectory tracings of mechanoreceptive central afferents in chick****Figure 3.32: Trajectory tracings of mechanoreceptive central afferents in chick**

(a-c) Example of two individual mechanoreceptive afferents by contralaterally-derived  $Is1^{Crest3+}$  sensory neurons in transverse E12 dorsal horn sections (a), a trajectory reconstruction of different sections (b) and a summarized model of mechanoreceptive afferents projecting from the dorsal funiculus (DF) to laminae III-V (c). Dotted lines differentiate white and gray matter. Numbers indicate respective laminae. LF, lateral funiculus. Scale bar: 100  $\mu$ m.

(d-f) Example of an individual mechanoreceptive afferent by contralaterally-derived  $Ntn1^{Mech1+}$  sensory neurons in transverse E12 dorsal horn sections (d), a trajectory reconstruction of different sections (e) and a summarized model of mechanoreceptive afferents entering the dorsal horn via the DF and terminating exclusively in laminae IV-V (f). Scale bar: 100  $\mu$ m.

Finally, proprioceptive collaterals transited the gray matter by projecting throughout the medial half of the dorsal horn, while neither type Ia nor type Ib/II afferents show differences regarding the position of their funicular entry points, or the angle of their initial trajectories (Figure 3.30 e-f and Figure 3.33 a-f). Furthermore, in analogy to previous observations, proprioceptive afferents showed an extensive axon branching along their trajectories before establishing their final connectivity in laminae VI and IX (Figure 3.33 g-n) (Chen *et al.*, 2006). Additionally,  $Is1^{Crest3-}$  and  $Avi^{Lucy1-}$ -tagged contralaterally-derived central afferent projections were mapped throughout gestation and reflected the established developmental sequence of somatosensory collateral extension into the spinal cord gray matter (Figure 3.34).

These observations thus support the long-standing idea that afferent connectivity in the spinal cord is established by a majority of central afferent collaterals that directly home in on their respective target zones (Figure 3.30 i) (Fitzgerald, 1987; Davis *et al.*, 1989; Ozaki and Snider, 1997; Redmond *et al.*, 1997; Fitzgerald, 2005).

Figure 3.33: Trajectory tracings of proprioceptive central afferents in chick

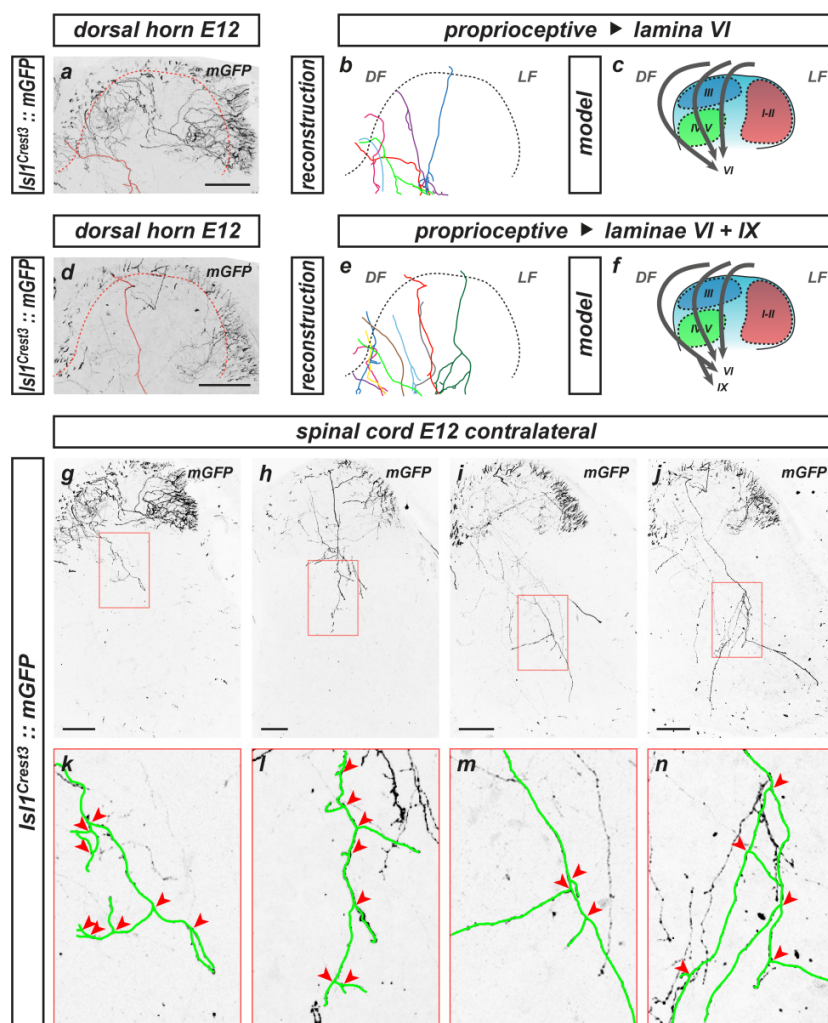


Figure 3.33: Trajectory tracings of proprioceptive central afferents in chick

(a-c) Example of an individual proprioceptive afferent by contralaterally-derived  $Isl1^{Crest3+}$  sensory neurons in transverse E12 dorsal horn sections (a), a trajectory reconstruction of different sections (b) and a summarized model of proprioceptive afferents projecting throughout the dorsal funiculus (DF) only to lamina VI (c). Dotted lines differentiate white and gray matter. Numbers indicate respective laminae. LF, lateral funiculus. Scale bar: 100  $\mu$ m.

(d-f) Example of an individual proprioceptive afferent by contralaterally-derived  $Isl1^{Crest3+}$  sensory neurons in transverse E12 dorsal horn sections (d), a trajectory reconstruction of different sections (e) and a summarized model of proprioceptive afferents projecting throughout the DF to lamina VI and lamina IX (f). Scale bar: 100  $\mu$ m.

(g-n) Sparse central afferent axon labeling by contralaterally-derived  $Isl1^{Crest3+}$ -labeled sensory neurons in transverse E12 spinal cord sections facilitates delineation of single axon projections (g-j). Detailed view of proprioceptive afferents (outlined in green) shows an extensive axon branching along their trajectories (arrowheads) (k-n). Scale bar: 100  $\mu$ m.



Figure 3.34: Tagging of contralateral central collaterals throughout gestation in chick

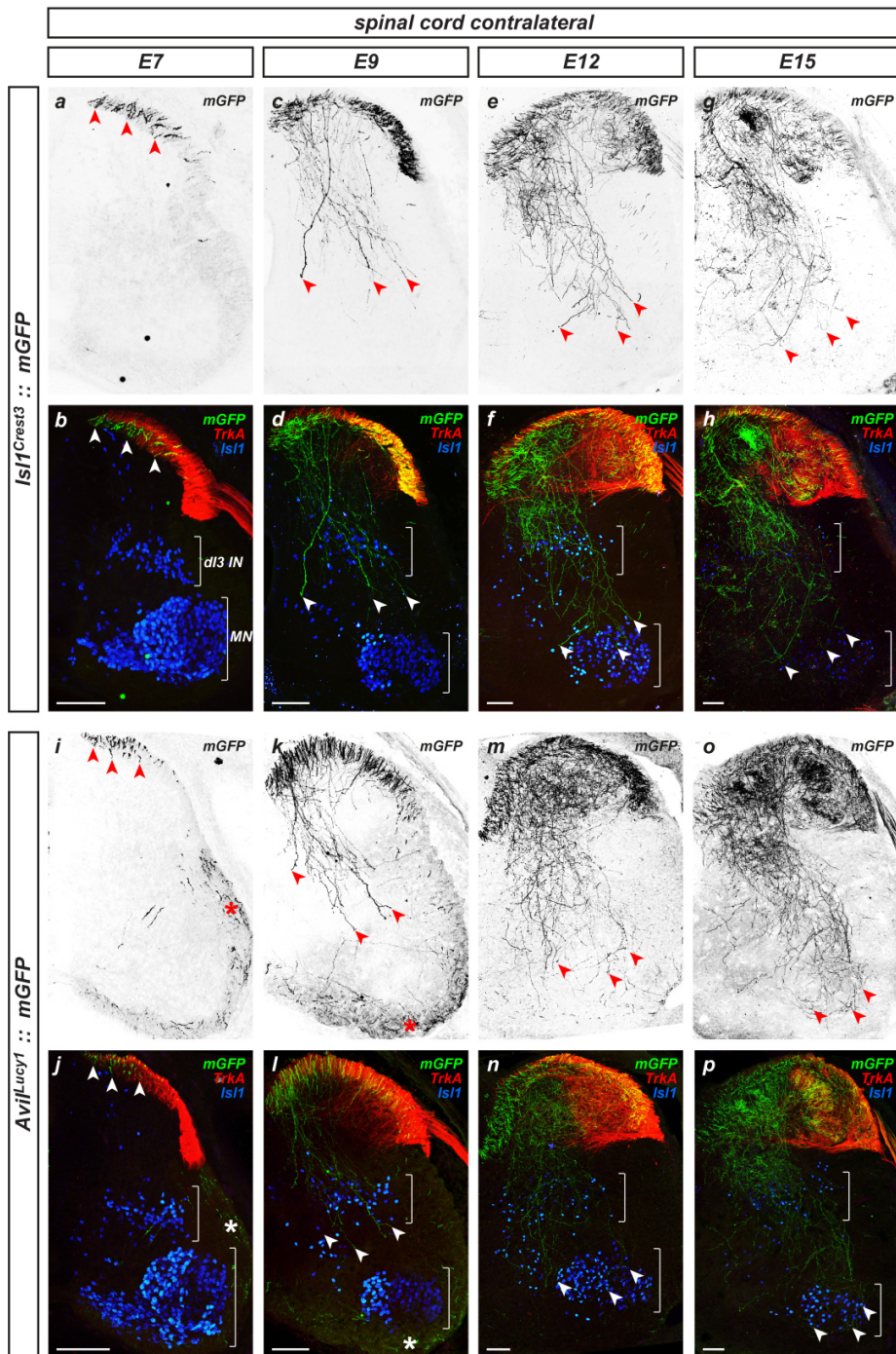


**Figure 3.34: Tagging of contralateral central collaterals throughout gestation in chick**  
 (a-p) Genetic tagging of contralateral central afferent projections by *Isl1<sup>Crest3</sup>* (a-h) and *Avil<sup>Lucy1</sup>* (i-p) throughout gestation in transverse sections from E7 to E15. Proprioceptive afferents are indicated by arrowheads, nociceptive sensory axons are labeled by TrkA, motor neurons (MN) and dorsal interneurons (dI3 IN) by Isl1. Asterisks, mGFP<sup>+</sup> ipsilateral commissural projections. Scale bar: 100  $\mu$ m.



### 3.7. Peripheral connectivity of *Ntng1*<sup>Mech1+</sup> somatosensory neurons

The topographic arrangement of sensory subtype-specific central connectivity in the dorsal horn of the spinal cord is expected to be reflected by the innervation of corresponding sensory end organs in defined regions in the periphery (Arber, 2012). Different types of functionally specialized LTMRs along with their corresponding receptor end organs in the skin encode the different qualities of touch (Li *et al.*, 2011). In mammals, rapidly adapting (RA) A $\beta$ -LTMRs innervate hair follicles, Meissner corpuscles and Pacinian corpuscles, that selectively respond to hair deflection and to low and high-frequency vibration, respectively (Lewin and Moshourab, 2004; Lumpkin *et al.*, 2010). Slowly adapting (SA) A $\beta$ -LTMRs terminate in Merkel discs and Ruffini corpuscles, which relay static responses to dermal stretch and indentation (Lewin and Moshourab, 2004; Lumpkin *et al.*, 2010). Pacinian corpuscles and Merkel cells are present in both glabrous and hairy skin. In contrast, Meissner corpuscles and Ruffini corpuscles are exclusively found in glabrous skin, whereas hair follicles are restricted to hairy skin. It is therefore possible to differentiate LTMRs due to their peripheral innervation of distinct morphologically unique end organs and their characteristic physiological properties. Although sensory end organs are well documented in mammals, there is only limited information on avian mechanoperception. In birds, two main types of mechanoreceptors transduce information: Herbst and Merkel corpuscles (Gottschaldt 1985; Necker 2000). The most common and widely distributed Herbst corpuscle, which is considered to resemble the Pacinian corpuscle of mammals, is sensitive to vibration and acceleration (Gottschaldt, 1985; Necker, 2000). Herbst corpuscles are thought to form terminal arborizations in the collar region of most feather follicles and to terminate in the dermis of glabrous skin in digits (Duc *et al.*, 1993). In contrast, Merkel cell receptors, which respond to pressure, are primarily found in featherless skin of avians and differ from Merkel cell-neurite complexes in mammals by accumulating and forming rudimentary Meissner-like corpuscles (Winkelmann and Myers, 1961; Duc *et al.*, 1993; Necker, 2000; Halata *et al.*, 2003). Unlike in mammals, Merkel corpuscles in chick are exclusively found in the superficial layer of the dermis, while the epidermis does not contain any nerve endings (Halata *et al.*, 2003). On the basis of electrophysiological studies, the literature is so far not

conclusive in ranking Herbst and Merkel corpuscles among defined RA or SA modalities (Necker, 1985; Gentle, 1989; Necker, 1990; Duc *et al.*, 1993).

**Figure 3.35: Analysis of  $Ntng1^{Mech1+}$  peripheral collaterals in chick glabrous skin**

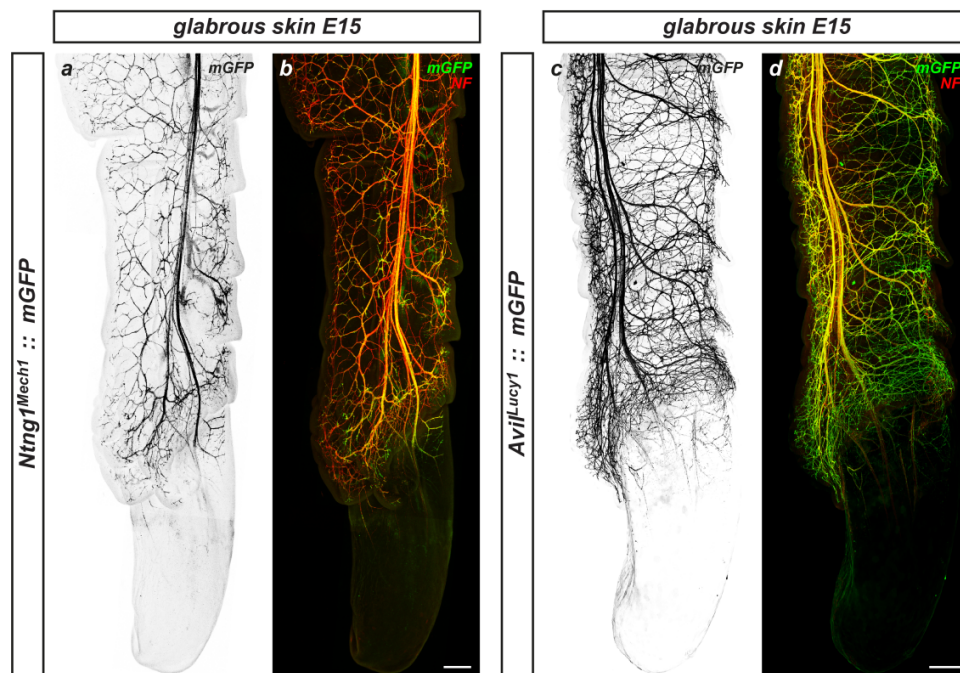


**Figure 3.35: Analysis of  $Ntng1^{Mech1+}$  peripheral collaterals in chick glabrous skin**  
**(a-d)** Genetic tagging of peripheral afferent projections by  $Ntng1^{Mech1}$  and  $Avil^{Lucy1}$  in digits at E15.  $Ntng1^{Mech1+}$  peripheral somatosensory afferents display a subtype-specific innervation of glabrous skin in the digit **(a-b)**, in contrast to highly complex innervation of  $Avil^{Lucy1+}$  somatosensory neurons including all mechanoreceptive and nociceptive subtypes **(c-d)**. Neurofilament (NF) labels total sensory projections. Scale bar: 200  $\mu\text{m}$ .

$Ntng1^{Mech1}$  appears to define a subset of LTMRs, whose central connectivity is restricted to laminae IV-V of the dorsal horn. In order to determine whether  $Ntng1^{Mech1+}$  and  $Ntng1^{Mech1-}$  neurons are tuned to specific mechanosensory submodalities and terminate in different sensory end organs in the dermis, the peripheral innervation of  $Ntng1^{Mech1+}$  DRG neurons was analyzed. In consistence with labeling central collaterals,  $Ntng1^{Mech1}$ -tagged peripheral projections were observed at different developmental stages at least until hatching. At E15,  $Ntng1^{Mech1+}$  peripheral sensory afferents displayed a subtype-specific innervation of the glabrous skin in digits (Figure 3.35 a-b), in contrast to the widely distributed and highly complex innervation of robustly labeled sensory projections by the pan-somatosensory marker  $Avil^{Lucy1}$

(Figure 3.35 c-d). No specific innervation of  $Ntng1^{Mech1+}$  LTMRs was detected in feathery skin of the hindlimb or the dorsal trunk (Figure 3.36 a-b), whereas  $Isl1^{Crest3-}$  tagged peripheral afferents were highly accumulated in collar regions of feather follicles and displayed a typical sensory innervation of feathery skin (Figure 3.36 c-d). Since  $Ntng1^{Mech1}$  did not drive expression in proprioceptive neurons, no musculature innervation of  $Ntng1^{Mech1+}$  peripheral collaterals could be observed.

**Figure 3.36: Analysis of  $Ntng1^{Mech1+}$  peripheral collaterals in chick feathery skin**

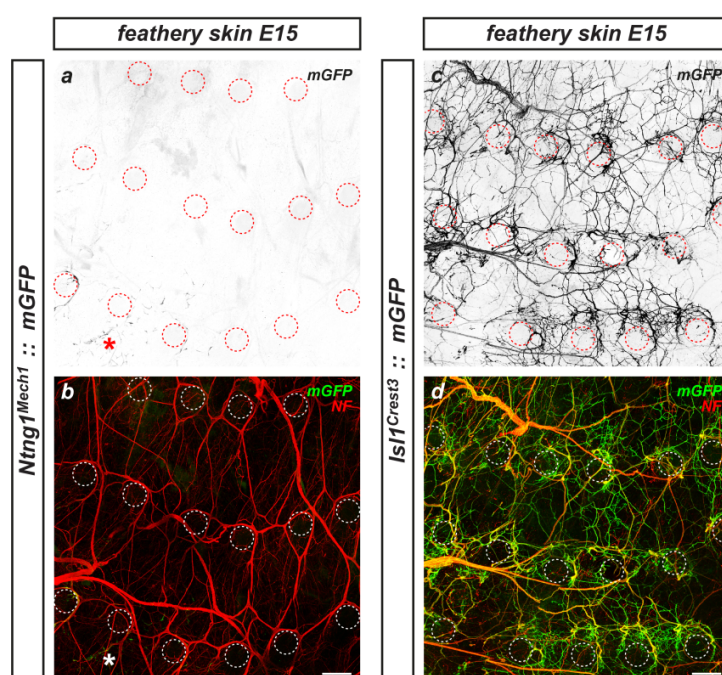


**Figure 3.36: Analysis of  $Ntng1^{Mech1+}$  peripheral collaterals in chick feathery skin**

(a-d) Genetic tagging of peripheral afferent projections by  $Ntng1^{Mech1}$  and  $Isl1^{Crest3}$  in the dorsal trunk at E15. No specific innervation of  $Ntng1^{Mech1+}$  peripheral afferents is detected in feathery skin (a-b). Sparse non-specific mGFP expression is detected in limited regions (asterisks). Peripheral projections labeled by pan-somatosensory marker  $Isl1^{Crest3}$  highly accumulate in collar regions of feather follicles (dotted lines) (c-d).  $Isl1^{Crest3+}$  axons show complete overlap with neurofilament (NF) illustrating a typical sensory skin innervation. Scale bar: 200  $\mu$ m.

Both of the main mechanoreceptor end organs, Herbst and Merkel corpuscles, are present in chick glabrous skin. In order to obtain more precise information, whether  $Ntng1^{Mech1+}$  DRG neurons terminate in a discrete sensory end organ, the peripheral innervation was analyzed morphologically in more detail. At E12,  $Ntng1^{Mech1+}$  peripheral endings were visualized in the plantar and scaly glabrous skin of the digits,

but no obvious end organ structures could be identified (Figure 3.37). At the latest analyzed embryonic stage, E19, *Ntn1*<sup>Mech1</sup>-tagged peripheral afferents were observed to project in dermal papillae in the plantar skin of the digits (Figure 3.38 a). Herein, *Ntn1*<sup>Mech1+</sup> peripheral endings appeared to terminate in rudimentary Meissner-form structures (Figure 3.38 b-c), which are suggested to correspond to a subset of chick Merkel corpuscles (Winkelman and Myers, 1961; Duc *et al.*, 1993). *Ntn1*<sup>Mech1</sup>-labeled peripheral afferents were also detected in scaly skin of the digits, but the sensory innervation could not be determined morphologically (data not shown). At the same time, *Avil*<sup>Lucy1</sup>-driven reporter gene expression in mechanoreceptive and nociceptive peripheral projections was detected in dermal papillae and other dermal regions of the glabrous skin in digits (Figure 3.38 d-f). In analogy with previous observations, no intraepidermal termination of sensory axons was observed in chick (Figure 3.38) (Halata *et al.*, 2003).

**Figure 3.37: Analysis of *Ntn1*<sup>Mech1+</sup> peripheral terminations in chick glabrous skin at E12**

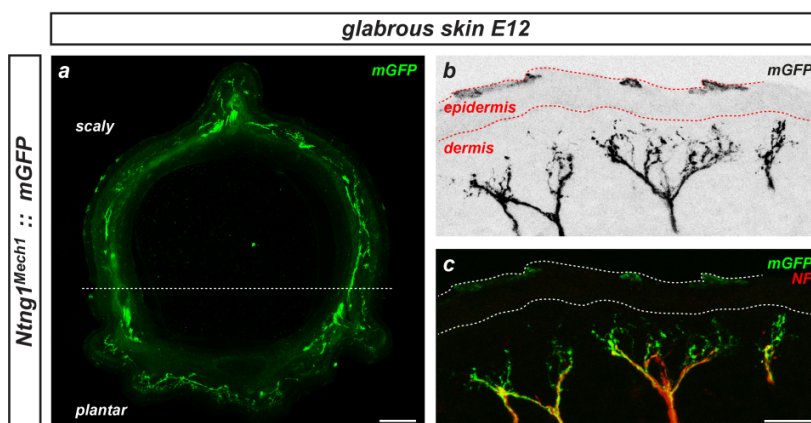


**Figure 3.37: Analysis of *Ntn1*<sup>Mech1+</sup> peripheral terminations in chick glabrous skin at E12**

(a-c) Visualization of *Ntn1*<sup>Mech1+</sup> peripheral endings in plantar and scaly glabrous skin of digits in transverse E12 sections (a). Dotted line differentiates plantar and scaly glabrous skin of the digit. Scale bar: 100  $\mu\text{m}$ . Detailed view does not reveal obvious receptor end organ structures at E12 (b-c). Neurofilament (NF) labels total sensory projections. Dotted lines demarcate epidermis and dermis. Scale bar: 25  $\mu\text{m}$ .

Altogether, *STEVE*-mediated stable genetic tagging of individual sensory subtypes and their circuits enables visualization and precise analysis of both central and peripheral connectivity in the chick primary somatosensory system. The peripheral innervation of *Ntn1*<sup>Mech1+</sup> A $\beta$ -LTMRs was exclusively found in glabrous skin, possibly

terminating in rudimentary Meissner-like corpuscles, which are primarily found in featherless skin of avians. Whether *Ntng1<sup>Mech1+</sup>*-tagged peripheral termination is indeed restricted to Meissner-like corpuscles or whether *Ntng1<sup>Mech1+</sup>* projections alternatively or additionally display a topographic ('distal-versus-proximal-limb') innervation pattern not strictly adhering to one specific LTRM type, could not be conclusively determined. Since Herbst corpuscles are also present in glabrous skin this needs to be further addressed.

**Figure 3.38: Analysis of *Ntng1<sup>Mech1+</sup>* peripheral terminations in chick glabrous skin at E19**

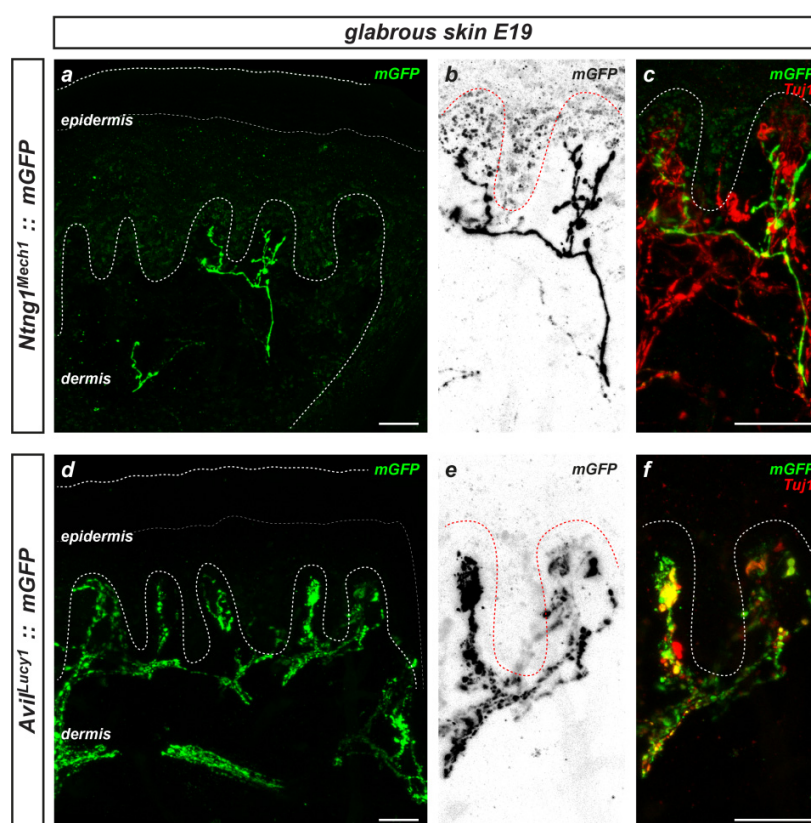


**Figure 3.38: Analysis of *Ntng1<sup>Mech1+</sup>* peripheral terminations in chick glabrous skin at E19**  
**(a-c)** *Ntng1<sup>Mech1+</sup>*-tagged peripheral afferents terminate in dermal papillae in the plantar skin of digits in transverse E19 sections **(a)**. Detailed view: *Ntng1<sup>Mech1+</sup>* peripheral endings innervate rudimentary Meissner-form structures **(b-c)**. Nociceptive and mechanoreceptive axons are labeled by  $\beta$ III-tubulin (TuJ1). Dotted lines demarcate epidermis and dermis. Scale bar: 25  $\mu$ m.  
**(d-f)** *Avil<sup>Lucy1+</sup>* mechanoreceptive and nociceptive peripheral afferents project in dermal papillae of glabrous skin in digits in transverse E19 sections **(d)**. Detailed view: *Avil<sup>Lucy1+</sup>* axon endings overlap with TuJ1 **(e-f)**. No intraepidermal termination of sensory axons is observed. Scale bar: 25  $\mu$ m.



### 3.8. Ntng1-NGL1 interactions in laminar targeting of sensory afferents

Precise central connectivity is a key step in the formation of well-defined neuronal circuits that relay and process sensory information. However, the transcriptional and signaling mechanisms that direct the distinct laminar target zone innervation remain poorly understood (Chen AI *et al.*, 2006). The comprehensive analysis comprising many sensory neuron characteristics identified *Ntng1<sup>Mech1</sup>* as a novel genetic marker, which has been shown to correspond to a discrete subclass of large-diameter A $\beta$ -LTMRs, possibly correlating with Meissner-like LTMRs. Based on five principle observations it may be suggested that Ntng1-NGL1 interactions have a function in specific laminar targeting within the developing spinal cord of vertebrates (see Figure 1.11 b). First, *Ntng1* is expressed in a subset of large-soma size somatosensory neurons in mouse DRGs (see Figure 1.11 a). Second, the selective interaction partner NGL1 appears to be expressed in the deeper laminae IV-V in mouse dorsal horn (see Figure 1.11 a). Third, the *Ntng1<sup>Mech1</sup>* enhancer derived from the *Ntng1* locus drives specific expression in a subset of A $\beta$ -LTMRs which project to a restricted target zone within laminae IV-V in the chick dorsal horn (see Figure 3.28). Fourth, Ntng1 and NGL1 proteins have been described to be highly enriched in developing pre- and postsynaptic terminals of neurons in vertebrates (Kim *et al.*, 2006; Brose, 2009; Woo *et al.*, 2009). And fifth, NetrinG-NGL interactions have been implicated in excitatory synapse formation and lamina-specific segmentation of dendrites in the hippocampus (Nishimura-Akiyoshi *et al.*, 2007; Woo *et al.*, 2009; Seiradake *et al.*, 2011). Consequently, the contribution of Ntng1-NGL1 interactions in laminar targeting of mechanoreceptive axons was addressed.

The impact of Ntng1-NGL1 interactions in somatosensory neuron subtypes concerning their axon projections to defined target zones in the spinal cord was examined by gain-of-function studies in late-gestation chick embryos (Chen AI *et al.*, 2006; Guo *et al.*, 2011). Through the combination of *STEVE* with the *Cre/loxP* system, a strategy was developed allowing specific and long-term expression of introduced transgenes at high expression levels (Figure 3.39) (Livet *et al.*, 2007). The transgene expression cassette of the *pCAG-loxP-ssFlag-IRES-mGFP/tdTomato-Tol2* is composed of the strong constitutive *CAG* promoter (1), a *loxP-STOP-loxP* cassette (2) for specific *Cre*

recombinase-mediated site-specific recombination as a driver for transgene activation, a signal sequence (3) for targeting proteins to the secretion pathway, a farnesylation plasma membrane insertion signal (4), and IRES coupled reporter genes (*mGFP* or *tdTomato*) (5) ensuring bicistronic expression of an epitope-tagged transgene and the fluorescent tracer. Additionally, the transgene expression cassette is flanked by *Tol2* sites (6) for transposase-mediated stable genomic integration (Kawakami and Shima, 1999; Sato *et al.*, 2007; Takahashi *et al.*, 2008). The mouse coding sequences of the transmembrane proteins Ntng1 and NGL1, which displayed extensive homology to the corresponding human and chick protein sequences, were introduced into the expression vector. In order to stably express NGL1 in the entire chick spinal cord, the ubiquitous *Cre* driver (*pPGK-Cre-bpA*) was used (Figure 3.39 a). Specific overexpression of Ntng1 in chick somatosensory neurons was achieved by *Isl1<sup>Crest3</sup>*-mediated *Cre* expression for selective *Cre* recombination in DRG neurons (Figure 3.39 b). Both transgene vectors directed intense membrane-localized transgene and reporter gene expression in all transfected neurons which was verified by detection with specific antibodies against mouse NGL1 and Ntng1 (Figure 3.40).

**Figure 3.39: Selective and stable transgene overexpression in late-gestation chick embryos**

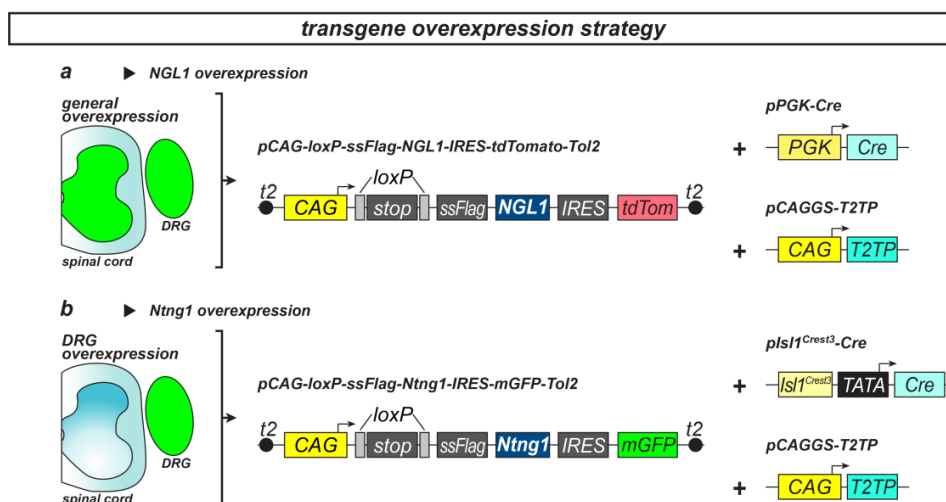


**Figure 3.39: Selective and stable transgene overexpression in late-gestation chick embryos**

**(a-b)** Strategy: Subcloning of transgenes NGL1 and Ntng1 into transposon-based expression construct *pCAG-loxP-ssFlag-IRES-mGFP/tdTomato-Tol2*. Co-electroporation with constitutive *Cre* driver (*PGK*) and transposase (*T2TP*) for stable ectopic NGL1 expression in entire spinal cord **(a)**. Co-electroporation with somatosensory-specific *Cre* driver (*Isl1<sup>Crest3</sup>*) and transposase (*T2TP*) for selective and stable ectopic Ntng1 expression in DRGs **(b)**.

**Figure 3.40: Verification of transgene overexpression in early stage chick embryos**

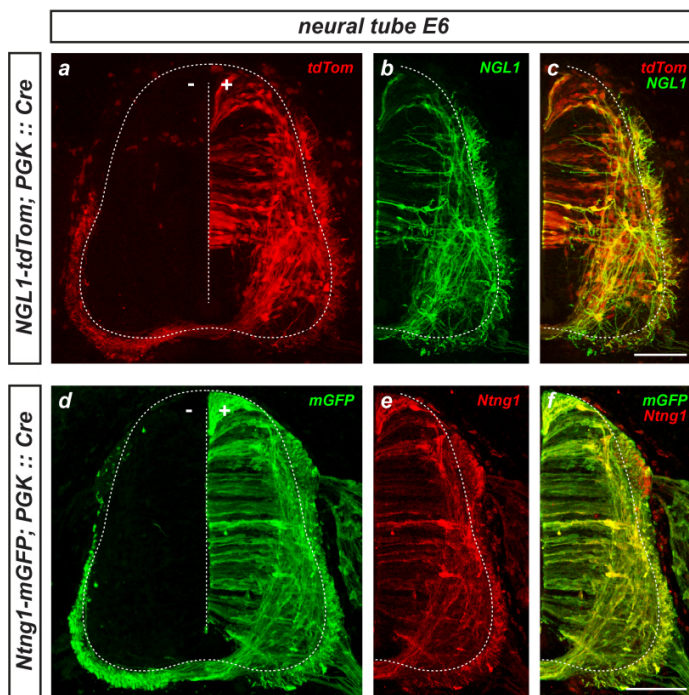


**Figure 3.40: Verification of transgene overexpression in early stage chick embryos**

(a-f) Verification of transgene expression constructs by general transgene overexpression via constitutive *Cre* driver (*pPGK-Cre*) in unilaterally transfected chick neural tube. The *NGL1* expression construct shows high level expression of fluorescent protein tdTomato (a) and membrane-localized mouse *NGL1* (b) in transverse neural tube sections at E6. Similarly, the *Ntng1* expression construct induces robust mGFP (d) and membrane-bound mouse *Ntng1* expression (e) in transfected cells of the neural tube at E6. Scale bar: 100  $\mu\text{m}$ .

*NGL1* is expressed in deeper laminae of the dorsal horn presumably corresponding to laminae IV-V (Figure 3.41 e). Hypothesizing that restricted expression of *NGL1* is involved in mediating the targeting of *Ntng1*<sup>+</sup> sensory collaterals in defined termination zones, ectopic expression of *NGL1* in all laminae of the dorsal horn would be expected to alter the central connectivity pattern of *Ntng1*<sup>+</sup> axons (Figure 3.41 f). Therefore, *NGL1* was ectopically expressed throughout all laminae of the dorsal horn and *Ntng1*<sup>Mech1</sup>-labeled central afferent collaterals were analyzed for their laminar targeting. Robust expression of *NGL1* and fluorescent reporter protein in all laminae of the dorsal horn was achieved (Figure 3.41 d), whereas dorsal horn laminar organization appeared unaffected (Figure 3.41 c). Like in control experiments, *Ntng1*<sup>Mech1+</sup> projections penetrated the superficial dorsal horn at the expected medial position and terminated in the ventromedial quadrant presumably corresponding to laminae IV-V



(compare Figure 3.41 a-c and Figure 3.28 c-d). No obvious shift in the distribution of  $Ntng1^{Mech1+}$  central collaterals to other NGL1 expressing laminae was detected.

**Figure 3.41: NGL1 overexpression analysis of chick somatosensory central connectivity**

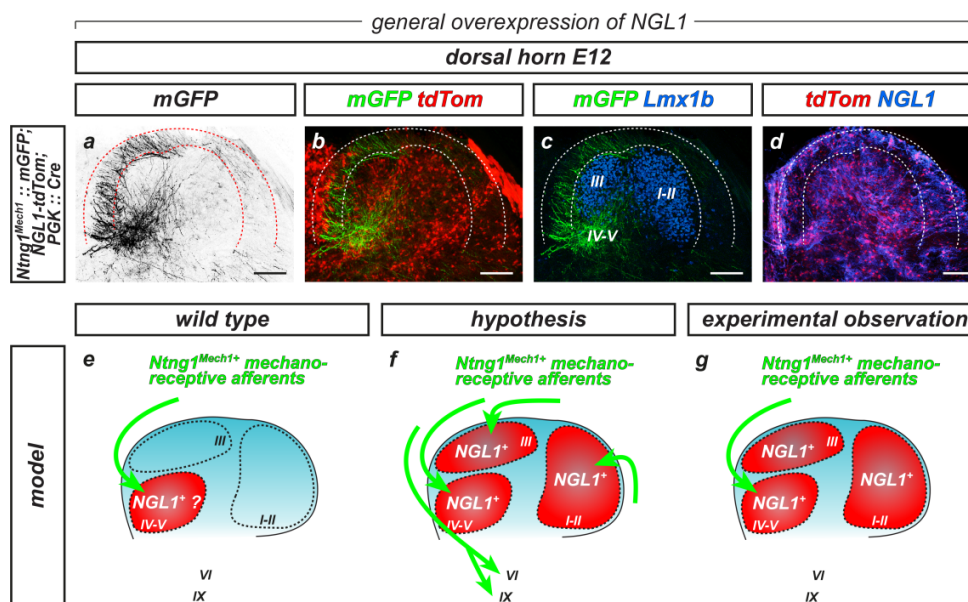


**Figure 3.41: NGL1 overexpression analysis of chick somatosensory central connectivity**

(a-d) General NGL1 overexpression in chick E12 spinal cord.  $Ntng1^{Mech1+}$  afferents terminate in confined domain ventrally of lamina III, presumably corresponding to laminae IV-V in transverse dorsal horn sections (a-c). High level co-expression of ectopic NGL1 and tdTomato in all laminae of the dorsal horn (b, d). Unaffected laminar organization based on laminae I-III marker Lmx1b (c). Dotted lines demarcate white and gray matter. Numbers indicate respective laminae. Scale bar: 100  $\mu$ m.

(e-h) Model: Putative restricted expression of NGL1 to laminae IV-V could mediate  $Ntng1^{Mech1+}$  sensory collaterals in defined termination zone (e). Ectopic expression of NGL1 in all laminae might alter  $Ntng1^{Mech1+}$  central connectivity pattern to all NGL1 expressing regions (f). No redirection of  $Ntng1^{Mech1+}$  central collaterals into different NGL1 expressing laminae was observed (g).

Alternatively, if Ntng1-NGL1 interaction indeed was a determinant for the specific termination pattern in LTMR circuits, the status of Ntng1 expression in sensory neurons should influence the positioning of their collaterals within the spinal cord (Figure 3.42 f). Ectopic expression of Ntng1 in prospective nociceptive and proprioceptive sensory neurons could therefore alter their axonal projections to adopt  $Ntng1^{+}$  LTMR-like features and to prompt axons to assume a medioventral position within the dorsal horn (laminae IV-V), which defines a region where interaction partner NGL1 is expected to be accumulated (Figure 3.42 g). Therefore, Ntng1 was overexpressed in all somatosensory neuron subtypes and the central innervation of

transfected neurons was observed. In congruence with the NGL1 overexpression analysis, no drastic influence of forced Ntng1 expression in the axonal trajectories of nociceptive, mechanoreceptive or proprioceptive neurons was observed (compare Figure 3.42 a-e and Figure 3.15 a-e).

**Figure 3.42: Ntng1 overexpression analysis of chick somatosensory central connectivity**

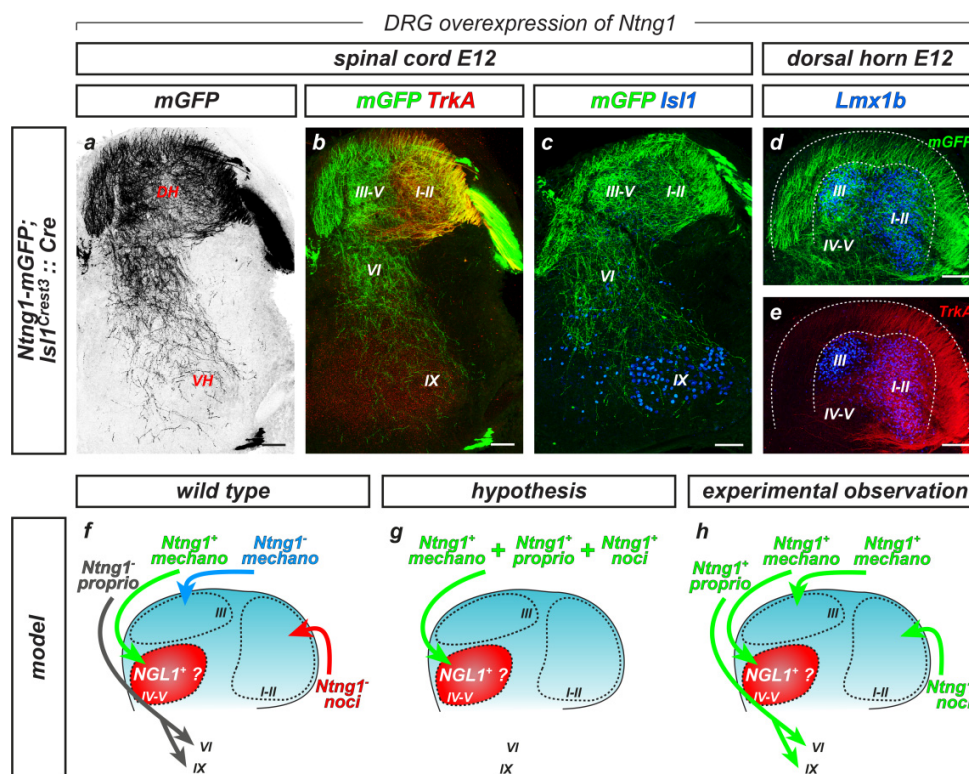


**Figure 3.42: Ntng1 overexpression analysis of chick somatosensory central connectivity**

(a-e) Selective Ntng1 overexpression in chick E12 DRGs. Ntng1<sup>+</sup> mGFP<sup>+</sup> central afferents terminate throughout the dorsal horn and intermediate and ventral spinal cord in transverse sections and are not biased to particular laminae (a-d). Nociceptive Ntng1<sup>+</sup> TrkA<sup>+</sup> projections converge in laminae I-II (b, e). Isl1 labels motor neurons in lamina IX and dI3 interneurons (c), Lmx1b labels laminae I-III neurons (d-e). Numbers indicate respective laminae. DH, dorsal horn; VH, ventral horn. Scale bar: 100  $\mu$ m.

(f-h) Model: Putative restricted expression of NGL1 in laminae IV-V could mediate Ntng1<sup>+</sup> mechanoreceptive collaterals into defined termination zone (f). Ectopic expression of Ntng1 in all somatosensory subtypes might alter the central connectivity pattern mainly to laminae IV-V (g). No obvious change in subtype-specific laminar targeting of nociceptive, mechanoreceptive and proprioceptive neurons was observed (h).

In summary, Ntng1<sup>Mech1+</sup> central collaterals were not redirected into different NGL1 expressing laminae by ectopic NGL1 expression throughout the dorsal horn

(Figure 3.41 g). In addition, ectopic expression of Ntng1 in all subtypes of somatosensory neurons did not change the subtype-specific laminar targeting pattern of nociceptive, mechanoreceptive and proprioceptive neurons (Figure 3.42 h). Hence, it can be concluded that, at least under conditions of forced expression in chick, neither Ntng1 nor its interaction partner NGL1 is sufficient to alter the overall central connectivity of axonal projections in the spinal cord. However, it cannot be excluded that Ntng1-NGL1 interactions play a role in fine-grained changes in laminar and sublamina targeting, like in the lamina-specific differentiation of dendrites. Through a novel *in silico*-to-*in vivo* screen for neuron subtype-specific gene regulatory elements, a unique LTMR circuit defined by Ntng1 activity was uncovered. This circuit appears to relay touch responses from Meissner-like glabrous skin A $\beta$ -LTMRs to laminae IV-V in the dorsal horn. However, deciphering the precise roles of endogenous Ntng1 activity in LTMRs, and that of its putative interaction partner NGL1 in the dorsal horn, during somatosensory circuit assembly or function remains to be addressed.

## 4. Discussion

### 4.1. *STEVE*-mediated stable genetic tagging of somatosensory neurons

The sense of touch is essential for a variety of behaviors in virtually all higher animal species (Lumpkin *et al.*, 2010). Formation and specification of precise sensory neuronal circuits during embryogenesis represents a crucial step in the development of a functional nervous system (Kandel *et al.*, 2000). However, little is known about molecular mechanisms underlying sensory neuron specification, the unique function of specialized sensory neurons, and the logic of sensory circuit organization, which is mainly due to the limited availability of sensory neuron subtype-specific markers facilitating their comprehensive analysis (Marmigère and Ernfors, 2007; Ma, 2009; Lumpkin *et al.*, 2010; Nilius, 2010; Li *et al.*, 2011; Lallemand and Ernfors, 2012). This study aimed at the identification of novel genetic markers for distinct sensory subtypes to provide more detailed insights into sensory neuron circuit organization and developmental assembly. These overall aims were addressed by screening for sensory neuron subtype-specific enhancer activities in a novel chick model system.

An extensive enhancer analysis in rodent transgenic animals, including screening of multiple genomic sequences for enhancer activities *in vivo*, implicates high costs, resource-intensiveness and lengthy generation times (Timmer *et al.*, 2001). The chicken as a complementary model system shares developmental and structural similarities to mammals, including universal conserved gene regulatory mechanisms, and provides a straightforward and rapid *in vivo* transfection with minimal time effort and low costs (Novitch *et al.*, 2001; Thaler *et al.*, 2002; Lee SK *et al.*, 2004; Dasen *et al.*, 2005; Uchikawa, 2008). Therefore, *in ovo* electroporation greatly facilitated an enhancer activity screen along with the study of sensory neuron specification and connectivity in vertebrates. A straightforward strategy was explored based on vertebrate transposon-based transgenesis, allowing for the first time effective, selective and stable genetic tagging of somatosensory neurons and their connectivity patterns in late-gestation chick embryos. The designed stable expression vector *STEVE*, including the minimal *TATA box* promoter and fluorescent reporter genes, provided the basis for a sensitive enhancer analysis by facilitating ready detection of

putative enhancer activities *in vivo*. Persistent expression in transfected cells at later developmental stages along with a long-term observation of enhancer activities was ensured by *ToI2* transposon-based random genomic integration. This was particularly necessitated by the high mitotic rates of neural crest cells (NCCs), causing non-integrated transgenes to disappear rapidly by dilution and progressive degradation (Kawakami and Shima, 1999; Sato *et al.*, 2007; Takahashi *et al.*, 2008; Yokota *et al.*, 2011). For high transfection efficiency in the sensory lineage, *in ovo* electroporation of the chick neural tube was consequently performed between Hamburger-Hamilton (HH) stages 11 and 13 before NCC emigration (Hamburger and Hamilton, 1951; Serbedzija *et al.*, 1990; Kasemeier-Kulesa *et al.*, 2005; Krispin *et al.*, 2010). Previous studies reported of biased transfection efficiency within the somatosensory lineage towards a particular somatosensory subtype (Chen Al *et al.*, 2006; George *et al.*, 2007). In contrast, *STEVE* provided unbiased stable transfection and expression in the entire spinal cord and dorsal root ganglia (DRGs), as verified with the constitutive *CAG* promoter, whereas the enhancer-less construct did not display activity in neural tissue. The effective method of *in ovo* electroporation for introducing exogenous DNA in combination with *STEVE* therefore created the prerequisites for the detection of cis-regulatory activities and their subsequent use for the stable genetic tagging of somatosensory neurons in late-gestation chick embryos that were inaccessible to previous methods.

#### 4.2. Establishment of *Isl1<sup>Crest3</sup>* and *Avil<sup>Lucy1</sup>* as pan-sensory neuron markers

In order to identify novel pan-sensory and sensory subtype-specific markers literature and gene expression data bases were screened for putative candidates expressed by DRG neurons (Yin *et al.*, 2002; Uemura *et al.*, 2005; Alvarez-Bolado and Eichele, 2006). Genomic comparison of chosen candidate gene loci between multiple species revealed a wide range of evolutionary conserved non-coding regions (ECRs) (Ovcharenko *et al.*, 2004). Based on homology and conservation of putative transcription factor binding sites the most promising ECRs were analyzed. It was found that five out of seven tested ECRs were driving reporter gene expression in neuronal

tissue of the chick, with both specific and non-specific activities (see Table 3.1). The general sensory neuron-specific enhancers *Isl1<sup>Crest3</sup>* and *Avil<sup>Lucy1</sup>*, as well as the mechanoreceptive neuron-specific enhancer *Ntng1<sup>Mech1</sup>* were discovered via this method by recapitulating the endogenous expression pattern of the corresponding genes in DRG neurons. These results confirmed the efficacy of the designed screening strategy for the rapid *in silico*-to-*in vivo* enhancer identification (Boffelli *et al.*, 2004; Uchikawa, 2008; Visel *et al.*, 2008). Additionally, the method enabled a significantly easier access to sensory neuron manipulation studies in both early and late-gestation embryos, compared to previous manipulation approaches (Chen AI *et al.*, 2006; George *et al.*, 2007). The analysis of identified ECRs supported previous observations that enhancers can modulate gene expression independently of their orientation or their distance to the gene transcription start (Khoury and Gruss, 1983; Blackwood and Kadonaga, 1998; Pennacchio *et al.*, 2006; Doh *et al.*, 2007). *Isl1<sup>Crest3</sup>*, for example, originally located more than 323 kb upstream of the gene transcription start, was subcloned just upstream to the reporter gene coding sequence in *STEVE* with any functional impairment, thereby demonstrating the relative independence between enhancer distance and its function in gene regulation. In accordance with previous studies, a high ECR sequence conservation is reflected by a high probability of enhancer activity of mouse genome-derived ECRs in the chick embryo, thus emphasizing the idea that mammals and avians share many basic gene regulatory mechanisms in the primary somatosensory system (Timmer *et al.*, 2001; Uchikawa *et al.*, 2004; Dasen *et al.*, 2005).

In this study, *Isl1<sup>Crest3</sup>* and *Avil<sup>Lucy1</sup>* were established as new pan-sensory neuron markers by driving a specific and strong reporter gene expression in somatosensory neurons from embryonic stages into adulthood in chick. Along with this, the pan-sensory markers provided both central and peripheral tagging of sensory axon collaterals and provided the feasibility to directly analyze the connectivity of somatosensory neurons throughout late gestation in chick embryos. The overall developmental sequence of nociceptive, mechanoreceptive and proprioceptive collateral extension into the gray matter in chick mirrored that observed in the mammalian spinal cord. However, the delay in the establishment of nociceptive compared to proprioceptive afferent connectivity observed in mammals appeared

temporally compressed in avians, likely reflecting an ontogenic adaptation in precocial birds (Fitzgerald, 1987; Mirnics and Koerber, 1995; Ozaki and Snider, 1997; Marmigère and Ernfors, 2007). Furthermore, these observations provided evidence that central connectivity in the spinal cord is established by a majority of central afferent collaterals that directly home in on their respective target laminae (Eide and Glover, 1997; Fitzgerald, 1987; Davis *et al.*, 1989; Ozaki and Snider, 1997; Redmond *et al.*, 1997; Fitzgerald, 2005).

As an exception to the above mentioned trend, the examined ECRs derived from the well-established nociceptive marker *TrkA* and the proprioceptive marker *Runx3* did not reflect the endogenous gene expression in sensory DRG neurons, and showed no or unspecific enhancer activity in the central and peripheral nervous system. Since many genes are regulated by complex arrays of enhancers for temporal and spatial gene expression, the discovery of the particular enhancers being responsible for sensory neuron-specific gene expression may not always be straightforward, often requiring more extensive experimental trials (Pennacchio *et al.*, 2006; Alberts *et al.*, 2008). Although highly conserved, no enhancer activity of *TrkA*<sup>ECR1</sup> and *Runx3*<sup>ECR3</sup> could be observed in neuronal tissue of the embryonic chick. One might speculate that these sequences might still include functional regulatory elements which could mediate enhancer activity in different tissue not accessible via chick neural tube electroporation or become active at stages that were not analyzed (Uchikawa *et al.*, 2003; Uchikawa, 2008; Visel *et al.*, 2009). Silencer and insulator elements in a gene locus indispensable for mediating a specific gene expression are, like enhancer elements, thought to be evolutionary highly conserved. Since it is impossible to distinguish between enhancer, silencer and insulator elements in a screen for ECRs, it could be possible that the chosen ECRs are silencers or insulators, which are not sufficient to drive a gene transcription (Blackwood and Kadonaga, 1998; Woolfe *et al.*, 2005; Visel *et al.*, 2009). The *Runx3*<sup>ECR1</sup>- and *Runx3*<sup>ECR2</sup>-driven non-specific expression in different subtypes of sensory DRG neurons in the late-gestation chick was not reflecting the endogenous gene expression normally restricted to the proprioceptive subtype. It is possible that the ECR-mediated expression becomes confined to the proprioceptive neuron subtype with additional enhancer and silencer elements which are necessary in the genomic locus to specify *Runx3* expression (Lee SK *et al.*, 2004; Doh *et al.*,

2007; Visel *et al.*, 2009). By analysis of further candidates, additional enhancers mediating expression in different somatosensory subtypes could be discovered. A comprehensive analysis with a variety of diverse sensory subtype-specific markers could provide a better understanding how specification, as well as precise circuitries of the different sensory neuron classes are established (Lallemend and Ernfors, 2012).

The ability to directly relate sensory identities in chick to specific sensory modalities in other vertebrate species is currently limited by the comparatively poorly resolved structure-function relationships in the avian somatosensory system. The improvement of this situation is, however, expected to go hand-in-hand with the ongoing identification and characterization of molecularly defined sensory neuron subclasses. By allowing systematic exploration of molecularly defined neuronal identities, the *STEVE*-based screening for cis-regulatory activities in chick offers a potentially powerful pre-screening platform for targeting discrete sensory neuronal populations in other vertebrate systems by uncovering principles of their specification and connectivity. While in many cases the mouse will likely remain the gold standard for the genetic dissection of neuronal circuits, the strategic use of auxiliary models facilitating rapid molecular identification and interrogation of neuronal identities could thereby accelerate the drive to map mammalian connectomes.

#### **4.3. Neurogenic equivalence of ipsilaterally and contralaterally migrating neural crest cells**

During early embryonic development, NCCs emigrate from the neural tube towards their respective peripheral targets, whereby some NCCs cross the neural tube midline and contribute to the contralateral NCC migratory stream (Serbedzija *et al.*, 1990; Frank and Sanes, 1991; Carmona-Fontaine *et al.*, 2008; Squire *et al.*, 2008). George and colleagues reported of lineage-restricted premigratory NCCs in diametrically opposed (ipsilateral and contralateral) migratory streams, such that contralaterally migrating NCCs are biased to generate nociceptive somatosensory neurons (George *et al.*, 2007; Lefcort and George, 2007; George *et al.*, 2010). The potential presence of



lineage-restricted NCC populations with unique migratory trajectories has far-reaching implications for understanding NCC biology, including the origin of pain-sensing circuits, and could have profound consequences for experimental strategies targeting ipsilateral or contralateral NCC derivatives.

Through *STEVE*-mediated direct cell lineage-tracking and systematic analysis of neuronal NCC progeny and their circuitries in chick conclusive evidence could be provided that ipsilateral and contralateral NCC streams are neurogenically equivalent and give rise to the same principal set of NCC derivatives, including peripheral neuron types and their circuitries. It is likely that the use of stable somatic transgenesis for tracking NCC lineages effectively sidestepped past limitations inherent to conventional plasmid-based transfection, thus, contributing to the different outcomes between this study and preceding experiments (George *et al.*, 2007). The limited intracellular half-life of non-integrating plasmid DNA confines lineage-tracking experiments to largely immature NCC progeny in DRGs (Yokota *et al.*, 2011). Moreover, in analogy to classical dye-tracing procedures, this might collude with fluctuating tracing efficacies to skew outcomes towards certain cell classes. This could be caused by disparate dilution rates in sub-lineages progressing through few or several cell divisions, especially in the highly proliferative NCC lineages (Stern and Fraser, 2001; Lacar *et al.*, 2010). These effects would have previously eluded detection by the omission of a direct comparative analysis of ipsilaterally- or contralaterally-derived DRG neuron classes, which is a prerequisite for conclusively assessing any neurogenic bias (or lack thereof) of ipsilateral or contralateral NCCs.

Based on obtained observations of *STEVE*-mediated unbiased bilateral targeting of DRG neurons, it is proposed that the entry of a contralateral migratory trajectory by some NCCs is most parsimoniously explained by stochastic events, likely resulting from homotypic interactions driving the initial pattern of NCC emigration (Carmona-Fontaine *et al.*, 2008). Both, ipsilateral and contralateral migratory streams would thereby derive from a common pool of precursors subjected to the same spatiotemporal factors influencing NCC potential (Le Douarin and Kalcheim, 1999; Anderson, 2000; Harris and Erickson, 2007; Krispin *et al.*, 2010). A practical consequence of this is the emerging possibility of using unbiased targeting of

contralateral NCC progeny, such as for the sparse labeling of peripheral neurons for in-depth circuit mapping (Jefferis and Livet, 2012; Chen AI *et al.*, 2006). This feature was utilized for the analysis of somatosensory subtype-specific central trajectories in the developing chick embryo (see Figure 3.23-3.26).

#### 4.4. A novel subclass of touch receptor neurons defined by *Ntng1<sup>Mech1</sup>*

Dependent on the specific functional characteristics associated with the detection of different touch stimuli, low-threshold mechanoreceptors (LTMRs) can be broadly subdivided in heavily myelinated rapidly adapting (RA) A $\beta$ -LTMRs, slowly adapting (SA) A $\beta$ -LTMRs, lightly myelinated A $\delta$ -LTMRs and unmyelinated C-LTMRs. The medium-diameter A $\delta$ -LTMRs and the small-diameter C-LTMRs differ morphologically and physiologically from the large-diameter A $\beta$ -LTMRs of both RA and SA types (Lewin and Moshourab, 2004; Lumpkin and Caterina, 2007; Ma, 2009). By demonstrating the feasibility of the *STEVE* system for the rapid identification and interrogation of neuronal subtype identities, *Ntng1<sup>Mech1</sup>* was shown to label a novel molecularly defined subset of sensory neurons whose anatomical, morphological, electrophysiological, functional and molecular characteristics correspond to a discrete subclass of A $\beta$ -LTMRs. Based on the similar *Ntng1<sup>Mech1</sup>*-mediated expression pattern in large-size sensory neurons and its close genomic localization to the gene transcription start, *Ntng1<sup>Mech1</sup>* is expected to correspond to an enhancer associated with the *Ntng1* gene and consistently to reflect the endogenous gene expression in sensory DRG neurons (Yin *et al.*, 2002; [www.brain-map.org](http://www.brain-map.org)). Nevertheless, a final validation for a direct association should be ultimately conducted via two-color fluorescence *in situ* hybridization analysis against the *Ntng1<sup>Mech1</sup>*-driven reporter gene and endogenous *Ntng1* or via co-expression analysis with specific antibodies against the reporter gene and chick *Ntng1* (Levsky and Singer, 2003).

In order to classify *Ntng1<sup>Mech1+</sup>* DRG neurons according to defined sensory neuron subtypes a comprehensive analysis addressing typical characteristics of sensory neuron subclasses was performed. *Ntng1<sup>Mech1</sup>* consistently labeled a population of

large-diameter sensory neurons clustered in the ventrolateral position of the DRGs, which is mainly occupied by mechanoreceptive and proprioceptive neurons in chick (Frank and Sanes, 1991; Harris and Erickson, 2007). More strikingly,  $Ntng1^{Mech1+}$  central axon collaterals projected into a highly confined region in the medial dorsal horn of the spinal cord which is the target zone of LTMRs in chick (Eide and Glover, 1997; Wild *et al.*, 2010). Furthermore,  $Ntng1^{Mech1}$ -labeled sensory collaterals separated from nociceptive central afferents targeting laminae I-II in the lateral dorsal horn and from proprioceptive afferents projecting to the intermediate and ventral spinal cord (Scott, 1992; Chen Ai *et al.*, 2006; Lallemand and Ernfors, 2012). By labeling the largest DRG neurons which are highly myelinated based on the co-expression with NF200, the properties of  $Ntng1^{Mech1+}$  neurons highly correlated with A $\beta$ -LTMR characteristics (Harper and Lawson, 1985; Lechner *et al.*, 2009). Based on these criteria,  $Ntng1^{Mech1}$ -tagged sensory neurons strongly differed from small-size lightly myelinated or unmyelinated nociceptive neurons, as well as from medium-diameter myelinated A $\delta$ -LTMRs and small-diameter unmyelinated C-LTMRs (Harper and Lawson, 1985; Marmigère and Ernfors, 2007). The electrophysiological analysis revealed that  $Ntng1^{Mech1+}$  DRG neurons represent a discrete population of sensory neurons with spike characteristics and mechanosensitive currents typical of embryonic LTMRs, concomitant with the exclusion of functional properties characteristic for nociceptive neurons (Koerber *et al.*, 1988; Djouhri *et al.*, 1998; Fang *et al.*, 2005; Lechner *et al.*, 2009). The stereotypic laminar connectivity pattern established by  $Ntng1^{Mech1+}$  DRG neurons displayed a selective termination within a medioventral domain presumably corresponding to laminae IV-V by excluding lamina III of the dorsal horn. Recent studies showed that the central collaterals of molecularly identified A $\beta$ -LTMRs, including both RA and SA types, broadly target laminae III to V, which is consistent with the connectivity patterns of morphologically or physiologically identified LTMRs in both, mammals and birds (Necker, 1990; Eide and Glover, 1997; Bourane *et al.*, 2009; Luo *et al.*, 2009; Honma *et al.*, 2010; Li *et al.*, 2011; Lallemand and Ernfors, 2012). Moreover, transganglionic tracing of morphologically identified skin mechanoreceptors in rat have previously revealed that A $\delta$ -LTMR afferents tend to be concentrated in laminae II (inner) and III (Light and Perl, 1979; Li *et al.*, 2011). It may therefore be tempting to speculate that A $\delta$ -LTMRs are  $Ntng1^{Mech1-}$ . The exclusion of

laminae I-III and restriction to laminae IV-V by  $Ntng1^{Mech1+}$  collaterals thus appears to uncover a novel molecularly defined subclass of A $\beta$ -LTMRs (Figure 4.1).

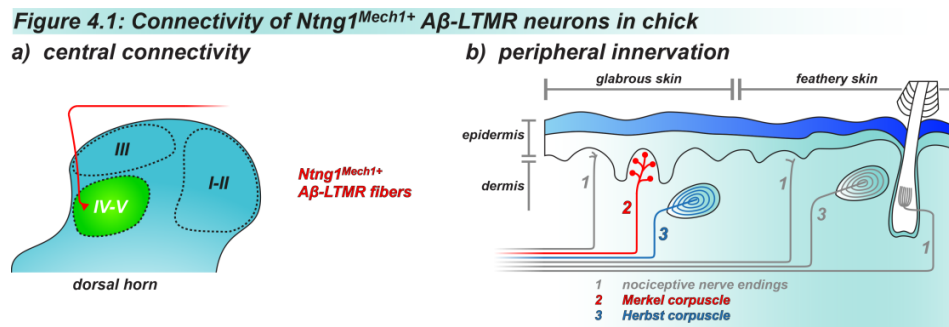


**Figure 4.1: Connectivity of  $Ntng1^{Mech1+}$  A $\beta$ -LTMR neurons in chick**

(a)  $Ntng1^{Mech1+}$  sensory neurons define a subclass of A $\beta$  low-threshold mechanoreceptors (LTMRs), whose central collaterals selectively terminate within a medioventral domain of the dorsal horn presumably corresponding to laminae IV-V. In contrast, all subtypes of A $\beta$ -LTMRs, including RA and SA types, project throughout laminae III-V.

(b)  $Ntng1^{Mech1+}$  peripheral collaterals innervate dermal papillae of glabrous skin, which are suggested to be associated with a subset of Merkel corpuscles in avians. Whether  $Ntng1^{Mech1+}$  axons also associate with Herbst corpuscles in glabrous skin needs to be determined. No  $Ntng1^{Mech1+}$ -labeled projections terminate in feathery skin. Feather follicles are associated with Herbst corpuscles and nociceptive nerve endings.

In analogy to the fine-grained laminar and sublaminar segregation patterns of molecularly defined nociceptor identities, the functional specialization of LTMRs could thus in general be expressed as unique labeled lines relaying submodalities to discrete laminar targets (Zylka *et al.*, 2005; Li *et al.*, 2011). Currently, it is generally believed that LTMRs arise from two early populations of mechanoreceptive progenitors expressing either Ret (earlyRet<sup>+</sup> population) or TrkB (TrkB<sup>+</sup> population) (Lallemend and Ernors, 2012). The earlyRet<sup>+</sup> lineage further subdivides which finally results in five molecularly unique lineages: Ret<sup>+</sup>/MafA<sup>+</sup> (1), Ret<sup>+</sup>/MafA<sup>+</sup>/TrkB<sup>+</sup> (2), Ret<sup>+</sup>/MafA<sup>+</sup>/TrkC<sup>+</sup> (3), Ret<sup>+</sup>/TH<sup>+</sup> (4) and TrkB<sup>+</sup> (5) (Bourane *et al.*, 2009; Luo *et al.*, 2009; Honma *et al.*, 2010; Abdo *et al.*, 2011; Heidenreich *et al.*, 2011; Li *et al.*, 2011; Wende *et al.*, 2012). In mammals, it has been speculated that the Ret<sup>+</sup>/MafA<sup>+</sup> subsets (lineages 1-3) of LTMR neurons could predominantly represent RA A $\beta$ -LTMRs, the Ret<sup>+</sup>/TH<sup>+</sup> subset (lineage 4) is predicted to label C-LTMRs, whereas the TrkB<sup>+</sup> population (lineage 5) was associated with A $\delta$ -LTMRs (Bourane *et al.*, 2009; Luo *et al.*, 2009; Heidenreich *et al.*, 2011; Li *et al.*, 2011; Wende *et al.*, 2012). Based on

current literature no specific markers for SA A $\beta$ -LTMRs have been identified yet. However, in most cases the correlation between the molecularly unique LTMR subtypes with distinct mechanoreceptive end organs needs to be determined in more detail. Additionally, the regulatory mechanisms regarding specification and connectivity of the different LTMR subtypes still remain unknown (Lallemend and Ernfors, 2012). Since the early development of sensory differentiation displays homology in vertebrates, it might be suggested that also later specification and maturation of LTMRs is highly conserved between mammals and avians (Koltzenburg and Lewin; 1997; Marmigère and Ernfors, 2007; Guo *et al.*, 2011).

In the present study, it was found that the *Ntng1*<sup>Mech1</sup>-tagged DRG neuron population partially overlaps with earlyRet<sup>+</sup> (lineages 1-4) and TrkB<sup>+</sup> (lineages 2+5) mechanoreceptive neurons, with 31% of *Ntng1*<sup>Mech1+</sup> neurons co-expressing Ret and 33% co-expressing TrkB. By assumption of no co-expression between Ret and TrkB in any of the LTMR lineages, which is actually present in lineage 2, at least 36% of *Ntng1*<sup>Mech1+</sup> neurons express neither Ret nor TrkB. This indication therefore points towards a molecularly novel Ret<sup>-</sup> TrkB<sup>-</sup> LTMR subtype defined by *Ntng1*<sup>Mech1</sup> (additionally to lineages 1-5), which has not yet been described. Based on this, it would be predicted that *Ntng1*<sup>Mech1+</sup> A $\beta$ -LTMRs are partially independent of the Neurotrophin Ret/Trk receptor signaling during development, which may be further clarified with a DRG explant culture assay (Bilsland *et al.*, 1999; Bourane *et al.*, 2009; Lechner *et al.*, 2009; Wang and Marquardt, 2012). Accordingly, by incubation of *Ntng1*<sup>Mech1</sup>-transfected sensory neurons with single growth factors (GDNF, NGF, BDNF, NT-3) the influence on differentiation, neurite outgrowth and survival of *Ntng1*<sup>Mech1+</sup> neurons could be analyzed in order to classify the *Ntng1*<sup>Mech1</sup> population more precisely (Figure 4.2). Analogous to the division of earlyRet<sup>+</sup> mechanoreceptors into diverse subclasses, *Ntng1*<sup>Mech1+</sup> neurons may thus be tentatively divided into *Ntng1*<sup>Mech1+</sup> (1'), *Ntng1*<sup>Mech1+</sup>/Ret<sup>+</sup> (2'), *Ntng1*<sup>Mech1+</sup>/TrkB<sup>+</sup> (3') and *Ntng1*<sup>Mech1+</sup>/TrkC<sup>+</sup> (4') A $\beta$ -LTMRs, whereas a potential overlap is considered to be possible between the Ret<sup>+</sup> and TrkB<sup>+</sup> subsets (2'+3'), as well as between the Ret<sup>+</sup> and TrkC<sup>+</sup> populations (2'+4'). However, given the apparent molecular heterogeneity of the larger class of A $\beta$ -LTMRs, and the smaller class of *Ntng1*<sup>Mech1+</sup> 'laminae IV-V' A $\beta$ -LTMRs, it is also

possible that the relationship between mechanosensory neuron subclass and Ret/Trk receptor expression is even more complex.

**Figure 4.2: DRG explant culture of  $Isl1^{Crest3+}$  somatosensory neurons in chick**

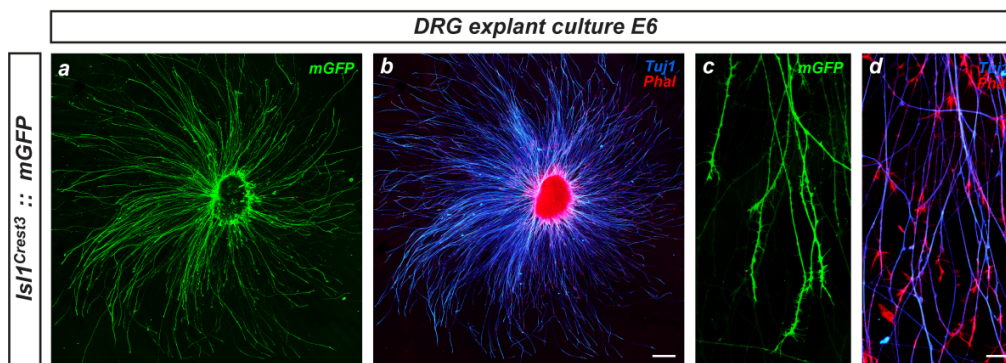


**Figure 4.2: DRG explant culture of  $Isl1^{Crest3+}$  somatosensory neurons in chick**

(a-d) Dorsal root ganglion (DRG) explant culture of  $Isl1^{Crest3}$ -tagged somatosensory neurons treated with NGF, BDNF and NT-3 shows neurite outgrowth (a-b). Somatosensory neurites are labeled by  $\beta$ III-tubulin (Tuj1), growth cones are labeled by F-actin marker Phalloidin (Phal). Scale bar: 200  $\mu$ m. Detailed view reveals Phal<sup>+</sup> growth cones (c-d). Scale bar: 25  $\mu$ m.

In mammals, the peripheral collaterals of RA A $\beta$ -LTMRs terminate in hair follicles, as well as Pacinian and Meissner corpuscles that dynamically respond to light touch, vibration, flutter and skin movements, while SA A $\beta$ -LTMRs innervate Merkel discs and Ruffini corpuscles that relay static responses to dermal stretch and indentation (Lewin and Moshourab, 2004; Lumpkin and Caterina, 2007; Ma, 2009). The A $\delta$ -fiber D-hair receptors and C-fiber LTMRs are associated with hair follicles (Lumpkin *et al.*, 2010; Li *et al.*, 2011). In contrast to the well characterized sensory end organs in mammals there is only limited information on avian mechanoperception and its adaptations in feathery versus hairy skin. In birds, detection of different touch stimuli appears to be mainly mediated by Herbst and Merkel corpuscles (Gottschaldt 1985; Necker 2000). Herbst corpuscles are considered as the avian equivalent of the mammalian Pacinian corpuscles, which respond to vibration and acceleration (Gottschaldt, 1985; Necker, 2000). The corpuscles are widely distributed throughout the feathery skin by forming terminals in the collar region of most feather follicles, but also innervate the dermis of glabrous skin (Duc *et al.*, 1993). Merkel cell receptors are primarily found in featherless skin of avians, where they respond to sustained pressure (Necker, 2000; Halata *et al.*, 2003). In contrast to mammals, Merkel cells here differ from mammalian

Merkel cell-neurite complexes by accumulating and forming rudimentary Meissner-like corpuscles exclusively present in the superficial layer of the dermis and being highly enriched in dermal papillae (Winkelman and Myers, 1961; Duc *et al.*, 1993). The electrophysiological classification of Herbst and Merkel corpuscles among defined RA or SA modalities is complicated by conflicting findings, with some groups reporting that both receptor types are RA, whereas others identified both RA and SA responses (Necker, 1985; Gentle, 1989; Necker, 1990; Duc *et al.*, 1993). The peripheral innervation of  $Ntng1^{Mech1+}$  A $\beta$ -LTMRs was exclusively found in plantar and scaly regions of the glabrous skin. The innervation of dermal papillae to rudimentary Meissner-like structures indicates that  $Ntng1^{Mech1+}$  axons terminate in this subset of avian Merkel corpuscles. Whether the  $Ntng1^{Mech1+}$  and  $Ntng1^{Mech1-}$  neurons are indeed tuned to specific mechanosensory submodalities awaits further study, however.

A co-labeling with sensory end organ specific markers could provide more precise conclusions of the  $Ntng1^{Mech1-}$ -mediated target specificity (Duc *et al.*, 1993). Since Herbst corpuscles are also present in glabrous skin it need to be determined whether the peripheral termination of  $Ntng1^{Mech1-}$ -tagged LTMRs is restricted to Merkel corpuscles or whether these projections alternatively or additionally display a topographic 'distal-versus-proximal-limb' innervation pattern. However, such a 'distal-versus-proximal-limb' regional specificity of the  $Ntng1^{Mech1}$  peripheral projections appears unlikely, as a topographic skin innervation pattern is generally thought to be reflected by central afferents that organize in column-like structures from medial to lateral throughout different laminae of the dorsal horn (Wild *et al.*, 2010; Li *et al.*, 2011). Since  $Ntng1^{Mech1+}$  central afferent collaterals occupy the entire medioventral domain of the dorsal horn presumably corresponding to laminae IV-V by excluding laminae I-III,  $Ntng1^{Mech1}$  is rather more likely restricted to a specific LTMR subtype. Due to the so far limited morphological and electrophysiological characterization of LTMR subtypes in avians and due to the difficulty of pinpointing the homologous mammalian sensory end organs, conclusive statements regarding the stereotypic sensory end organ innervation of  $Ntng1^{Mech1+}$  LTMRs remain challenging. In order to address the issue of a precise electrophysiological characterization of the avian LTMR subtypes, including  $Ntng1^{Mech1-}$ -tagged neurons, particularly with regard to their response properties to different stimuli, *in vitro* skin nerve preparations will have to be

performed (Lewin and Moshourab, 2004; Heidenreich *et al.*, 2011; Wende *et al.*, 2012). Therefore, a novel not-yet-described strategy was designed to selectively tag and record single axons of a defined population in the chick. Since the avian transient receptor potential cation channel V1 (TrpV1), in contrast to the mammalian form, is insensitive to capsaicin, mammalian TrpV1 will be selectively expressed in *Ntng1*<sup>Mech1+</sup> peripheral axons, which then can be recognized after capsaicin exposure of the skin (Wood *et al.*, 1988; Jordt and Julius, 2002). Subsequently, the responses of *Ntng1*<sup>Mech1+</sup> axons can be recorded after variable mechanical stimulation of the skin (vibration, sustained pressure, etc.) in order to classify the LTMR population among defined RA or SA modalities. *Isl1*<sup>Crest3</sup>- or *Avil*<sup>Lucy1</sup>-driven TrpV1 in all somatosensory subtypes might serve as a reference for the different response properties present in the chick somatosensory circuitry.

Finally, the overall aim for the near future is to recapitulate, verify and to in depth characterize the *Ntng1*<sup>Mech1</sup>-mediated LTMR subtype-specific expression in the mouse via specific antibodies against *Ntng1*, as well as by stable transgenesis, as the mouse serves as a well-established model system in regard to study the development and the function of somatosensory circuitries (Luo *et al.*, 2009; Heidenreich *et al.*, 2011). While there is a lack of information regarding the specific mechanosensory modality they relay, *Ntng1*<sup>Mech1+</sup> neurons constitute a novel molecularly unique subclass of A $\beta$ -LTMRs. Moreover, the accelerated identification of molecularly defined somatosensory neuron subclasses by *STEVE*-based transgenesis in chick may accelerate the comprehensive mapping of neuronal identities associated with mechanosensory (sub)modalities.

#### 4.5. NetrinG-NGL interactions in mechanoreceptive circuit formation

*Ntng1*<sup>Mech1</sup> defines a novel subclass of large-diameter A $\beta$ -LTMRs whose central collaterals selectively terminate within a defined domain of the dorsal horn presumably corresponding to laminae IV-V. Since NetrinG-NGL interactions have been implicated in excitatory synapse formation and lamina-specific segmentation of dendrites in the



hippocampus, these new results could indicate a function of Ntng1 for the development of precise mechanoreceptive connectivity (Brose, 2009; Woo *et al.*, 2009). In order to analyze the impact of the cell adhesion molecules Ntng1 and its ligand NGL1 in somatosensory connectivity, a strategy for gain-of-function studies in late-gestation chick embryos, which is based on *STEVE* and the *Cre/loxP* system, was developed enabling specific and long-term expression of introduced transgenes.

NGL1 expression is expected to be restricted to the deeper laminae of the dorsal horn presumably corresponding to laminae IV-V. If Ntng1-NGL1 interactions would be the determinants for laminar targeting of Ntng1<sup>+</sup> sensory collaterals in their defined termination zone of the dorsal horn, ectopic expression of NGL1 in all laminae should be able to alter the central connectivity pattern of Ntng1<sup>+</sup> axons. Alternatively, ectopic expression of Ntng1 in prospective nociceptive and proprioceptive sensory neurons should be able to alter their axonal projections to adopt Ntng1<sup>+</sup> LTMR-like features and to redirect their axons towards regions in the dorsal horn where interaction partner NGL1 is expected to be accumulated. Primary experiments showed that Ntng1<sup>Mech1+</sup> central collaterals were not redirected into different NGL1 expressing laminae by ectopic NGL1 expression throughout the dorsal horn. Furthermore, no change in the phenotypic laminar targeting of Ntng1 expressing nociceptive, mechanoreceptive and proprioceptive neurons was observed. These primary observations lead to the conclusion that Ntng1-NGL1 interactions are not sufficient to alter the stereotypic laminar targeting of somatosensory projections in the spinal cord. However, it cannot be excluded that Ntng1-NGL1 interactions might be involved in fine-grained changes in laminar and sublaminal connectivity, in analogy to the lamina-specific dendrite segmentation in hippocampal neurons observed by previous studies (Nishimura-Akiyoshi *et al.*, 2007; Seiradake *et al.*, 2011). The design of a more precise and more sensitive analysis, which facilitates the detection of changes at sublaminal levels, is essential to reach the final conclusion regarding the Ntng1-NGL1 function in central targeting of LTMR afferents. *In vitro* studies might address the individual influence of Ntng1-NGL1 interactions in axon guidance of A $\beta$ -LTMR neurons with less interference factors, compared to *in vivo* studies. The stripe assay, for example, has been proven to be powerful in uncovering guidance cues and mechanisms in many principal neuronal projections (Knöll *et al.*, 2007; Kao and Kania, 2011). Consequently,

*Ntng1<sup>Mech1</sup>*-tagged somatosensory neurons in DRG explant cultures could be analyzed for their extending neurites along ligands printed in a striped pattern in order to study the responses of growing axons to Ntng1-NGL1 signaling. Furthermore, coculture of *Ntng1<sup>Mech1</sup>*-transfected DRG explants with NGL1 expressing cell aggregates could address the attractive or repulsive Ntng1-NGL1 interaction present in LTMR afferents (He and Tessier-Lavigne, 1997; Anderson *et al.*, 2003). Ntng1-NGL1 adhesion might also be involved in peripheral targeting of A $\beta$ -LTMR collaterals. Since the analysis of peripheral skin innervation in avians is difficult, due to limited information about the mechanoreceptive end organ organization, transgenic mice, carrying the *Ntng1<sup>Mech1</sup>* expression cassette, could bridge the gap between the molecular identity of the A $\beta$ -LTMR subpopulation and their precise peripheral and central circuit formation.

The assembly of neuronal circuits relies on a complex interplay of diverse combinations of different adhesion systems that work in parallel and trigger the precise cell-type specific connectivity (Brose, 2009; Lallemand and Ernfors, 2012). Dysfunction of one component, for example Ntng1-NGL1 interactions in LTMR circuitries, may therefore not necessarily result in a drastically altered connectivity, because of remaining and partially redundant factors. Interestingly, the NetrinG family member Ntng2 and its ligand NGL2 display a comparable expression pattern like Ntng1 in large-diameter DRG neurons and NGL1 in the deeper laminae of the dorsal horn, respectively (Yin *et al.*, 2002; [www.brain-map.org](http://www.brain-map.org)). If both Ntng1 and Ntng2 are co-expressed in the same LTMR population, these highly homologous factors would be likely to act in a redundant manner to achieve laminar targeting specificity. Another possibility might be, in analogy to their roles in the organization of lamina/pathway-specific dendrite differentiation in the hippocampal neurons, that Ntng1 and Ntng2 are expressed in different somatosensory subpopulations mediating specific central innervation in discrete domains of the spinal cord. The study of *Ntng1/Ntng2* double knockout mice could reveal new insights regarding these issues (Nishimura-Akiyoshi *et al.*, 2007). In the future, it will be interesting to decipher more precisely, which additional factors provoke the differentiation towards the *Ntng1<sup>Mech1</sup>*-specific subclass of large-diameter A $\beta$ -LTMRs, how regulatory mechanisms mediate the unique organization of this circuit and what kind of touch responses are relayed by the *Ntng1<sup>Mech1+</sup>* Meissner-like glabrous skin LTMRs to laminae IV-V in the dorsal horn.

## 5. Summary

The assembly of circuitries for somatosensory perception relies on a complex interplay of neuronal diversification, specification, phenotypic modulation and establishment of precise connectivity patterns during embryogenesis. However, little is known about the molecular mechanisms controlling the establishment of well-defined somatosensory connectivity, which is to a large part due to the limitation of sensory neuron subtype-specific molecular markers. This study aimed at the identification of novel genetic markers for distinct somatosensory neuron subtypes to provide more detailed insights into primary somatosensory circuit formation, organization and function. These aims were addressed by a newly established *in silico*-to-*in vivo* screen for neuron subtype-specific enhancer activities in the chick.

The designed strategy, based on the stable expression system *STEVE*, facilitated the detection of cis-regulatory activities and their subsequent use for the rapid, efficient and stable genetic tagging of somatosensory neurons in chick embryos at late-gestation stages that were inaccessible to previous methods. The feasibility of the system for the rapid identification and interrogation of sensory neuronal identities was demonstrated by the establishment of *Isl1<sup>Crest3</sup>* and *Avil<sup>Lucy1</sup>* as pan-somatosensory neuron markers. These newly identified enhancers mediated a specific and robust reporter gene expression in somatosensory neurons from embryonic stages at least until hatching and facilitated both central and peripheral visualization of sensory axon collaterals. A detailed reconstruction of the sensory trajectories regarding their phenotypic laminar targeting revealed new insights in the complex central connectivity of the different somatosensory lineages. Furthermore, *STEVE*-based direct lineage-tracking and systematic analysis of neural crest cell progeny in chick provided conclusive evidence that ipsilateral and contralateral neural crest streams are neurogenically equivalent, giving rise to the same principal set of derivatives, including peripheral neuron types and their circuitries.

Through the selective screen for sensory neuron subtype-specific gene regulatory elements and the subsequent comprehensive analysis comprising many sensory neuron characteristics, *Ntng1<sup>Mech1</sup>* was identified as a novel genetic marker for a

discrete subclass of large-diameter A $\beta$  low-threshold mechanoreceptors. Ntng1 activity thereby uncovered a novel circuit that appears to relay touch responses from Meissner-like glabrous skin mechanoreceptive neurons exclusively to laminae IV-V in the dorsal horn. Ongoing work is directed at deciphering the precise roles of endogenous Ntng1 activity in this subclass of A $\beta$  low-threshold mechanoreceptors, and that of its putative interaction partner NGL1 in the dorsal horn, during somatosensory circuit assembly.

Taken together, this study designed a simple screening strategy that permits rapid, efficient and stable genetic tagging of neuronal subtypes *in vivo*, which thus provides the basis for the systematic discovery of late-onset sensory neuron subtype-specific gene regulatory activities. Thereby, a novel molecularly defined subclass of touch receptor neurons was uncovered, thus providing the utility of the system for uncovering the neural basis of discrete sensory modalities relayed by the primary somatosensory system. In addition, the system facilitated stable cell fate-tracking, which unraveled outstanding features of the primary somatosensory neuron lineage. Besides facilitating the genetic dissection of the somatosensory system, the strategy also offers an effective pre-screening platform for targeting genetically identified neuronal subtypes in other vertebrate species.

## 6. References

Abdel Samad O, Liu Y, Yang FC, Kramer I, Arber S, Ma Q. Characterization of two Runx1-dependent nociceptor differentiation programs necessary for inflammatory versus neuropathic pain. *Mol Pain*. 2010 Jul 30;6:45.

Abdo H, Li L, Lallemand F, Bachy I, Xu XJ, Rice FL, Ernfors P. Dependence on the transcription factor Shox2 for specification of sensory neurons conveying discriminative touch. *Eur J Neurosci*. 2011 Nov;34(10):1529-41.

Alberts B, Johnson A, Lewis J, Raff M, Roberts K, Walter P. *Molecular biology of the cell*. 5th edition. Garland Science. New York. 2008.

Alvarez-Bolado G, Eichele G. Analysing the developing brain transcriptome with the GenePaint platform. *J Physiol*. 2006 Sep 1;575(Pt 2):347-52. Review.

Anderson DJ. Genes, lineages and the neural crest: a speculative review. *Philos Trans R Soc Lond B Biol Sci*. 2000 Jul 29;355(1399):953-64. Review.

Anderson CN, Ohta K, Quick MM, Fleming A, Keynes R, Tannahill D. Molecular analysis of axon repulsion by the notochord. *Development*. 2003 Mar;130(6):1123-33.

Aoki-Suzuki M, Yamada K, Meerabux J, Iwayama-Shigeno Y, Ohba H, Iwamoto K, Takao H, Toyota T, Suto Y, Nakatani N, Dean B, Nishimura S, Seki K, Kato T, Itohara S, Nishikawa T, Yoshikawa T. A family-based association study and gene expression analyses of netrin-G1 and -G2 genes in schizophrenia. *Biol Psychiatry*. 2005 Feb 15;57(4):382-93.

Arber S. Motor circuits in action: specification, connectivity, and function. *Neuron*. 2012 Jun 21;74(6):975-89. Review.

Archer HL, Evans JC, Millar DS, Thompson PW, Kerr AM, Leonard H, Christodoulou J, Ravine D, Lazarou L, Grove L, Verity C, Whatley SD, Pilz DT, Sampson JR, Clarke AJ. NTNG1 mutations are a rare cause of Rett syndrome. *Am J Med Genet A*. 2006 Apr 1;140(7):691-4.

Bachy I, Franck MC, Li L, Abdo H, Pattyn A, Ernfors P. The transcription factor Cux2 marks development of an A-delta sublineage of TrkA sensory neurons. *Dev Biol*. 2011 Dec 1;360(1):77-86.

Biederer T. Hooking up new synapses. *Nat Neurosci*. 2006 Oct;9(10):1203-4.

Bilsland J, Rigby M, Young L, Harper S. A rapid method for semi-quantitative analysis of neurite outgrowth from chick DRG explants using image analysis. *J Neurosci Methods*. 1999 Oct 15;92(1-2):75-85.

Blackwood EM, Kadonaga JT. Going the distance: a current view of enhancer action. *Science*. 1998 Jul 3;281(5373):60-3. Review.

Boffelli D, Nobrega MA, Rubin EM. Comparative genomics at the vertebrate extremes. *Nat Rev Genet.* 2004 Jun;5(6):456-65. Review.

Borg I, Freude K, Kübart S, Hoffmann K, Menzel C, Laccone F, Firth H, Ferguson-Smith MA, Tommerup N, Ropers HH, Sargan D, Kalscheuer VM. Disruption of Netrin G1 by a balanced chromosome translocation in a girl with Rett syndrome. *Eur J Hum Genet.* 2005 Aug;13(8):921-7.

Bourane S, Garces A, Venteo S, Pattyn A, Hubert T, Fichard A, Puech S, Boukhaddaoui H, Baudet C, Takahashi S, Valmier J, Carroll P. Low-threshold mechanoreceptor subtypes selectively express MafA and are specified by Ret signaling. *Neuron.* 2009 Dec 24;64(6):857-70.

Briscoe J, Pierani A, Jessell TM, Ericson J. A homeodomain protein code specifies progenitor cell identity and neuronal fate in the ventral neural tube. *Cell.* 2000 May 12;101(4):435-45.

Bronner-Fraser M, Fraser SE. Cell lineage analysis reveals multipotency of some avian neural crest cells. *Nature.* 1988 Sep 8;335(6186):161-4.

Bronner-Fraser M. Development. Making sense of the sensory lineage. *Science.* 2004 Feb 13;303(5660):966-8.

Brose N. Synaptogenic proteins and synaptic organizers: "many hands make light work". *Neuron.* 2009 Mar 12;61(5):650-2.

Brown AG. The dorsal horn of the spinal cord. *Q J Exp Physiol.* 1982 Apr;67(2):193-212.

Carmona-Fontaine C, Matthews HK, Kuriyama S, Moreno M, Dunn GA, Parsons M, Stern CD, Mayor R. Contact inhibition of locomotion *in vivo* controls neural crest directional migration. *Nature.* 2008 Dec 18;456(7224):957-61.

Chandrashekar J, Kuhn C, Oka Y, Yarmolinsky DA, Hummler E, Ryba NJ, Zuker CS. The cells and peripheral representation of sodium taste in mice. *Nature.* 2010 Mar 11;464(7286):297-301.

Chen HH, Hippenmeyer S, Arber S, Frank E. Development of the monosynaptic stretch reflex circuit. *Curr Opin Neurobiol.* 2003 Feb;13(1):96-102. Review.

Chen AI, de Nooij JC, Jessell TM. Graded activity of transcription factor Runx3 specifies the laminar termination pattern of sensory axons in the developing spinal cord. *Neuron.* 2006 Feb 2;49(3):395-408.

Chen CL, Broom DC, Liu Y, de Nooij JC, Li Z, Cen C, Samad OA, Jessell TM, Woolf CJ, Ma Q. Runx1 determines nociceptive sensory neuron phenotype and is required for thermal and neuropathic pain. *Neuron.* 2006 Feb 2;49(3):365-77.

Chiang C, Litingtung Y, Lee E, Young KE, Corden JL, Westphal H, Beachy PA. Cyclopia and defective axial patterning in mice lacking Sonic hedgehog gene function. *Nature*. 1996 Oct 3;383(6599):407-13.

Copp AJ, Greene ND, Murdoch JN. The genetic basis of mammalian neurulation. *Nat Rev Genet*. 2003 Oct;4(10):784-93. Review.

Dasen JS, Tice BC, Brenner-Morton S, Jessell TM. A Hox regulatory network establishes motor neuron pool identity and target-muscle connectivity. *Cell*. 2005 Nov 4;123(3):477-91.

Davis BM, Frank E, Johnson FA, Scott SA. Development of central projections of lumbosacral sensory neurons in the chick. *J Comp Neurol*. 1989 Jan 22;279(4):556-66.

Delprat B, Michel V, Goodyear R, Yamasaki Y, Michalski N, El-Amraoui A, Perfettini I, Legrain P, Richardson G, Hardelin JP, Petit C. Myosin XVa and whirlin, two deafness gene products required for hair bundle growth, are located at the stereocilia tips and interact directly. *Hum Mol Genet*. 2005 Feb 1;14(3):401-10.

Djohri L, Bleazard L, Lawson SN. Association of somatic action potential shape with sensory receptive properties in guinea-pig dorsal root ganglion neurones. *J Physiol*. 1998 Dec 15;513 (Pt 3):857-72.

Doh ST, Zhang Y, Temple MH, Cai L. Non-coding sequence retrieval system for comparative genomic analysis of gene regulatory elements. *BMC Bioinformatics*. 2007 Mar 15;8:94.

Drew LJ, Wood JN, Cesare P. Distinct mechanosensitive properties of capsaicin-sensitive and -insensitive sensory neurons. *J Neurosci*. 2002 Jun 15;22(12):RC228.

Duc C, Barakat-Walter I, Droz B. Calbindin D-28k- and substance P-immunoreactive primary sensory neurons: peripheral projections in chick hindlimbs. *J Comp Neurol*. 1993 Aug 1;334(1):151-8.

Eastwood SL, Harrison PJ. Decreased mRNA expression of netrin-G1 and netrin-G2 in the temporal lobe in schizophrenia and bipolar disorder. *Neuropsychopharmacol*. 2008 Mar;33(4):933-45.

Echelard Y, Vassileva G, McMahon AP. Cis-acting regulatory sequences governing Wnt-1 expression in the developing mouse CNS. *Development*. 1994 Aug;120(8):2213-24.

Eide AL, Glover JC. Developmental dynamics of functionally specific primary sensory afferent projections in the chicken embryo. *Anat Embryol (Berl)*. 1997 Mar;195(3):237-50.

Ericson J, Thor S, Edlund T, Jessell TM, Yamada T. Early stages of motor neuron differentiation revealed by expression of homeobox gene *Islet-1*. *Science*. 1992 Jun 12;256(5063):1555-60.

- Ernfors P. Local and target-derived actions of neurotrophins during peripheral nervous system development. *Cell Mol Life Sci.* 2001 Jul;58(8):1036-44. Review.
- Fang X, McMullan S, Lawson SN, Djouhri L. Electrophysiological differences between nociceptive and non-nociceptive dorsal root ganglion neurones in the rat *in vivo*. *J Physiol.* 2005 Jun 15;565(Pt 3):927-43.
- Fariñas I, Wilkinson GA, Backus C, Reichardt LF, Patapoutian A. Characterization of neurotrophin and Trk receptor functions in developing sensory ganglia: direct NT-3 activation of TrkB neurons *in vivo*. *Neuron.* 1998 Aug;21(2):325-34.
- Fitzgerald M. Prenatal growth of fine-diameter primary afferents into the rat spinal cord: a transganglionic tracer study. *J Comp Neurol.* 1987 Jul 1;261(1):98-104.
- Fitzgerald M. The development of nociceptive circuits. *Nat Rev Neurosci.* 2005 Jul;6(7):507-20. Review.
- Frank E, Sanes JR. Lineage of neurons and glia in chick dorsal root ganglia: analysis *in vivo* with a recombinant retrovirus. *Development.* 1991 Apr;111(4):895-908.
- Frenzel H, Bohlender J, Pinsker K, Wohlleben B, Tank J, Lechner SG, Schiska D, Jaijo T, Rüschemdorf F, Saar K, Jordan J, Millán JM, Gross M, Lewin GR. A genetic basis for mechanosensory traits in humans. *PLoS Biol.* 2012;10(5):e1001318.
- Fünfschilling U, Ng YG, Zang K, Miyazaki J, Reichardt LF, Rice FL. TrkC kinase expression in distinct subsets of cutaneous trigeminal innervation and nonneuronal cells. *J Comp Neurol.* 2004 Dec 20;480(4):392-414.
- Gascon E, Gaillard S, Malapert P, Liu Y, Rodat-Despoix L, Samokhvalov IM, Delmas P, Helmbacher F, Maina F, Moqrich A. Hepatocyte growth factor-Met signaling is required for Runx1 extinction and peptidergic differentiation in primary nociceptive neurons. *J Neurosci.* 2010 Sep 15;30(37):12414-23.
- Gentle MJ. Cutaneous sensory afferents recorded from the nervus intramandibularis of *Gallus gallus var domesticus*. *J Comp Physiol A.* 1989 Feb;164(6):763-74.
- George L, Chaverra M, Todd V, Lansford R, Lefcort F. Nociceptive sensory neurons derive from contralaterally migrating, fate-restricted neural crest cells. *Nat Neurosci.* 2007 Oct;10(10):1287-93.
- George L, Kasemeier-Kulesa J, Nelson BR, Koyano-Nakagawa N, Lefcort F. Patterned assembly and neurogenesis in the chick dorsal root ganglion. *J Comp Neurol.* 2010 Feb 15;518(4):405-22.
- Gilbert SF. *Developmental Biology*. 6th edition. Sinauer Associates. Sunderland. 2000.
- Golden JP, Hoshi M, Nassar MA, Enomoto H, Wood JN, Milbrandt J, Gereau RW 4th, Johnson EM Jr, Jain S. RET signaling is required for survival and normal function of nonpeptidergic nociceptors. *J Neurosci.* 2010 Mar 17;30(11):3983-94.



Gottschaldt KM. Structure and function of avian somatosensory receptors. In: King AS, McLelland J. Form and function in birds. Vol 3. Academic Press. London. 1985.

Goulding M. Circuits controlling vertebrate locomotion: moving in a new direction. *Nat Rev Neurosci*. 2009 Jul;10(7):507-18. Review.

Greene ND, Copp AJ. Development of the vertebrate central nervous system: formation of the neural tube. *Prenat Diagn*. 2009 Apr;29(4):303-11. Review.

Guo T, Mandai K, Condie BG, Wickramasinghe SR, Capecchi MR, Ginty DD. An evolving NGF-Hoxd1 signaling pathway mediates development of divergent neural circuits in vertebrates. *Nat Neurosci*. 2011 Jan;14(1):31-6.

Hamburger V, Hamilton HL. A series of normal stages in the development of the chick embryo. *J Morphol* 1951 Jan;88(1):49-92.

Hari L, Brault V, Kléber M, Lee HY, Ille F, Leimeroth R, Paratore C, Suter U, Kemler R, Sommer L. Lineage-specific requirements of beta-catenin in neural crest development. *J Cell Biol*. 2002 Dec 9;159(5):867-80.

Hari L, Miescher I, Shakhova O, Suter U, Chin L, Taketo M, Richardson WD, Kessarlis N, Sommer L. Temporal control of neural crest lineage generation by Wnt/ $\beta$ -catenin signaling. *Development*. 2012 Jun;139(12):2107-17.

Harris ML, Erickson CA. Lineage specification in neural crest cell pathfinding. *Dev Dyn*. 2007 Jan;236(1):1-19. Review.

Hasegawa H, Abbott S, Han BX, Qi Y, Wang F. Analyzing somatosensory axon projections with the sensory neuron-specific Advillin gene. *J Neurosci*. 2007 Dec 26;27(52):14404-14.

Halata Z, Grim M, Bauman KI. Friedrich Sigmund Merkel and his "Merkel cell", morphology, development, and physiology: review and new results. *Anat Rec A Discov Mol Cell Evol Biol*. 2003 Mar;271(1):225-39. Review.

Harper AA, Lawson SN. Conduction velocity is related to morphological cell type in rat dorsal root ganglion neurones. *J Physiol*. 1985 Feb;359:31-46.

He Z, Tessier-Lavigne M. Neuropilin is a receptor for the axonal chemorepellent Semaphorin III. *Cell*. 1997 Aug 22;90(4):739-51.

Heidenreich M, Lechner SG, Vardanyan V, Wetzel C, Cremers CW, De Leenheer EM, Aránguez G, Moreno-Pelayo MÁ, Jentsch TJ, Lewin GR. KCNQ4 K(+) channels tune mechanoreceptors for normal touch sensation in mouse and man. *Nat Neurosci*. 2011 Nov 20;15(1):138-45.

Helms AW, Johnson JE. Specification of dorsal spinal cord interneurons. *Curr Opin Neurobiol*. 2003 Feb;13(1):42-9. Review.

- Hippenmeyer S, Kramer I, Arber S. Control of neuronal phenotype: what targets tell the cell bodies. *Trends Neurosci.* 2004 Aug;27(8):482-8. Review.
- Honma Y, Kawano M, Kohsaka S, Ogawa M. Axonal projections of mechanoreceptive dorsal root ganglion neurons depend on Ret. *Development.* 2010 Jul;137(14):2319-28.
- Hu J, Lewin GR. Mechanosensitive currents in the neurites of cultured mouse sensory neurones. *J Physiol.* 2006 Dec 15;577(Pt 3):815-28.
- Huang EJ, Wilkinson GA, Fariñas I, Backus C, Zang K, Wong SL, Reichardt LF. Expression of Trk receptors in the developing mouse trigeminal ganglion: *in vivo* evidence for NT-3 activation of TrkA and TrkB in addition to TrkC. *Development.* 1999 May;126(10):2191-203.
- Huang EJ, Reichardt LF. Neurotrophins: roles in neuronal development and function. *Annu Rev Neurosci.* 2001;24:677-736. Review.
- Huang X, Saint-Jeannet JP. Induction of the neural crest and the opportunities of life on the edge. *Dev Biol.* 2004 Nov 1;275(1):1-11. Review.
- Inoue H, Nojima H, Okayama H. High efficiency transformation of *Escherichia coli* with plasmids. *Gene.* 1990 Nov 30;96(1):23-8.
- Inoue K, Ozaki S, Shiga T, Ito K, Masuda T, Okado N, Iseda T, Kawaguchi S, Ogawa M, Bae SC, Yamashita N, Itohara S, Kudo N, Ito Y. Runx3 controls the axonal projection of proprioceptive dorsal root ganglion neurons. *Nat Neurosci.* 2002 Oct;5(10):946-54.
- Inoue K, Ito K, Osato M, Lee B, Bae SC, Ito Y. The transcription factor Runx3 represses the neurotrophin receptor TrkB during lineage commitment of dorsal root ganglion neurons. *J Biol Chem.* 2007 Aug 17;282(33):24175-84.
- Jefferis GS, Livet J. Sparse and combinatorial neuron labelling. *Curr Opin Neurobiol.* 2012 Feb;22(1):101-10.
- Jessell TM. Neuronal specification in the spinal cord: inductive signals and transcriptional codes. *Nat Rev Genet.* 2000 Oct;1(1):20-9.
- Jones AR, Overly CC, Sunkin SM. The Allen Brain Atlas: 5 years and beyond. *Nat Rev Neurosci.* 2009 Nov;10(11):821-8.
- Jordt SE, Julius D. Molecular basis for species-specific sensitivity to "hot" chili peppers. *Cell.* 2002 Feb 8;108(3):421-30.
- Kandel ER, Schwartz JH, Jessell TM. *Principles of Neural Science.* 4th edition. McGraw-Hill. New York. 2000.
- Kao TJ, Kania A. Ephrin-mediated cis-attenuation of Eph receptor signaling is essential for spinal motor axon guidance. *Neuron.* 2011 Jul 14;71(1):76-91.

- Kasemeier-Kulesa JC, Kulesa PM, Lefcort F. Imaging neural crest cell dynamics during formation of dorsal root ganglia and sympathetic ganglia. *Development*. 2005 Jan;132(2):235-45.
- Kawakami K, Shima A. Identification of the *To/2* transposase of the medaka fish *Oryzias latipes* that catalyzes excision of a nonautonomous *To/2* element in zebrafish *Danio rerio*. *Gene*. 1999 Nov 15;240(1):239-44.
- Khoury G, Gruss P. Enhancer elements. *Cell*. 1983 Jun;33(2):313-4. Review.
- Kim J, Lo L, Dormand E, Anderson DJ. SOX10 maintains multipotency and inhibits neuronal differentiation of neural crest stem cells. *Neuron*. 2003 Apr 10;38(1):17-31.
- Kim S, Burette A, Chung HS, Kwon SK, Woo J, Lee HW, Kim K, Kim H, Weinberg RJ, Kim E. NGL family PSD-95-interacting adhesion molecules regulate excitatory synapse formation. *Nat Neurosci*. 2006 Oct;9(10):1294-301.
- Kim IJ, Zhang Y, Yamagata M, Meister M, Sanes JR. Molecular identification of a retinal cell type that responds to upward motion. *Nature*. 2008 Mar 27;452(7186):478-82.
- King MC, Wilson AC. Evolution at two levels in humans and chimpanzees. *Science*. 1975 Apr 11;188(4184):107-16. Review.
- Kléber M, Lee HY, Wurdak H, Buchstaller J, Riccomagno MM, Ittner LM, Suter U, Epstein DJ, Sommer L. Neural crest stem cell maintenance by combinatorial Wnt and BMP signaling. *J Cell Biol*. 2005 Apr 25;169(2):309-20.
- Knöll B, Weini C, Nordheim A, Bonhoeffer F. Stripe assay to examine axonal guidance and cell migration. *Nat Protoc*. 2007;2(5):1216-24.
- Koerber HR, Druzinsky RE, Mendell LM. Properties of somata of spinal dorsal root ganglion cells differ according to peripheral receptor innervated. *J Neurophysiol*. 1988 Nov;60(5):1584-96.
- Koltzenburg M, Lewin GR. Receptive properties of embryonic chick sensory neurons innervating skin. *J Neurophysiol*. 1997 Nov;78(5):2560-8.
- Kramer I, Sigrist M, de Nooij JC, Taniuchi I, Jessell TM, Arber S. A role for Runx transcription factor signaling in dorsal root ganglion sensory neuron diversification. *Neuron*. 2006 Feb 2;49(3):379-93.
- Krispin S, Nitzan E, Kassem Y, Kalcheim C. Evidence for a dynamic spatiotemporal fate map and early fate restrictions of premigratory avian neural crest. *Development*. 2010 Feb;137(4):585-95.
- Koerber HR, Druzinsky RE, Mendell LM. Properties of somata of spinal dorsal root ganglion cells differ according to peripheral receptor innervated. *J Neurophysiol*. 1988 Nov;60(5):1584-96.

- Lacar B, Young SZ, Platel JC, Bordey A. Imaging and recording subventricular zone progenitor cells in live tissue of postnatal mice. *Front Neurosci*. 2010 Jul 19;4.
- Ladle DR, Pecho-Vrieseling E, Arber S. Assembly of motor circuits in the spinal cord: driven to function by genetic and experience-dependent mechanisms. *Neuron*. 2007 Oct 25;56(2):270-83. Review.
- Lallemend F, Ernfors P. Molecular interactions underlying the specification of sensory neurons. *Trends Neurosci*. 2012 Jun;35(6):373-81.
- Lanier J, Dykes IM, Nissen S, Eng SR, Turner EE. Brn3a regulates the transition from neurogenesis to terminal differentiation and represses non-neural gene expression in the trigeminal ganglion. *Dev Dyn*. 2009 Dec;238(12):3065-79.
- Lau J, Minett MS, Zhao J, Dennehy U, Wang F, Wood JN, Bogdanov YD. Temporal control of gene deletion in sensory ganglia using a tamoxifen-inducible Advillin-Cre-ERT2 recombinase mouse. *Mol Pain*. 2011 Dec 21;7:100.
- Le Douarin NM, Kalcheim C. *The Neural Crest*. Cambridge Univ. Press. Cambridge. 1999.
- Le Dréau G, Martí E. Dorsal-ventral patterning of the neural tube: A tale of three signals. *Dev Neurobiol*. 2012 Dec;72(12):1471-81.
- Lechner SG, Frenzel H, Wang R, Lewin GR. Developmental waves of mechanosensitivity acquisition in sensory neuron subtypes during embryonic development. *EMBO J*. 2009 May 20;28(10):1479-91.
- Lecoin L, Rocques N, El-Yakoubi W, Ben Achour S, Larcher M, Pouponnot C, Eychène A. MafA transcription factor identifies the early ret-expressing sensory neurons. *Dev Neurobiol*. 2010 Jun;70(7):485-97.
- Lee KJ, Jessell TM. The specification of dorsal cell fates in the vertebrate central nervous system. *Annu Rev Neurosci*. 1999;22:261-94. Review.
- Lee HY, Kléber M, Hari L, Brault V, Suter U, Taketo MM, Kemler R, Sommer L. Instructive role of Wnt/beta-catenin in sensory fate specification in neural crest stem cells. *Science*. 2004 Feb 13;303(5660):1020-3.
- Lee SK, Jurata LW, Funahashi J, Ruiz EC, Pfaff SL. Analysis of embryonic motoneuron gene regulation: derepression of general activators function in concert with enhancer factors. *Development*. 2004 Jul;131(14):3295-306.
- Lefcort F, George L. Neural crest cell fate: to be or not to be prespecified. *Cell Adh Migr*. 2007 Oct-Dec;1(4):199-201. Review.
- Levanon D, Bettoun D, Harris-Cerruti C, Woolf E, Negreanu V, Eilam R, Bernstein Y, Goldenberg D, Xiao C, Fliegau M, Kremer E, Otto F, Brenner O, Lev-Tov A, Groner Y. The Runx3 transcription factor regulates development and survival of TrkC dorsal root ganglia neurons. *EMBO J*. 2002 Jul 1;21(13):3454-63.

- Levsky JM, Singer RH. Fluorescence in situ hybridization: past, present and future. *J Cell Sci.* 2003 Jul 15;116(Pt 14):2833-8. Review.
- Lewin GR, Moshourab R. Mechanosensation and pain. *J Neurobiol.* 2004 Oct;61(1):30-44. Review.
- Li L, Rutlin M, Abaira VE, Cassidy C, Kus L, Gong S, Jankowski MP, Luo W, Heintz N, Koerber HR, Woodbury CJ, Ginty DD. The functional organization of cutaneous low-threshold mechanosensory neurons. *Cell.* 2011 Dec 23;147(7):1615-27.
- Lichtman JW, Sanes JR. Ome sweet ome: what can the genome tell us about the connectome? *Curr Opin Neurobiol.* 2008 Jun;18(3):346-53. Review.
- Liem KF Jr, Tremml G, Jessell TM. A role for the roof plate and its resident TGFbeta-related proteins in neuronal patterning in the dorsal spinal cord. *Cell.* 1997 Oct 3;91(1):127-38.
- Liem KF Jr, Jessell TM, Briscoe J. Regulation of the neural patterning activity of sonic hedgehog by secreted BMP inhibitors expressed by notochord and somites. *Development.* 2000 Nov;127(22):4855-66.
- Light AR, Perl ER. Spinal termination of functionally identified primary afferent neurons with slowly conducting myelinated fibers. *J Comp Neurol.* 1979 Jul 15;186(2):133-50.
- Lin JC, Ho WH, Gurney A, Rosenthal A. The netrin-G1 ligand NGL-1 promotes the outgrowth of thalamocortical axons. *Nat Neurosci.* 2003 Dec;6(12):1270-6.
- Linhoff MW, Laurén J, Cassidy RM, Dobie FA, Takahashi H, Nygaard HB, Airaksinen MS, Strittmatter SM, Craig AM. An unbiased expression screen for synaptogenic proteins identifies the LRRTM protein family as synaptic organizers. *Neuron.* 2009 Mar 12;61(5):734-49.
- Liu Y, Yang FC, Okuda T, Dong X, Zylka MJ, Chen CL, Anderson DJ, Kuner R, Ma Q. Mechanisms of compartmentalized expression of Mrg class G-protein-coupled sensory receptors. *J Neurosci.* 2008 Jan 2;28(1):125-32.
- Liu Y, Ma Q. Generation of somatic sensory neuron diversity and implications on sensory coding. *Curr Opin Neurobiol.* 2011 Feb;21(1):52-60. Review.
- Livet J, Weissman TA, Kang H, Draft RW, Lu J, Bennis RA, Sanes JR, Lichtman JW. Transgenic strategies for combinatorial expression of fluorescent proteins in the nervous system. *Nature.* 2007 Nov 1;450(7166):56-62.
- Luo W, Wickramasinghe SR, Savitt JM, Griffin JW, Dawson TM, Ginty DD. A hierarchical NGF signaling cascade controls Ret-dependent and Ret-independent events during development of nonpeptidergic DRG neurons. *Neuron.* 2007 Jun 7;54(5):739-54.

- Luo W, Enomoto H, Rice FL, Milbrandt J, Ginty DD. Molecular identification of rapidly adapting mechanoreceptors and their developmental dependence on ret signaling. *Neuron*. 2009 Dec 24;64(6):841-56.
- Lumpkin EA, Caterina MJ. Mechanisms of sensory transduction in the skin. *Nature*. 2007 Feb 22;445(7130):858-65. Review.
- Lumpkin EA, Marshall KL, Nelson AM. The cell biology of touch. *J Cell Biol*. 2010 Oct 18;191(2):237-48. Review.
- Lumsden A, Krumlauf R. Patterning the vertebrate neuraxis. *Science*. 1996 Nov 15;274(5290):1109-15. Review.
- Ma Q, Fode C, Guillemot F, Anderson DJ. Neurogenin1 and neurogenin2 control two distinct waves of neurogenesis in developing dorsal root ganglia. *Genes Dev*. 1999 Jul 1;13(13):1717-28.
- Ma L, Merenmies J, Parada LF. Molecular characterization of the TrkA/NGF receptor minimal enhancer reveals regulation by multiple cis elements to drive embryonic neuron expression. *Development*. 2000 Sep;127(17):3777-88.
- Ma L, Lei L, Eng SR, Turner E, Parada LF. Brn3a regulation of TrkA/NGF receptor expression in developing sensory neurons. *Development*. 2003 Aug;130(15):3525-34.
- Ma Q. RETouching upon mechanoreceptors. *Neuron*. 2009 Dec 24;64(6):773-6.
- Maher B. ENCODE: The human encyclopaedia. *Nature*. 2012 Sep 6;489(7414):46-8.
- Marmigère F, Montelius A, Wegner M, Groner Y, Reichardt LF, Ernfors P. The Runx1/AML1 transcription factor selectively regulates development and survival of TrkA nociceptive sensory neurons. *Nat Neurosci*. 2006 Feb;9(2):180-7.
- Marmigère F, Ernfors P. Specification and connectivity of neuronal subtypes in the sensory lineage. *Nat Rev Neurosci*. 2007 Feb;8(2):114-27. Review.
- Maro GS, Vermeren M, Voiculescu O, Melton L, Cohen J, Charnay P, Topilko P. Neural crest boundary cap cells constitute a source of neuronal and glial cells of the PNS. *Nat Neurosci*. 2004 Sep;7(9):930-8.
- Marquardt T, Ashery-Padan R, Andrejewski N, Scardigli R, Guillemot F, Gruss P. Pax6 is required for the multipotent state of retinal progenitor cells. *Cell*. 2001 Apr 6;105(1):43-55.
- Martin-Zanca D, Barbacid M, Parada LF. Expression of the trk proto-oncogene is restricted to the sensory cranial and spinal ganglia of neural crest origin in mouse development. *Genes Dev*. 1990 May;4(5):683-94.

- Mburu P, Mustapha M, Varela A, Weil D, El-Amraoui A, Holme RH, Rump A, Hardisty RE, Blanchard S, Coimbra RS, Perfettini I, Parkinson N, Mallon AM, Glenister P, Rogers MJ, Paige AJ, Moir L, Clay J, Rosenthal A, Liu XZ, Blanco G, Steel KP, Petit C, Brown SD. Defects in whirlin, a PDZ domain molecule involved in stereocilia elongation, cause deafness in the whirler mouse and families with DFNB31. *Nat Genet.* 2003 Aug;34(4):421-8.
- McEvelly RJ, Erkman L, Luo L, Sawchenko PE, Ryan AF, Rosenfeld MG. Requirement for Brn-3.0 in differentiation and survival of sensory and motor neurons. *Nature.* 1996 Dec 12;384(6609):574-7.
- Meerabux JM, Ohba H, Fukasawa M, Suto Y, Aoki-Suzuki M, Nakashiba T, Nishimura S, Itohara S, Yoshikawa T. Human netrin-G1 isoforms show evidence of differential expression. *Genomics.* 2005 Jul;86(1):112-6.
- Messersmith EK, Leonardo ED, Shatz CJ, Tessier-Lavigne M, Goodman CS, Kolodkin AL. Semaphorin III can function as a selective chemorepellent to pattern sensory projections in the spinal cord. *Neuron.* 1995 May;14(5):949-59.
- Mirnic K, Koerber HR. Prenatal development of rat primary afferent fibers: II. Central projections. *J Comp Neurol.* 1995 May 15;355(4):601-14.
- Molliver DC, Wright DE, Leitner ML, Parsadanian AS, Doster K, Wen D, Yan Q, Snider WD. IB4-binding DRG neurons switch from NGF to GDNF dependence in early postnatal life. *Neuron.* 1997 Oct;19(4):849-61.
- Mombaerts P, Wang F, Dulac C, Chao SK, Nemes A, Mendelsohn M, Edmondson J, Axel R. Visualizing an olfactory sensory map. *Cell.* 1996 Nov 15;87(4):675-86.
- Montelius A, Marmigère F, Baudet C, Aquino JB, Enerbäck S, Ernfors P. Emergence of the sensory nervous system as defined by Foxs1 expression. *Differentiation.* 2007 Jun;75(5):404-17.
- Muhr J, Graziano E, Wilson S, Jessell TM, Edlund T. Convergent inductive signals specify midbrain, hindbrain, and spinal cord identity in gastrula stage chick embryos. *Neuron.* 1999 Aug;23(4):689-702.
- Muramatsu T, Mizutani Y, Ohmori Y, Okumura J. Comparison of three nonviral transfection methods for foreign gene expression in early chicken embryos *in ovo*. *Biochem Biophys Res Commun.* 1997 Jan 13;230(2):376-80.
- Nakagawa S, Takeichi M. Neural crest emigration from the neural tube depends on regulated cadherin expression. *Development.* 1998 Aug;125(15):2963-71.
- Nakamura S, Senzaki K, Yoshikawa M, Nishimura M, Inoue K, Ito Y, Ozaki S, Shiga T. Dynamic regulation of the expression of neurotrophin receptors by Runx3. *Development.* 2008 May;135(9):1703-11.

- Nakashiba T, Nishimura S, Ikeda T, Itohara S. Complementary expression and neurite outgrowth activity of netrin-G subfamily members. *Mech Dev.* 2002 Feb;111(1-2):47-60.
- Necker, R. Observations on the function of a slowly-adapting mechanoreceptor associated with filoplumes in the feathered skin of pigeons. *Journal of comparative physiology A.* 1985;156(3):391-394.
- Necker, R. Sensory representation of the wing in the spinal dorsal horn of the pigeon. *Exp Brain Res.* 1990;81(2):403-412.
- Necker, R. The somatosensory system. In: Sturkie PD, Whittow GC. *Sturkie's avian physiology.* 5th edition. Academic Press. London. 2000.
- Nectoux J, Girard B, Bahi-Buisson N, Prieur F, Afenjar A, Rosas-Vargas H, Chelly J, Bienvenu T. Netrin G1 mutations are an uncommon cause of atypical Rett syndrome with or without epilepsy. *Pediatr Neurol.* 2007 Oct;37(4):270-4.
- Niimi K, Nishimura-Akiyoshi S, Nakashiba T, Itohara S. Monoclonal antibodies discriminating netrin-G1 and netrin-G2 neuronal pathways. *J Neuroimmunol.* 2007 Dec;192(1-2):99-104.
- Nilius B. Pressing and squeezing with Piezos. *EMBO Rep.* 2010 Dec;11(12):902-3.
- Nishimura-Akiyoshi S, Niimi K, Nakashiba T, Itohara S. Axonal netrin-Gs transneuronally determine lamina-specific subdendritic segments. *Proc Natl Acad Sci U S A.* 2007 Sep 11;104(37):14801-6.
- Nobrega MA, Ovcharenko I, Afzal V, Rubin EM. Scanning human gene deserts for long-range enhancers. *Science.* 2003 Oct 17;302(5644):413.
- Novitsch BG, Chen AI, Jessell TM. Coordinate regulation of motor neuron subtype identity and pan-neuronal properties by the bHLH repressor Olig2. *Neuron.* 2001 Sep 13;31(5):773-89.
- O'Connor DH, Huber D, Svoboda K. Reverse engineering the mouse brain. *Nature.* 2009 Oct 15;461(7266):923-9. Review.
- Ohtsuki T, Horiuchi Y, Koga M, Ishiguro H, Inada T, Iwata N, Ozaki N, Ujike H, Watanabe Y, Someya T, Arinami T. Association of polymorphisms in the haplotype block spanning the alternatively spliced exons of the NTNG1 gene at 1p13.3 with schizophrenia in Japanese populations. *Neurosci Lett.* 2008 Apr 25;435(3):194-7.
- Ovcharenko I, Nobrega MA, Loots GG, Stubbs L. ECR Browser: a tool for visualizing and accessing data from comparisons of multiple vertebrate genomes. *Nucleic Acids Res.* 2004 Jul 1;32(Web Server issue):W280-6.
- Ozaki S, Snider WD. Initial trajectories of sensory axons toward laminar targets in the developing mouse spinal cord. *J Comp Neurol.* 1997 Apr 7;380(2):215-29.



- Patel TD, Jackman A, Rice FL, Kucera J, Snider WD. Development of sensory neurons in the absence of NGF/TrkA signaling *in vivo*. *Neuron*. 2000 Feb;25(2):345-57.
- Patel TD, Kramer I, Kucera J, Niederkofler V, Jessell TM, Arber S, Snider WD. Peripheral NT3 signaling is required for ETS protein expression and central patterning of proprioceptive sensory afferents. *Neuron*. 2003 May 8;38(3):403-16.
- Peier AM, Moqrich A, Hergarden AC, Reeve AJ, Andersson DA, Story GM, Earley TJ, Dragoni I, McIntyre P, Bevan S, Patapoutian A. A TRP channel that senses cold stimuli and menthol. *Cell*. 2002 Mar 8;108(5):705-15.
- Pennacchio LA, Ahituv N, Moses AM, Prabhakar S, Nobrega MA, Shoukry M, Minovitsky S, Dubchak I, Holt A, Lewis KD, Plajzer-Frick I, Akiyama J, De Val S, Afzal V, Black BL, Couronne O, Eisen MB, Visel A, Rubin EM. *In vivo* enhancer analysis of human conserved non-coding sequences. *Nature*. 2006 Nov 23;444(7118):499-502.
- Pennisi E. Genomics. ENCODE project writes eulogy for junk DNA. *Science*. 2012 Sep 7;337(6099):1159, 1161.
- Perez SE, Rebelo S, Anderson DJ. Early specification of sensory neuron fate revealed by expression and function of neurogenins in the chick embryo. *Development*. 1999 Apr;126(8):1715-28.
- Pla P, Moore R, Morali OG, Grille S, Martinozzi S, Delmas V, Larue L. Cadherins in neural crest cell development and transformation. *J Cell Physiol*. 2001 Nov;189(2):121-32. Review.
- Pond A, Roche FK, Letourneau PC. Temporal regulation of neuropilin-1 expression and sensitivity to semaphorin 3A in NGF- and NT3-responsive chick sensory neurons. *J Neurobiol*. 2002 Apr;51(1):43-53.
- Prabhakar S, Visel A, Akiyama JA, Shoukry M, Lewis KD, Holt A, Plajzer-Frick I, Morrison H, Fitzpatrick DR, Afzal V, Pennacchio LA, Rubin EM, Noonan JP. Human-specific gain of function in a developmental enhancer. *Science*. 2008 Sep 5;321(5894):1346-50.
- Ravenall SJ, Gavazzi I, Wood JN, Akopian AN. A peripheral nervous system actin-binding protein regulates neurite outgrowth. *Eur J Neurosci*. 2002 Jan;15(2):281-90.
- Rebelo S, Reguenga C, Lopes C, Lima D. Prrxl1 is required for the generation of a subset of nociceptive glutamatergic superficial spinal dorsal horn neurons. *Dev Dyn*. 2010 Jun;239(6):1684-94.
- Redmond L, Xie H, Ziskind-Conhaim L, Hockfield S. Cues intrinsic to the spinal cord determine the pattern and timing of primary afferent growth. *Dev Biol*. 1997 Feb 15;182(2):205-18.

- Riddell JS, Hadian M. Interneurons in pathways from group II muscle afferents in the lower-lumbar segments of the feline spinal cord. *J Physiol*. 2000 Jan 1;522 Pt 1:109-23.
- Ruhrberg C, Schwarz Q. In the beginning: Generating neural crest cell diversity. *Cell Adh Migr*. 2010 Oct-Dec;4(4):622-30. Review.
- Sambrook J, Russell DW. *Molecular Cloning: A laboratory manual*. 3rd edition. Cold Spring Harbor Laboratory Press. New York. 2001.
- Sander M, Paydar S, Ericson J, Briscoe J, Berber E, German M, Jessell TM, Rubenstein JL. Ventral neural patterning by Nkx homeobox genes: Nkx6.1 controls somatic motor neuron and ventral interneuron fates. *Genes Dev*. 2000 Sep 1;14(17):2134-9.
- Sato Y, Kasai T, Nakagawa S, Tanabe K, Watanabe T, Kawakami K, Takahashi Y. Stable integration and conditional expression of electroporated transgenes in chicken embryos. *Dev Biol*. 2007 May 15;305(2):616-24.
- Sauka-Spengler T, Bronner-Fraser M. A gene regulatory network orchestrates neural crest formation. *Nat Rev Mol Cell Biol*. 2008 Jul;9(7):557-68. Review.
- Scott SA. *Sensory Neurons: Diversity, Development, and Plasticity*. Oxford University Press. New York. 1992.
- Scott A, Hasegawa H, Sakurai K, Yaron A, Cobb J, Wang F. Transcription factor short stature homeobox 2 is required for proper development of tropomyosin-related kinase B-expressing mechanosensory neurons. *J Neurosci*. 2011 May 4;31(18):6741-9.
- Seiradake E, Coles CH, Perestenko PV, Harlos K, McIlhinney RA, Aricescu AR, Jones EY. Structural basis for cell surface patterning through NetrinG-NGL interactions. *EMBO J*. 2011 Sep 23;30(21):4479-88.
- Serbedzija GN, Fraser SE, Bronner-Fraser M. Pathways of trunk neural crest cell migration in the mouse embryo as revealed by vital dye labelling. *Development*. 1990 Apr;108(4):605-12.
- Smeyne RJ, Klein R, Schnapp A, Long LK, Bryant S, Lewin A, Lira SA, Barbacid M. Severe sensory and sympathetic neuropathies in mice carrying a disrupted Trk/NGF receptor gene. *Nature*. 1994 Mar 17;368(6468):246-9.
- Snider WD, Wright DE. Neurotrophins cause a new sensation. *Neuron*. 1996 Feb;16(2):229-32. Review.
- Squire L, Berg D, Bloom F, Du Lac S, Ghosh A, Spitzer N. *Fundamental Neuroscience*. 3rd edition. Academic Press. Amsterdam. 2008.
- Stern CD, Fraser SE. Tracing the lineage of tracing cell lineages. *Nat Cell Biol*. 2001 Sep;3(9):E216-8. Review.

Sun Y, Dykes IM, Liang X, Eng SR, Evans SM, Turner EE. A central role for Islet1 in sensory neuron development linking sensory and spinal gene regulatory programs. *Nat Neurosci*. 2008 Nov;11(11):1283-93.

Sürmeli G, Akay T, Ippolito GC, Tucker PW, Jessell TM. Patterns of spinal sensory-motor connectivity prescribed by a dorsoventral positional template. *Cell*. 2011 Oct 28;147(3):653-65.

Takahashi Y, Watanabe T, Nakagawa S, Kawakami K, Sato Y. Transposon-mediated stable integration and tetracycline-inducible expression of electroporated transgenes in chicken embryos. *Methods Cell Biol*. 2008;87:271-80. Review.

Takashima Y, Ma L, McKemy DD. The development of peripheral cold neural circuits based on TRPM8 expression. *Neuroscience*. 2010 Aug 25;169(2):828-42.

Tanabe Y, Jessell TM. Diversity and pattern in the developing spinal cord. *Science*. 1996 Nov 15;274(5290):1115-23. Review.

Thaler JP, Lee SK, Jurata LW, Gill GN, Pfaff SL. LIM factor Lhx3 contributes to the specification of motor neuron and interneuron identity through cell-type-specific protein-protein interactions. *Cell*. 2002 Jul 26;110(2):237-49.

Thaler JP, Koo SJ, Kania A, Lettieri K, Andrews S, Cox C, Jessell TM, Pfaff SL. A postmitotic role for Isl-class LIM homeodomain proteins in the assignment of visceral spinal motor neuron identity. *Neuron*. 2004 Feb 5;41(3):337-50.

Theveneau E, Mayor R. Neural crest delamination and migration: from epithelium-to-mesenchyme transition to collective cell migration. *Dev Biol*. 2012 Jun 1;366(1):34-54.

Timmer J, Johnson J, Niswander L. The use of *in ovo* electroporation for the rapid analysis of neural-specific murine enhancers. *Genesis*. 2001 Mar;29(3):123-32.

Tsuchida T, Ensini M, Morton SB, Baldassare M, Edlund T, Jessell TM, Pfaff SL. Topographic organization of embryonic motor neurons defined by expression of LIM homeobox genes. *Cell*. 1994 Dec 16;79(6):957-70.

Uchikawa M, Ishida Y, Takemoto T, Kamachi Y, Kondoh H. Functional analysis of chicken Sox2 enhancers highlights an array of diverse regulatory elements that are conserved in mammals. *Dev Cell*. 2003 Apr;4(4):509-19.

Uchikawa M, Takemoto T, Kamachi Y, Kondoh H. Efficient identification of regulatory sequences in the chicken genome by a powerful combination of embryo electroporation and genome comparison. *Mech Dev*. 2004 Sep;121(9):1145-58. Review.

Uchikawa M. Enhancer analysis by chicken embryo electroporation with aid of genome comparison. *Dev Growth Differ*. 2008 Aug;50(6):467-74.

- Uemura O, Okada Y, Ando H, Guedj M, Higashijima S, Shimazaki T, Chino N, Okano H, Okamoto H. Comparative functional genomics revealed conservation and diversification of three enhancers of the *isl1* gene for motor and sensory neuron-specific expression. *Dev Biol*. 2005 Feb 15;278(2):587-606.
- Visel A, Prabhakar S, Akiyama JA, Shoukry M, Lewis KD, Holt A, Plajzer-Frick I, Afzal V, Rubin EM, Pennacchio LA. Ultraconservation identifies a small subset of extremely constrained developmental enhancers. *Nat Genet*. 2008 Feb;40(2):158-60.
- Visel A, Rubin EM, Pennacchio LA. Genomic views of distant-acting enhancers. *Nature*. 2009 Sep 10;461(7261):199-205. Review.
- Wang L, Marquardt T. Direct live monitoring of heterotypic axon-axon interactions *in vitro*. *Nat Protoc*. 2012 Jan 26;7(2):351-63.
- Wende H, Lechner SG, Cheret C, Bourane S, Kolanczyk ME, Pattyn A, Reuter K, Munier FL, Carroll P, Lewin GR, Birchmeier C. The transcription factor c-Maf controls touch receptor development and function. *Science*. 2012 Mar 16;335(6074):1373-6.
- Wild JM, Krützfeldt NO, Altshuler DL. Trigeminal and spinal dorsal horn (dis)continuity and avian evolution. *Brain Behav Evol*. 2010;76(1):11-9.
- Winkelman RK, Myers TT 3rd. The histochemistry and morphology of the cutaneous sensory end-organs of the chicken. *J Comp Neurol*. 1961 Aug;117:27-35.
- Woo J, Kwon SK, Kim E. The NGL family of leucine-rich repeat-containing synaptic adhesion molecules. *Mol Cell Neurosci*. 2009 Sep;42(1):1-10. Review.
- Wood JN, Winter J, James IF, Rang HP, Yeats J, Bevan S. Capsaicin-induced ion fluxes in dorsal root ganglion cells in culture. *J Neurosci*. 1988 Sep;8(9):3208-20.
- Woodbury CJ, Scott SA. Somatotopic organization of hindlimb skin sensory inputs to the dorsal horn of hatchling chicks (*Gallus g. domesticus*). *J Comp Neurol*. 1991 Dec 8;314(2):237-56.
- Woolfe A, Goodson M, Goode DK, Snell P, McEwen GK, Vavouri T, Smith SF, North P, Callaway H, Kelly K, Walter K, Abnizova I, Gilks W, Edwards YJ, Cooke JE, Elgar G. Highly conserved non-coding sequences are associated with vertebrate development. *PLoS Biol*. 2005 Jan;3(1):e7.
- Woolfe JM, Kluender KR, Levi DM, Bartoshuk LM, Herz RS, Klatzky RL, Lederman SJ, Merfeld DM. *Sensation and Perception*. 2nd edition. Sinauer Associates. Sunderland. 2008.
- Wray GA, Babbitt CC. Genetics. Enhancing gene regulation. *Science*. 2008 Sep 5;321(5894):1300-1.
- Yin Y, Miner JH, Sanes JR. Laminets: laminin- and netrin-related genes expressed in distinct neuronal subsets. *Mol Cell Neurosci*. 2002 Mar;19(3):344-58.

Yokota Y, Saito D, Tadokoro R, Takahashi Y. Genomically integrated transgenes are stably and conditionally expressed in neural crest cell-specific lineages. *Dev Biol*. 2011 May 15;353(2):382-95.

Zhang F, Aravanis AM, Adamantidis A, de Lecea L, Deisseroth K. Circuit-breakers: optical technologies for probing neural signals and systems. *Nat Rev Neurosci*. 2007 Aug;8(8):577-81. Review.

Zhang W, Rajan I, Savelieva KV, Wang CY, Vogel P, Kelly M, Xu N, Hasson B, Jarman W, Lanthorn TH. Netrin-G2 and netrin-G2 ligand are both required for normal auditory responsiveness. *Genes Brain Behav*. 2008 Jun;7(4):385-92.

Zhou Y, Yamamoto M, Engel JD. GATA2 is required for the generation of V2 interneurons. *Development*. 2000 Sep;127(17):3829-38.

Zurborg S, Piszczek A, Martínez C, Hublitz P, Al Banchaabouchi M, Moreira P, Perlas E, Heppenstall PA. Generation and characterization of an Advillin-Cre driver mouse line. *Mol Pain*. 2011 Sep 11;7:66.

Zylka MJ, Rice FL, Anderson DJ. Topographically distinct epidermal nociceptive circuits revealed by axonal tracers targeted to Mrgprd. *Neuron*. 2005 Jan 6;45(1):17-25.

[ecrbrowser.dcode.org](http://ecrbrowser.dcode.org)

[www.brain-map.org](http://www.brain-map.org)

## 7. Acknowledgements

First of all, I would like to thank Dr. Till Marquardt for giving me the opportunity to be a doctoral student under his supervision. I am very grateful for the scientific training, the long-lasting support, the encouragement and his unlimited optimism and creativity over the last five years.

I would like to thank Prof. Dr. Gregor Eichele and Prof. Dr. Klaus-Armin Nave for their scientific support and helpful discussions as members of my thesis committee. My thankfulness also goes to the additional committee members, Prof. Dr. Ernst Wimmer, Prof. Dr. André Fischer and Dr. Camin Dean, for taking their time to evaluate my work.

I am very grateful to Dr. Stefan Lechner and Prof. Dr. Gary Lewin for the great collaboration, which hopefully will be rewarded soon with a publication.

Dr. Till Marquardt assembled an international extraordinary team that worked in a professional and at the same time supportive and helpful atmosphere. For that, I thank all the former and current colleagues and friends: Dr. Liang Wang, Dr. Daniel Müller, Dr. David Herholz, Dr. Pitchaiah Cherukuri, Dr. Tsung-I Lee, Chor Hoon Poh, Heiko Röhse, Bianca Schnepf, Camille Lancelin and all my bachelor students. Special gratitude goes to Alexandra Klusowski for her enormous support.

I would like to express my gratitude to the Göttingen Graduate School for Neurosciences and Molecular Biosciences (GGNB) and the Center for Molecular Physiology of the Brain (CMPB), as well as its coordinators for their assistance.

Furthermore, I would like to thank all my friends in and out of Göttingen. Special thanks go to my parents for their endless support, their patience and their love.

Finally, I would like to thank Alice. Thank you for your love.

## 8. Curriculum Vitae

### LUKAS CYGANEK

#### PERSONAL DATA

---

- Personal status: single
- Nationality: german
- Day of birth: November 9th 1983
- Place of birth: Neustadt, Poland

#### HIGHER EDUCATION

---

- July 2009 – Dec. 2012 Ph.D. thesis titled  
*“Exploring the neural basis of touch through selective and stable genetic tagging in the chick somatosensory system”*  
at European Neuroscience Institute Göttingen,  
Workgroup Developmental Neurobiology
- Oct. 2004 – June 2009 Studies at Georg-August-University Göttingen  
,Lehramt am Gymnasium' - Chemistry / Biology  
First State Examination ,Lehramt am Gymnasium'
- July 2008 – Jan. 2009 Final thesis titled  
*“Identification of regulatory elements involved in functional specification of fast and slow motor neurons”*  
at European Neuroscience Institute Göttingen,  
Workgroup Developmental Neurobiology
- Apr. 2007 – Aug. 2007 ERASMUS-stay at University Autònoma de Barcelona, Spain;  
Workgroup Analytic Chemistry, Sensors and Biosensors
- Apr. 2004 – Sept. 2004 Studies at Georg-August University Goettingen  
Diploma Chemistry

#### SCHOOL EDUCATION

---

- Aug. 2000 – June 2003 Attendance of the ,Gymnasiale Oberstufe' at  
Modellschule Obersberg in Bad Hersfeld,  
completed university entrance diploma
- Aug. 1994 – June 2000 Attendance of the ,Gymnasium' at  
Konrad-Duden-Schule in Bad Hersfeld

## 9. Declaration

I hereby declare that I prepared this thesis, entitled “Exploring the neural basis of touch through selective and stable genetic tagging in the chick somatosensory system”, on my own and with no other sources and aids than quoted.

Lukas Cyganek

Göttingen, November 2012